



HAL
open science

Persistent gas emission originating from a deep basaltic magma reservoir of an active volcano: the case of Aso volcano, Japan

Masataka Kawaguchi, Toshiaki Hasenaka, Kenneth T. Koga, Estelle F. Rose-Koga, Atsushi Yasuda, Natsumi Hokanishi, Yasushi Mori, Kenji Shimizu, Takayuki Ushikubo

► **To cite this version:**

Masataka Kawaguchi, Toshiaki Hasenaka, Kenneth T. Koga, Estelle F. Rose-Koga, Atsushi Yasuda, et al.. Persistent gas emission originating from a deep basaltic magma reservoir of an active volcano: the case of Aso volcano, Japan. Contributions to Mineralogy and Petrology, In press. hal-03029942v1

HAL Id: hal-03029942

<https://hal.science/hal-03029942v1>

Submitted on 29 Nov 2020 (v1), last revised 8 Oct 2021 (v2)

HAL is a multi-disciplinary open access archive for the deposit and dissemination of scientific research documents, whether they are published or not. The documents may come from teaching and research institutions in France or abroad, or from public or private research centers.

L'archive ouverte pluridisciplinaire **HAL**, est destinée au dépôt et à la diffusion de documents scientifiques de niveau recherche, publiés ou non, émanant des établissements d'enseignement et de recherche français ou étrangers, des laboratoires publics ou privés.

Contributions to Mineralogy and Petrology

Persistent gas emission originating from a deep basaltic magma reservoir of an active volcano: the case of Aso volcano, Japan

--Manuscript Draft--

Manuscript Number:	CTMP-D-20-00146R1	
Full Title:	Persistent gas emission originating from a deep basaltic magma reservoir of an active volcano: the case of Aso volcano, Japan	
Article Type:	Original Paper	
Keywords:	Melt inclusion; Volatile element; Magma mixing; Primitive magma; Storage depth; Excess degassing	
Corresponding Author:	Masataka Kawaguchi Kumamoto University Kumamoto, JAPAN	
Corresponding Author Secondary Information:		
Corresponding Author's Institution:	Kumamoto University	
Corresponding Author's Secondary Institution:		
First Author:	Masataka Kawaguchi	
First Author Secondary Information:		
Order of Authors:	Masataka Kawaguchi Toshiaki Hasenaka Kenneth T. Koga Estelle F. Rose-Koga Atsushi Yasuda Natsumi Hokanishi Yasushi Mori Kenji Shimizu Takayuki Ushikubo	
Order of Authors Secondary Information:		
Funding Information:	Japan Society for the Promotion of Science (17K05682)	Prof. Toshiaki Hasenaka
	Ministry of Education, Culture, Sports, Science and Technology	Prof. Toshiaki Hasenaka
	Campus France (JP19-00641)	Mr. Masataka Kawaguchi
	Région Auvergne-Rhône-Alpes (SCUSI)	Dr. Estelle F. Rose-Koga
Abstract:	Volcanic gas emission is considered to reflect the degassing of magma beneath volcanoes. The combined observations of gas measurement and petrological study are expected to constrain the volatile concentrations and storage depths of the pre-eruptive and primitive magma. Aso volcano (Japan) is a constantly-monitored, persistently-degassing volcano, and an ideal site to acquire gas and petrologic data. We analyzed the melt inclusions and phenocryst minerals of Holocene basaltic eruption products, and reported their major and volatile element concentrations. The samples showed abundant evidence of magma mixing, such as reverse mineral zoning, and highly variable mineral and glass compositions. SiO ₂ measured in melt inclusions varied from 46.0 to 65.8 wt. %. High-volatile concentration, S up to 3750	

	<p>ppm, were only found in mafic melt inclusions hosted by high-Fo olivine phenocrysts (~Fo82). The pre-eruptive storage depths were determined from volatile concentrations: 2 km and 4 km depth for Strombolian eruption and sub-Plinian eruption, respectively. The volatile-rich primitive magma, one endmember of the mixed-magma, originated from a deeper level (>10 km) than these magma reservoirs. Initial volatile concentrations of the primitive magma were determined using multiple constraints: >4.68 wt. % H₂O, 400 - 750 ppm CO₂, 3750 ppm S, 716 ppm Cl, and 324 ppm F. The observed variation of volcanic gas composition was best explained by the mixing of the gas segregated from at least a depth of 10 km, with that from the shallow reservoirs. This study illustrated the method to identify the primitive mafic magma responsible for deep volatile flux in a mature volcano with complex magmatic processes.</p>
<p>Response to Reviewers:</p>	<p>Dear Prof. Grove and reviewers:</p> <p>Thank you for your thoughtful and constructive feedback regarding our manuscript titled "Persistent gas emission originating from a deep basaltic magma reservoir of an active volcano: the case of Aso volcano, Japan". Please find attached our revised manuscript and responses to the reviewer's comments. We have carefully read all comments and revised the manuscript accordingly.</p> <p>In this revision, we rearranged the discussion order and added sentences to make it clearer. As suggested by the reviewers, we have also examined another degassing model and compared with our melt inclusion data, which is now enclosed into supplementary material. In addition, following the reviewer's suggestion, we have added a new summary figure for conclusion. Our manuscript has been greatly improved in other respects as well by the reviewers contributions.</p> <p>Lastly, thank you again for giving us the opportunity to strengthen our manuscript with your valuable comments and queries. We have worked hard to incorporate your feedback and hope that the revised version is now suitable for publication.</p> <p>Sincerely, Masataka Kawaguchi</p>

[Click here to view linked References](#)

Persistent gas emission originating from a deep basaltic magma reservoir of an active volcano: the case of Aso volcano, Japan

Masataka Kawaguchi**,

1. Graduate School of Science and Technology, Kumamoto University, 2-39-1 Kurokami, Chuo-ku, Kumamoto-shi, Kumamoto 860-8555, Japan, 181d9061@st.kumamoto-u.ac.jp

2. Université Clermont Auvergne, CNRS, IRD, OPGC, Laboratoire Magmas et Volcans, F-63000 Clermont-Ferrand, France, masataka.kawaguchi@etu.uca.fr

Toshiaki Hasenaka, Center for Water Cycle, Marine Environment and Disaster management, Kumamoto University, 2-39-1 Kurokami, Chuo-ku, Kumamoto-shi, Kumamoto 860-8555, Japan, hasenaka@kumamoto-u.ac.jp

Kenneth T. Koga, Université Clermont Auvergne, CNRS, IRD, OPGC, Laboratoire Magmas et Volcans, F-63000 Clermont-Ferrand, France, ken.koga@uca.fr

Estelle F. Rose-Koga, Université Clermont Auvergne, CNRS, IRD, OPGC, Laboratoire Magmas et Volcans, F-63000 Clermont-Ferrand, France, estelle.koga@uca.fr

Atsushi Yasuda, Earthquake Research Institute, The University of Tokyo, 1-1-1 Yayoi, Bunkyo-ku, Tokyo 113-0032, Japan, yasuda@eri.u-tokyo.ac.jp

Natsumi Hokanishi, Earthquake Research Institute, The University of Tokyo, 1-1-1 Yayoi, Bunkyo-ku, Tokyo 113-0032, Japan, hokanishi@eri.u-tokyo.ac.jp

Yasushi Mori, Kitakyushu Museum of Natural History and Human History, 2-4-1, Higashida, Yahatahigashi-ku, Kitakyushu 805-0071, Japan, mori@kminh.jp

Kenji Shimizu, Kochi Institute for Core Sample Research, Japan Agency for Marine–Earth Science and Technology (JAMSTEC), 200 Monobe-otsu Nankoku, Kochi 783-8502, Japan, shimmy@jamstec.go.jp

Takayuki Ushikubo, Kochi Institute for Core Sample Research, Japan Agency for Marine–Earth Science and Technology (JAMSTEC), 200 Monobe-otsu Nankoku, Kochi 783-8502, Japan, ushikubot@jamstec.go.jp

** Indicate the corresponding author

1
2
3 **35 Abstract**

4 36 Volcanic gas emission is considered to reflect the degassing of magma beneath
5 37 volcanoes. The combined observations of gas measurement and petrological study are
6 38 expected to constrain the volatile concentrations and storage depths of the pre-eruptive
7 39 and primitive magma. Aso volcano (Japan) is a constantly-monitored, persistently-
8 40 degassing volcano, and an ideal site to acquire gas and petrologic data. We analyzed the
9 41 melt inclusions and phenocryst minerals of Holocene basaltic eruption products, and
10 42 reported their major and volatile element concentrations. The samples showed abundant
11 43 evidence of magma mixing, such as reverse mineral zoning, and highly variable mineral
12 44 and glass compositions. SiO₂ measured in melt inclusions varied from 46.0 to 65.8 wt. %.
13 45 High-volatile concentration, S up to 3750 ppm, were only found in mafic melt inclusions
14 46 hosted by high-Fo olivine phenocrysts (~Fo82). The pre-eruptive storage depths were
15 47 determined from volatile concentrations: 2 km and 4 km depth for Strombolian eruption
16 48 and sub-Plinian eruption, respectively. The volatile-rich primitive magma, one
17 49 endmember of the mixed-magma, originated from a deeper level (>10 km) than these
18 50 magma reservoirs. Initial volatile concentrations of the primitive magma were determined
19 51 using multiple constraints: >4.68 wt. % H₂O, 400 - 750 ppm CO₂, 3750 ppm S, 716 ppm
20 52 Cl, and 324 ppm F. The observed variation of volcanic gas composition was best
21 53 explained by the mixing of the gas segregated from at least a depth of 10 km, with that
22 54 from the shallow reservoirs. This study illustrated the method to identify the primitive
23 55 mafic magma responsible for deep volatile flux in a mature volcano with complex
24 56 magmatic processes.

25
26
27
28
29
30
31
32
33
34 **57 Keywords**

35
36 58 Melt inclusion, Volatile element, Magma mixing, Primitive magma, Storage
37 59 depth, Excess degassing.

38
39
40 **60 Introduction**

41 61 Arc volcanoes are known for their explosive eruptions driven by abundant
42 62 dissolved volatile elements in their magma. It has been recognized that gas exsolution is
43 63 the key player triggering rapid magma ascent and eruption (Roggensack *et al.* 1997; Pioli
44 64 *et al.* 2009; Edmonds and Wallace 2017). Therefore, volcanic gas emission is considered
45 65 to reflect the degassing of magma beneath volcanoes, and is one of the commonly
46 66 observed and monitored activities, even in the quiescent period. Such persistent degassing
47 67 of active volcanoes has been seen in arc volcanoes of the world (e.g. Miyakejima,
48 68 Shinohara *et al.* 2003; Stromboli, Burton *et al.* 2007). Typically, volatile element
49 69 behavior in magmas is governed by their solubility, and the amounts of volatile elements
50 70 issued from magma are closely related to their pre-eruptive abundance. Thus, it is critical
51 71 to determine the depths at which magmas were present, and their initial compositions
52 72 through the studies of volcanic products. To investigate pre-eruptive volatile
53 73 concentration and possibly primitive concentration, the study of melt inclusions is a

1
2 74 powerful tool since the melt is trapped in a host crystal at depth, and isolated from
3 interaction with surrounding magma (e.g. Anderson 1973; Sisson and Layne 1993;
4 75 Wallace 2005). In fact, melt inclusions are not perfectly isolated from surrounding
5 76 magmas since H⁺ can diffuse through the host olivine (e.g. Gaetani *et al.* 2012) and CO₂
6 77 can be redistributed in shrinkage bubbles (e.g. Tucker *et al.* 2019). Therefore, H₂O and
7 78 CO₂ measurements in melt inclusions are regarded as minimum values indicating the
8 79 condition of last equilibration. However, several studies have pointed out discrepancies
9 80 between total masses of emitted gas measurements and melt inclusion-estimation of
10 81 dissolved gas in glasses (e.g. Wallace 2005; Shinohara 2008). This is commonly referred
11 82 to as “excess degassing”, and is observed in subduction zone volcanism (e.g. Métrich and
12 83 Wallace 2008; Roberge *et al.* 2009; Wallace and Edmonds 2011; de Moor *et al.* 2017). It
13 84 appears necessary to reconcile the melt inclusion-based volatile budget with the surface
14 85 observation and this is the task we want to tackle in this study.
15 86

16 87 Aso volcano (Japan) is the ideal study site to compare gas emissions and
17 88 petrological samples, including melt inclusions. It is a constantly monitored persistent
18 89 degassing volcano since the 1970s, emitting more than 100 - 200 tons of SO₂ a day, even
19 90 during the quiescent period (e.g. Mori *et al.* 2013; Shinohara *et al.* 2018; Japan
20 91 Meteorological Agency (JMA) 2020). In addition, Holocene eruptions from Aso
21 92 produced olivine-bearing tephra samples, ideal for finding quenched melt inclusions. For
22 93 example, a recent melt inclusion study of historical Aso eruption products reported a
23 94 shallow storage depth of erupted magma and a large excess of SO₂ degassing from Aso
24 95 volcano (Saito *et al.* 2018). However, this previous study did not report volatile element
25 96 concentrations of a primitive magma. Moreover, geophysical studies revealed multiple
26 97 magma reservoirs with depths down to 24 km (below sea level: bsl) (Sudo and Kong
27 98 2001; Sudo *et al.* 2006; Abe *et al.* 2010; Hata *et al.* 2016).
28 99

29 100 In this study, we analyzed the bulk tephra of less evolved erupted products,
30 101 matrix glasses, melt inclusions (glass and host minerals) to obtain information on the pre-
31 102 eruptive magma process, storage depth and characteristics of primitive magma of Aso
32 103 volcano. This paper reports the first petrological description of the deep magma reservoirs
33 104 of Aso volcano using melt inclusion data and corroborating gas composition model. Our
34 105 petrological constraints on a magma plumbing system give us the primitive H₂O, CO₂, F,
35 Cl, and S concentrations of Aso, a persistently-degassing active volcano.
36

37 106 **Samples and methods**

38 107 *Geological setting of Aso volcano and its cones*

39 108 Aso volcano, located in central Kyushu Island of the Southwest Japan Arc, is
40 109 one of the most active volcanoes of the volcanic front related to the Philippine sea plate
41 110 subduction (Nakada and Kamata 1991; Kamata 1998; Miyoshi *et al.* 2008a, b). It has
42 111 been active for at least 0.8 million years (e.g. Watanabe *et al.* 1989). Its activity is
43 112 characterized by two different types of volcanisms: caldera-forming gigantic pyroclastic-
44 113 flow eruptions (from 270 ka to 89 ka), and post-caldera extrusive activities (<89 ka) (Ono
45
46
47

1
2 114 and Watanabe 1985). In the post-caldera stage, various types of magma (basalt to rhyolite)
3 115 were erupted from, at least, 17 observable vents in the caldera (Watanabe 2001; Miyoshi
4 116 *et al.* 2005).

5 117 Holocene activities are well described in tephrostratigraphic studies
6 118 (Miyabuchi and Watanabe 1997; Miyabuchi 2009, 2010, 2017). The tephra is mostly
7 119 basaltic and limited to the ejections from central cones. The last silicic eruption deposited
8 120 Aso central cone pumice 1 (ACP1; Takada 1989) at 4.0 ka (Miyabuchi and Watanabe
9 121 1997; Hirata *et al.* 2020). ACP1 is the only silicic product in Holocene, which is dacitic
10 122 banded pumice related to the effusion of Akamizu andesite lava flow (Miyabuchi 2017).
11 123 Subsequently, volcanic activity of Kishimadake (3.7 ka), Ojodake (3.5 ka), Komezuka
12 124 and Kamikomezuka cones (3.0 ka) was derived from basaltic to basaltic andesite magmas
13 125 (Fig. 1; Miyabuchi and Watanabe 1997; Miyabuchi 2010; Hirata *et al.* 2020). Nakadake
14 126 cone is formed in three stages: old volcanic (22 – 7.3 ka), young volcanic (7.3 – 3.7 ka)
15 127 and youngest pyroclastic stages (<3.7 ka; Ono and Watanabe 1985; Miyabuchi 2009).
16 128 Today, Nakadake is the only active central cone since the last eruption of Kamikomezuka
17 129 (*ca.* 3.0 ka). All basaltic rocks in the post-caldera stage of Aso volcano evolved to low-
18 130 Mg high-alumina basalt (MgO < 6.1 wt.%; Kuno 1960; Sisson and Grove 1993).

19 131 The magma chambers beneath Aso caldera have been described by geophysical
20 132 surveys. Abe *et al.* (2010) reported a large low-velocity layer (LVL) from a depth of 11
21 133 to 25 km (for consistency hereafter, all the depths in the paper are referred as depths from
22 134 the vent of the edifice, adding 1 km to the depth below sea level), by receiver function
23 135 tomography. Hata *et al.* (2016) identified the magma pathway from 21 km deep beneath
24 136 the caldera by electromagnetic survey, and reported two anomaly centers (C1 and C2)
25 137 separated by 3 km in horizontal distance. C1 is located 5 km beneath Kishimadake cone,
26 138 which corresponds to the main magma chamber feeding present-day Nakadake eruptions.
27 139 This is in good agreement with earlier studies that reported the C1 chamber between 4
28 140 and 10 km depth, by deformation analysis of the volcano (Sudo *et al.* 2006) and seismic
29 141 low-velocity anomaly (Sudo and Kong 2001). C2 is located 3 km beneath Nakadake cone.
30 142 However, this C2 anomaly is geographically offsetted from the crater of Nakadake, and
31 143 instead, a crack-like conduit extending from 0.3 to 2.8 km. A continuing passage was
32 144 identified beneath this cracked-conduit, based on a region of lack of seismic reflectors at
33 145 a depth from 2.5 to 4.5 km beneath the crater based on a 3-D seismic reflection analysis
34 146 (Tsutsui and Sudo 2004). In this paper, we call this shallow magma passage as C2.

35 147 36 148 37 149 ***Tephra and scoria descriptions***

38 150 We collected tephra deposits of eruptions from Kishimadake (*ca.* 3.7 ka),
39 151 Ojodake (*ca.* 3.5 ka), Kamikomezuka (*ca.* 3.0 ka) and Nakadake (the youngest pyroclastic
40 152 cone; <3.7 ka). Tephra samples were specifically collected to avoid the diffusive volatile-
41 153 loss and daughter mineral crystallization within melt inclusions (Danyushevsky *et al.*
42 154 2002; Lloyd *et al.* 2013). Furthermore, we focused on recent (3.7 ka to present) eruption

1
2 155 activities of basalt to basaltic andesite composition involving olivine phenocrysts. The
3
4 156 sample set was therefore used to obtain information about crustal magma evolution and
5
6 157 the volatile characteristics of magmas. All tephra samples contain phenocrysts of
7
8 158 plagioclase, olivine, clinopyroxene, orthopyroxene, and opaque minerals. Detailed
9 159 descriptions of these tephra are found in Miyabuchi (2009, 2010).

10
11 160 Five tephra samples used in this study correspond to the eruptions of four cones:
12 161 Kishimadake scoria (KSS), Ojodake scoria (OJSU and OJSL), Kamikomezuka scoria
13 162 (KKO), and Nakadake scoria (NKD14). Specifically, KSS, OJSU, and OJSL were
14 163 collected from a tephra deposit site (A9418 section reported by Watanabe 1991;
15 164 Miyabuchi and Watanabe 1997; Fig. 1). KSS was collected from the lowest unit of sub-
16 165 Plinian scoria-fall deposits in the N6 stage. It is a vesicular basaltic black scoria with a
17 166 maximum size of 4.8 cm (Miyabuchi and Watanabe 1997). OJSU and OJSL were
18 167 collected from the uppermost and lowest unit of sub-Plinian scoria-fall deposits in the N4
19 168 stage, respectively. OJSU and OJSL are reddish-brown, weakly altered basaltic scoria,
20 169 with a maximum size of 4.6 cm (Miyabuchi and Watanabe 1997). These deposits
21 170 represent sub-Plinian eruption events, which are the biggest eruption events in Holocene
22 171 (each with approximately 0.06 km³, VEI 3, Miyabuchi 2009). KKO was collected from
23 172 Kamikomezuka cone, because the tephra deposit away from the edifice has not been
24 173 identified presently. We sampled the black scoria from the outer part of the edifice from
25 174 a road-cut outcrop, avoiding oxidized reddish scoria. KKO is poorly sorted, non-welded,
26 175 vesicular scoria, ranging from cm-size to cow-dung bomb (tens of cm). NKD14 was
27 176 collected from the crater rim of Nakadake cone's first crater, immediately after the
28 177 eruption of Nov. 27, 2014. The samples were cm-size, well-vesiculated, black scoria. The
29 178 eruption of Nakadake cone in the period 2014 - 2015 is the first magmatic eruption in 24
30 179 years (Ikebe *et al.* 2008; JMA 2016). In the most violent phase, Strombolian eruptions
31 180 occurred with ejections of scoria lapilli and bombs at Nakadake cone's first crater (Yokoo
32 181 and Miyabuchi 2015).

182 183 ***Melt inclusion preparation***

184
185 These 5 tephra samples were used for petrological observation and chemical
186 analysis (*i.e.* bulk rock, phenocrysts and melt inclusions). Samples were washed in an
187 ultrasonic bath, and only lapilli-size scoria (up to 6 cm) were chosen. Five grams of each
188 sample were powdered using a ball milling machine with an alumina cup and a ball, for
189 bulk rock X-ray fluorescence analysis (XRF). Olivine, pyroxene, and plagioclase crystals
190 were handpicked under an optical microscope from scoria crushed by hand and sieved
191 (from 0.25 to 1 mm). The picked crystals were mounted in resin and polished until the
192 melt inclusion was exposed. They were then measured using an electron probe micro-
193 analyzer (EPMA) and a reflectance Fourier transform infrared spectroscope (FTIR).
194 Selected olivine crystals hosting melt inclusions of KSS and NKD14 were removed from
195 the resin after EPMA and FTIR analyses, then mounted together in indium for secondary
ion mass spectrometry (SIMS).

1
2 196

3
4 197 *Analytical methods*

5
6 198 Bulk rock major and trace elements

7
8
9 199 Bulk rock major and trace elements were determined by XRF on flux-fused
10 200 disks using a Philips PANalytical MagiX PRO spectrometer at the Kitakyushu Museum
11 201 of Natural History and Human History. The detailed analytical procedures are described
12 202 by Mori and Mashima (Mori and Mashima 2005). Accuracy was reported as ± 0.1 %
13 203 relative for SiO₂ and for trace elements, and varied from 5 to 25 ppm (Table 1).

14
15
16
17 204 Major and volatile elements in melt inclusion, mineral and glass

18
19
20 205 Major elements, S, and Cl concentrations were determined in melt inclusions,
21 206 host minerals and groundmass glasses using a JXA8800R electron probe microanalyzer
22 207 at the Earthquake Research Institute (ERI), University of Tokyo. The analytical settings
23 208 were 15kV acceleration voltage, 12 nA beam current, with counting times for Na, Al, K,
24 209 Fe, Mg, Si, Ti, V, Mn, and Ca at 20 s, and 30 s for Ni, Cr in mafic minerals and for S and
25 210 Cl in hydrous melt. Beam diameter was set at 10 μm for glass and plagioclase, and
26 211 focused (1 μm) for other minerals. During melt inclusion and groundmass glass analysis,
27 212 Na and K were always measured in the first analytical cycle to minimize alkali loss
28 213 (Devine *et al.* 1995). All analyses applied oxide ZAF correction. Analytical uncertainties
29 214 are <0.7% relative for Si, <1% relative for Al, Fe, Mg, and Ca, <5% relative for Ti and
30 215 Na, <10% relative for K, and <20% relative for Mn, V, Ni, Cr, S, and Cl.

31 216 In addition to the EPMA analysis, the core and rim compositions of phenocrysts
32 217 were analyzed by energy-dispersive X-ray spectroscopy (EDS, AZtec system; Oxford
33 218 Instruments) connected to a JEOL JSM-7001F field-emission electron microscope (FE-
34 219 SEM) at Kumamoto University, using 15 kV acceleration voltage and 1 nA beam current.
35 220 The beam diameter settings were the same as the EPMA setting at the University of Tokyo
36 221 for all the host minerals. Analytical uncertainties are typically 0.5% relative for SiO₂, 1%
37 222 relative for Al₂O₃, 1.5% relative for FeO, 0.5% relative for MgO, 2% relative for TiO₂
38 223 and Na₂O, 1.5% relative for K₂O, 1% relative for CaO. Other minor elements such as
39 224 MnO and P₂O₅ can be as high as 20% relative.

40 225 Water concentrations in melt inclusions were determined by FTIR micro-
41 226 reflectance spectroscopy using a JASCO FT-IR-660 plus, equipped with an IRT-30VC
42 227 analytical microscope at the ERI, following the procedures described by Yasuda (2014).
43 228 The IR spectra were obtained using 15 \times 15 to 60 \times 60 μm^2 rectangular apertures, and by
44 229 accumulating 220 to 1500 scans, over a range of 400 to 7800 cm^{-1} . A gold mirror was
45 230 used as a reflectance reference. Water concentrations were quantified using an empirical
46 231 linear relationship for basalt to rhyolite compositions for total H₂O concentrations,
47 232 measured in the 3650 cm^{-1} wavelength region. The analytical uncertainty (2σ) of the FTIR
48 233 reflectance spectroscopy was < 0.3 wt. %. While the detection limit of the method

234 strongly depended on the sample, we estimated the detection limits as 0.14 wt. % (Yasuda
235 2014).

236 H₂O, CO₂, F, S, and Cl concentrations in selected melt inclusions were
237 determined by a SIMS (Cameca IMS-1280HR of Kochi Institute, JAMSTEC, Japan)
238 following the procedure described by Shimizu *et al.* (2017). This analytical method favors
239 a weaker primary current (up to 0.5 nA) than in previous studies (1-1.5 nA primary
240 current; Le Voyer *et al.* 2010; Helo *et al.* 2011; Rose-Koga *et al.* 2012, 2014; 20 nA
241 primary current in Hauri *et al.* 2002) and uses in-house standards covering the
242 concentration range found in the natural samples in this study. In short, a 20 keV (10 keV
243 at the ion source and 10 keV at the sample surface) Cs⁺ ion beam of 300–500 pA was
244 defocused to be 10-15 μm in diameter. Secondary ions were accelerated at 10 kV. A -10
245 keV electron beam with a diameter of ~100 μm was applied for electrostatic charge
246 compensation of the analysis area. The field aperture was set at the size corresponding to
247 5 x 5 μm on the sample surface. Mass resolving power was set at ~6000 to separate mass
248 interferences (for example, to separate ³⁴S¹H interference on ³⁵Cl requires 5120 MRP;
249 Burdo and Morrison 1971). Negative secondary ions of ¹²C, ¹⁶OH, ¹⁹F, ³⁰Si, ³¹P, ³²S, and
250 ³⁵Cl and the mass position of 11.9 amu were measured by an axial electron multiplier
251 using the peak switching method. An analysis consisted of 10 cycles, and the total
252 measurement time for each analysis was ~6 min. Repeated analysis of a secondary
253 basaltic glass standard from East Pacific Rise, EPR-G3 (Shimizu *et al.* 2017), yielded a
254 relative standard deviation (1σ) for H₂O, CO₂, F, Cl, and S of 1.4, 3.2, 1.5, 2.5, and 0.9%,
255 respectively. This SIMS analysis was conducted after EPMA analysis. Therefore,
256 although we were careful to polish the sample with alumina powder again before SIMS
257 analysis, measured CO₂ concentrations were reported in the supplementary material but
258 not used due to possible carbon contamination. The measured values for S and Cl agreed
259 within 25% between EPMA and SIMS analysis. So when volatile elements were
260 measured by two methods, we adopted SIMS values rather than EPMA because analytical
261 uncertainty of these elements by SIMS are generally lower (e.g. Rose-Koga *et al.* 2020).
262 In this study, we did not find satisfactory agreement between H₂O determined by FTIR
263 and by SIMS (uncertainty of FTIR measurements is close to 40%) so in the following,
264 we only consider H₂O concentrations measured by SIMS, based on the better detection
265 limit and precision of the method.

266 Sulfur speciation analysis

267 Selected inclusions were analyzed for SKα peak positions to constrain the *f*O₂
268 conditions of the glasses. The wavelength of SKα radiation [λ (SKα)] for melt inclusions
269 was measured using the EPMA following the procedures described by Yasuda *et al.*
270 (2001), based on the method of Wallace and Carmichael (1994) and Carroll and
271 Rutherford (1988). Sulfur speciation as the proportion of S⁶⁺ over a total S content was
272 determined by measuring a relative shift from the peak position of an anhydrite mineral

1
2 273 (Carroll and Rutherford 1988), with an assumption that S^{2-} and S^{6+} are the only two
3 274 relevant species in silicate melt (Jugo *et al.* 2010). To avoid sulfur oxidation due to
4 275 prolonged beam exposure (*i.e.* Rowe *et al.* 2007), we conducted a measurement with
5 276 multiple spots for each melt inclusion. Therefore, we added up the wavelength scan data
6 277 of individual spots to determine the precise peak position. A Gaussian curve fitting was
7 278 used for sulfur peak deconvolution. Analytical uncertainty ranges from 5 to 10% relative
8 279 (Table S1).
9
10
11

12 280 **Data processing: Post-entrapment crystallization correction**

13 281
14 282 Major and volatile element data for all melt inclusions hosted in olivine were
15 283 corrected for the effects of post-entrapment crystallization (PEC; e.g. Danyushevsky *et al.*
16 284 al. 2000) by incremental calculation of equilibrium olivine (0.1 wt. % step) adding into
17 285 the residual melt, until the melt reaching equilibrium with host olivine (Toplis 2005),
18 286 following the procedures described in Danyushevsky *et al.* (2000). The melt Fe^{2+}/Fe^{Total}
19 287 ratios were calculated from the empirical equation of Kilinc *et al.* (1983), assuming a
20 288 constant fO_2 ($\Delta FMQ + 1.0$) based on measured $SK\alpha$ peak shifts of all eruptions (Jugo *et al.*
21 289 al. 2010). Temperatures of olivine-melt equilibrium were calculated using the olivine-
22 290 saturated melt thermometer of Sugawara (2000), corrected for the effect of water on
23 291 olivine liquidus temperature according to Médard and Grove (2008). We assumed an
24 292 average H_2O concentration of NKD14 and KSS analyzed by SIMS for melt inclusions
25 293 that were not analyzed individually for H_2O . Note, K_D and temperature were recalculated
26 294 at each increment of olivine addition. The melt inclusions were not corrected for post-
27 295 entrapment diffusive Fe-loss (Danyushevsky *et al.* 2000), as total FeO concentrations in
28 296 melt inclusions are either the same or higher than those in bulk rocks. Corrected volatile
29 297 concentrations were adjusted assuming volatiles are perfectly incompatible to host
30 298 minerals and corrected values are used in the figures and reported in Table 2 (raw
31 299 uncorrected data in supplementary material S1).
32
33
34
35
36
37
38
39

40 300 Plagioclase-, clinopyroxene-, and orthopyroxene-hosted melt inclusions were
41 301 not corrected for PEC because there is no universally accepted procedure, although some
42 302 attempts have been reported (Yasuda *et al.* 2001; Neave *et al.* 2017; Hartley *et al.* 2018).
43 303 Among these samples, only the melt inclusions in equilibrium with host minerals were
44 304 used for the magmatic temperature calculation, in which the exchange coefficients were
45 305 within expected range of basaltic composition: $(K_D(Fe-Mg)_{cpx-liq} = 0.28 \pm 0.08$, $K_D(Fe-$
46 306 $Mg)_{opx-liq} = 0.29 \pm 0.06$, and $K_D(An-Ab)_{pl-liq} = 0.27 \pm 0.01$ or 0.1 ± 0.05 (depending on
47 307 the calculated temperature; Putirka 2008).
48
49
50
51
52
53

54 308 **Results**

55 309 The analysis of five scoria from Aso edifices produced data of major elements
56 310 for bulk rocks along with 204 melt inclusion data (major and volatile element
57 311 concentrations) and host mineral compositions. More than 890 point-analyses were made
58 312 to determine major element compositions of groundmass glasses and phenocrysts (core
59
60
61
62
63
64
65

1
2 313 and rim; Tables 1 – 3 and S1 – S3).

3 314
4 315 ***Petrography***

5 316 All samples were porphyritic with approximately 40 vol.% crystals. Plagioclase,
6 317 clinopyroxene, olivine plus minor orthopyroxene, and opaque minerals were present. In
7 318 all samples, plagioclase phenocrysts commonly showed dusty zone and honeycomb
8 319 texture (Fig. 2a), and all orthopyroxene phenocrysts had reaction rims of olivine and
9 320 clinopyroxene (Fig. 2b). Aggregates of phenocrysts (i.e. plagioclase, clinopyroxene,
10 321 olivine, and opaque minerals) were frequently found in all samples (Fig. 2c). The
11 322 groundmass consisted of microlites of plagioclase, clinopyroxene, olivine, and magnetite.
12 323 The groundmass of KSS occasionally showed the heterogeneous mingling texture where
13 324 crystals are relatively abundant (Fig. 2d).

14 325
15 326 ***Host mineral compositions***

16 327 The olivine phenocrysts were grouped into two types based on the core Fo
17 328 contents [$\text{Mg} / (\text{Fe} + \text{Mg}) \times 100$ in mole], as low-Fo (62 to 72) and high-Fo (72 to 82)
18 329 (Fig. 3a). High-Fo olivine was observed only in KKO, OJSU, OJSL, and KSS. Low-Fo
19 330 olivine was found in all samples. As Fo content of the phenocryst rims ranged from 68 to
20 331 78 in KKO, OJSU, OJSL, and KSS, and from 64 to 67 in NKD14 (Table S3), generally
21 332 low-Fo olivine phenocrysts were reversely zoned, whereas olivine phenocrysts in NKD14
22 333 were homogeneous. All high-Fo olivine phenocrysts were normally zoned.
23 334 Clinopyroxene and orthopyroxene phenocryst cores in all samples were in the range of
24 335 65-76 and 61-71, respectively ($\text{Mg\#} = [\text{Mg} / (\text{Fe} + \text{Mg}) \times 100$ in mole]). The majority of
25 336 clinopyroxene phenocrysts in KKO, OJSU, OJSL, and KSS were reversely zoned. Mg#
26 337 of NKD14 varied little, at ~70. The compositions in the rims of olivine and clinopyroxene
27 338 phenocrysts were the same as the minerals found in reaction rims of orthopyroxene
28 339 phenocrysts. The plagioclase phenocrysts were also divided into two types based on the
29 340 normal and reverse zoning patterns. The An content [$\text{Ca} / (\text{Ca} + \text{Na}) \times 100$ in mole] of
30 341 the plagioclase phenocryst cores was within the 55-93 range.

31 342
32 343 ***Major and volatile elements in melt inclusions***

33 344 The tephra samples of this study were basaltic to basaltic andesite with SiO_2
34 345 ranging from 51.5 to 54.3 wt. % (large circles in Fig. 3c). Melt composition in inclusions
35 346 varied significantly more than that of the bulk tephra composition: SiO_2 ranging from
36 347 46.0 to 65.8 wt. %. This range mostly overlapped with the compositional variation of
37 348 post-caldera volcanic products (grey circles in Fig. 3c). The melt inclusion compositions
38 349 of NKD14 were generally similar to evolved matrix glass and varied little, and were
39 350 distinguished from the melt inclusions of KKO, OJSU, OJSL, and KSS.

40 351 In our sample set, the core composition of host olivines were clearly divided
41 352 into two groups with Fo72 representing the divide (Fig. 3a). We interpreted that olivines
42 353 have grown from two distinctively different lavas, which we called mafic and felsic.

1
2 354 Based on the anti-correlation of SiO₂ concentration in olivine-hosted melt inclusions with
3 355 host Fo content, we concluded that magma composition can be divided into two groups
4 356 above and below 55 wt.% SiO₂. The high SiO₂ corresponded to low-Fo olivine and low
5 357 SiO₂ corresponded to high-Fo olivine. Thus, in the following we grouped all the melt
6 358 inclusions lower than 55 wt.% SiO₂ in a mafic group, and others in a felsic group. S
7 359 concentration in melt inclusions correlates well with host Fo content and is anti-correlated
8 360 with SiO₂ (Fig. 3a) and K₂O, indicating a mafic volatile-rich (with S up to 3750 ppm and
9 361 Cl up to 1311 ppm) magma, and a felsic volatile-poor magma (Fig. 3b). NKD14
10 362 inclusions were notably different, with less than 434 ppm S, indicating extensive
11 363 degassing. Melt inclusion Cl concentrations varied from 530 ppm to 1311 ppm (Table 2
12 364 and Table S1; SIMS value is preferred to EMP value when both are reported). F
13 365 concentrations were determined only on a subset of olivine-hosted melt inclusions and
14 366 therefore there are fewer data. F concentrations varied between 258 and 853 ppm (Table
15 367 2 and Table S1). F and Cl correlates with SiO₂ and K₂O and anti-correlate with host Fo
16 368 content. H₂O concentrations measured in melt inclusions vary between 0.47 to 2.89 wt.%
17 369 (NKD14-Olivine-4-m4 and KSS-Olivine-4-m11, respectively; Table 2 and Table S1).

370 **Discussion**

371 *Evidence for magma mixing*

372 Zoning in magmatic minerals characterizes their crystallization in a magma
373 chamber and can trace the history of magma cooling (e.g. Costa *et al.* 2008), and magma
374 mixing (e.g. Sakuyama 1979). Among the tephra samples in this study, phenocrysts in
375 every sample indicate textural evidence of magma mixing that could have been produced
376 by the introduction of hotter magma: for example, the reverse zoning and disequilibrium
377 texture, such as the honey-comb texture of plagioclase and reaction rim of orthopyroxene
378 (Fig. 2a and 2b; Tsuchiyama 1985). The coexistence of normally zoned plagioclase and
379 olivine phenocrysts with these disequilibrium phenocrysts suggests that magma mixing
380 of at least two distinct components has occurred (e.g. Sakuyama 1979). This
381 interpretation is supported by the compositional variation of the melt inclusions; felsic
382 melt inclusions are hosted in reversely zoned phenocrysts such as plagioclase,
383 clinopyroxene, orthopyroxene, and low-Fo olivine. Mafic melt inclusions are hosted in
384 high-Fo olivine and some of plagioclase (Fig. 3).

385 The presence of orthopyroxenes surrounded by reaction rims and An-rich zones
386 in the middle part of plagioclases in NKD14 (Fig. 2f) indicates that the 2014 magma is
387 also the result of mixing. Such petrological features are found in magmatic products of
388 every Nakadake eruption (Miyoshi *et al.* 2005). Thus, we consider that all the Nakadake
389 eruption products are the result of magma mixing, rather than the derivatives from a single
390 parental magma. In addition, Miyoshi *et al.* (2005) also show that the compositional
391 variation in the trace elements in the post-caldera basaltic rocks of Aso volcano is
392 consistent with a magma mixing model and not with a fractional crystallization process.
393 Therefore, at least two types of magmas are present beneath the Nakadake cone, and feed

1
2 394 its eruption.
3
4 395

5 396 ***Characterization of mixing endmembers***

6 397 We conducted a two-component mixing model calculation of two distinct
7
8 398 magmas, one silicic endmember and one mafic endmember, based on the major element
9
10 399 variation of melt inclusions (see Supplementary document S4). The model used the most
11
12 400 primitive basaltic melt (Melt ID: 2-m1 hosted in an olivine) and the most SiO₂-rich dacitic
13
14 401 melt (Melt ID: d2-m1 hosted in a plagioclase) of KSS as the mafic and silicic endmember,
15
16 402 respectively. The major element variation was well reproduced with the mixing model
17
18 403 for melt inclusions of all host minerals (Fig. S4-5). While the major variance of
19
20 404 concentration variations was explained by a simple mixing process, in close inspection of
21
22 405 trends, it is likely that crystal fractionation contributed to the dispersion from the mixing
23
24 406 model. It should also be noted that the mixing model required the presence of independent
25
26 407 mixing endmembers, it does not constrain their origin.

27 408 It is important to note that there is a surface expression of this silicic
28
29 409 endmember in the Aso eruption products, while the mixing endmember is set by a melt
30
31 410 inclusion. Major element compositions of ACP1 dacitic pumice (Takada 1989), the only
32
33 411 Holocene felsic product erupted three hundred years before that of KSS, are similar to the
34
35 412 endmember, and this indicates the presence of the silicic magma. Furthermore, the
36
37 413 presence of a banded pumice was reported in ACP1 prior to KSS (Miyabuchi 2017). This
38
39 414 banded texture is evidence of magma mingling and therefore the mixing trend is unlikely
40
41 415 a result of assimilation and crystal fractionation of single parental magma. The cores of
42
43 416 reversely zoned phenocrysts of KSS scoria samples were formed at equilibrium
44
45 417 conditions with the silicic endmember. Therefore, the temperature of silicic endmember
46
47 418 magma was determined with a two-pyroxene thermometer by pairing core compositions
48
49 419 (Putirka 2008). The estimated temperatures of the silicic endmember are 1010-1025°C
50
51 420 for KKO, OJSU, OJSL, and KSS ($\pm 13^\circ\text{C}$, 1σ for samples, while standard error of the
52
53 421 thermometer is $\pm 38^\circ\text{C}$). We adopted this estimated range as the temperature of the silicic
54
55 422 endmember magma. These estimated temperatures are higher than those of typical dacitic
56
57 423 magma with 4 - 5 wt. % H₂O (e.g. 770 – 915 °C for Mount St. Helens, Gardner *et al.*
58
59 424 1995) and lower than that estimated for a completely anhydrous dacitic magmas, for
60
61 425 example Puna Geothermal Venture Wellfield, Hawaii have the highest temperature
62
63 426 estimates 1050°C (Teplow *et al.* 2009). This silicic endmember magma (T between 1010-
64
65 427 1025°C) will mix with the mafic endmember (most likely hotter) magma at temperature
66
67 428 presumably higher than 1010-1025°C.

68 429 Basaltic lava corresponding to the pure mafic endmember is absent among the
69
70 430 eruption products of the entire post caldera stage (Miyoshi *et al.* 2005), while it is found
71
72 431 in olivine-hosted melt inclusion. Many tephra of this study also contain normally zoned
73
74 432 phenocrysts with high-Fo and high-An cores. As for the case of the silicic endmember, it
75
76 433 is possible to assume the equilibrium of these cores with the mafic endmember melt. We
77
78 434 therefore calculated the magmatic temperature of the pure mafic endmember, using

1
2 435 Sakuyama's method (Sakuyama *et al.* 2014), which involves the combined application of
3 436 a plagioclase-melt hygrometer (Lange *et al.* 2009) and an olivine-saturated melt
4 437 geothermometer (Sugawara 2000; Médard and Grove 2008). This method accounts for
5 438 the H₂O-dependency of the olivine thermometer by simultaneously solving for H₂O and
6 439 temperature using an additional constraint from the plagioclase hygrometer. The resulting
7 440 temperature of mafic endmember magma varies between 1051 – 1063 °C, depending on
8 441 the assumed pressure condition of the magma chamber (0.1 - 0.5 GPa, respectively). In
9 442 addition, the entrapment temperature of the endmember inclusion (KSS-2-m1) is 1092
10 443 °C based on the olivine-liquidus thermometer (Table S1, Sugawara 2000; Médard and
11 444 Grove 2008). Considering the uncertainties of the thermometry methods, these
12 445 temperature estimates are likely representing the range for the mafic magma. By taking
13 446 the high temperature result (~1090 °C), the temperature difference between mafic and
14 447 felsic (1010-1025 °C) endmembers is at least 65 °C.

15 448 The mixing trend among volatile elements is present and generally consistent
16 449 with the trend of major elements. However, in detail, there are systematic disparities from
17 450 the mixing curve (Supplementary document S4). Notably, abundances of H₂O, S, and Cl
18 451 for NKD14 sample, are depleted compared to the mixing trend traced by KSS melt
19 452 inclusions (Fig. S4-4). This is best explained by significant degassing occurring
20 453 during/after magma mixing. Furthermore, there is no single melt inclusion uniquely
21 454 representing suitable mafic endmember volatile concentrations. The sample KSS-2-m1 is
22 455 selected as the major element endmember, but its H₂O contents are not the highest values.
23 456 From the inspection of the trend, we inferred that the mafic endmember must have higher
24 457 volatile content thus most likely lost water after its entrapment. If melt inclusions formed
25 458 at a deeper depth, and were stored in a shallower magma chamber, it is expected that H⁺
26 459 diffusion through the olivine would equilibrate the melt inclusion with the surrounding
27 460 magma (Portnyagin *et al.* 2008; Chen *et al.* 2011; Gaetani *et al.* 2012; Bucholz *et al.*
28 461 2013; Ferriss *et al.* 2016). Complete re-equilibrated melt inclusion would have erased the
29 462 mixing trend. It is not the case here, we have found suitable endmember volatile element
30 463 concentrations that satisfy the general trend. Because the mafic endmember magma is
31 464 expected to be volatile-rich, it's H₂O concentration has to be higher than the H₂O of the
32 465 mixed-magma (e.g. that of the melt inclusions). The maximum estimated H₂O
33 466 concentration (4.68 wt. %) based on the hygrometer discussed above is therefore taken as
34 467 the concentration for the volatile-rich mafic endmember. This value of 4.68 wt.% H₂O is
35 468 higher, by about 2 wt. %, than the highest H₂O concentration measured in the melt
36 469 inclusion. Sakuyama's method implicitly ignores the CO₂ activity in magma, and predicts
37 470 lower H₂O content when considering CO₂-bearing system (by 0.9 wt. % less H₂O,
38 471 assessed from an experimental result of Melekhova *et al.* 2017). Furthermore, this volatile
39 472 content is the value at the condition of olivine - plagioclase crystallization, most likely of
40 473 the cooling magma in the crust. At this point, we have no other constraint on the H₂O
41 474 concentration of the mafic endmember and the primary magma could have an even higher
42 475 H₂O content.

1
2 476
3
4 477 ***Volatile concentrations of primitive basaltic melt***

5 478 The melt inclusions similar to the mafic endmember of the mixing model
6 479 showed element concentrations with primitive character, such as low incompatible
7 480 element concentrations (low K₂O, Cl, and F), and higher volatile element such as S.
8 481 However, H₂O concentration is likely equilibrated to a lower pressure conditions, and
9 482 CO₂ concentration in melt inclusion appears to be low. While these melt inclusions are
10 483 hosted in high Fo olivine, the H₂O and CO₂ abundances are not of primitive character.
11 484 On the contrary, as F, S, and Cl are not expected to diffuse through the host olivine, and
12 485 at the time of entrapment, they retain the value closest to the primitive magma. In an
13 486 attempt to constrain the mafic endmember composition, compositional trends are
14 487 examined with ratios of S, Cl, and F over K₂O. These ratios are less affected by
15 488 crystallization within melt inclusions and before entrapment, assuming the strong
16 489 incompatibility of K₂O in magmatic minerals near basaltic liquidus (Fig. 4). Because the
17 490 composition of the mafic endmember points towards that of the primitive magma, the
18 491 maximum values are taken from Fig. 4a, b, and c, as the primitive volatile ratios: S/K₂O
19 492 = 0.711, Cl/K₂O = 0.170, and F/K₂O = 0.047.

20 493 Dissolved S concentrations, up to 3750 ppm in the mafic group melt inclusions,
21 494 are higher than many melt inclusions from subduction-like hydrous basalt (Fig. 5a; S
22 495 mostly between 900 and 2500 ppm; e.g. Wallace 2005), while high S content appears to
23 496 occur in oxidized magmas (Roggensack 2001; Webster *et al.* 2010). Our primitive magma
24 497 S estimate is therefore 3750 ppm, the highest measured concentration in a melt inclusion
25 498 of the mafic group. We also noted that S concentration of half of the melt inclusions are
26 499 supersaturated in sulfide, plotting above the sulfur concentration at sulfide saturation
27 500 (SCSS, Fig. 5b), while no sulfide is found in the melt inclusions or in the groundmass.
28 501 These sulfide supersaturated melt inclusions must be at high *f*O₂ condition, so that the
29 502 concentration of sulfide-precipitating S²⁻ in magma is lower than SCSS. In fact, it has
30 503 been shown that arc basalt magmas have higher oxygen fugacities than MORB magmas
31 504 (e.g. Wallace 2005; Kelley and Cottrell 2009). In addition to this, the redox state of the
32 505 melt inclusions was determined and ranges from FMQ + 0.68 to FMQ + 1.41 (Average =
33 506 1.05, 1σ = 0.17, corresponding to S⁶⁺/S_{total} = 0.14 - 0.85, Table S1). Such oxidizing
34 507 conditions allow for (i) higher S solubility in the mafic magma (Carroll and Rutherford
35 508 1985; Jugo *et al.* 2010) and (ii) the presence of both S²⁻ and S⁶⁺ in the melt. Fig. 5b also
36 509 shows a dashed line expected for the SCSS corrected for abundance of S²⁻ species
37 510 (S⁶⁺/S_{total} = 0.85). Such first order correction puts all of our melt inclusion to be below
38 511 sulfur saturation, consistent with our observation. Also, S concentrations of all the melt
39 512 inclusions are under-saturated with respect to anhydrite saturation (SCAS was from 5300
40 513 to 6000 ppm, Li and Ripley 2009; Baker and Moretti 2011). The elevated S concentrations
41 514 in the undersaturated oxidized melt are therefore considered to represent, less-degassed,
42 515 non-sulfide-fractionated, S concentrations, at least at the condition of the shallow storage
43 516 depth.

1
2 517 Similarly, we also consider that the mafic endmember Cl and F concentrations
3
4 518 are representative of primary concentrations, as the exsolution pressure of Cl and F is at
5
6 519 shallower depths (~100 MPa for Cl and ~10 MPa for F; Spilliaert *et al.* 2006) than for
7
8 520 other volatile species. Cl concentration in the Aso primitive magma was 716 ppm (took
9
10 521 the value of the mafic end member melt inclusion: KSS-2-m1) which is higher than that
11
12 522 of MORB (Fig. 6; max 500 ppm Cl, Le Voyer *et al.* 2015), as it is interpreted as the
13
14 523 addition of Cl to the subarc mantle from the subducting slab (e.g. Straub and Layne 2003).
15
16 524 On the contrary, F concentration in the primitive magma was 324 ppm, which is the same
17
18 525 order of magnitude as that of MORB (max 500 ppm, Le Voyer *et al.* 2015). This suggests
19
20 526 that F addition to the subarc mantle was insignificant.

21
22 527 The Cl/F ratios of melt inclusions globally reflect the composition of the slab-
23
24 528 agent added to the mantle source as F fractionate from Cl depending on the physical
25
26 529 character of the flux leaving the slab (Le Voyer *et al.* 2010; Van den Bleeken and Koga
27
28 530 2015; Narvaez *et al.* 2018). Observed Cl/F ratio of melt inclusions from Aso volcano are
29
30 531 relatively high (from 1 to 2.5, Fig. 6) compared with that of MORB (Saal *et al.* 2002;
31
32 532 Wanless and Shaw 2012; Wanless *et al.* 2014, 2015; Le Voyer *et al.* 2017; Shimizu *et al.*
33
34 533 2019). Because Cl/F values in arc magma are characterized by several parameters such
35
36 534 as the composition of slab, nature of the fluid and fractionating minerals in residual slab,
37
38 535 and the degree of melting of arc magma, the physical character of slab derived flux is
39
40 536 determined with a set of assumptions. In any case, the primitive magmas with MORB-
41
42 537 like F concentration and a high Cl/F value (2.2) are found among the melt inclusions of
43
44 538 calc-alkaline arc magmas in a typically “cold” subduction setting (Straub and Layne
45
46 539 2003; Rose-Koga *et al.* 2014). The halogen characteristics of our Aso melt inclusions
47
48 540 were in the range of typical arc magma, and the value of the primitive magma was close
49
50 541 to the melt inclusions of Iwate volcano, a prototypical example of the arc magma derived
51
52 542 from aqueous fluid driven from a cold oceanic crust (Rose-Koga *et al.* 2014). This
53
54 543 indication is consistent with studies based on high bulk B/Nb ratios indicating aqueous
55
56 544 fluid additions from the subducting Philippine sea plate in the source of the Aso basalt-
57
58 545 basaltic andesite rocks (Miyoshi *et al.* 2008a, b). Other studies based on Sr, Nd, and Pb
59
60 546 isotope variations of Quaternary lavas in the northern Kyushu area also support the model
61
62 547 of slab-derived aqueous fluid addition from the subducted Philippine sea plate beneath
63
64 548 Aso volcano (Shibata *et al.* 2014).
65

549 550 ***Storage depth of the magma mixture***

551 Solubility of volatiles in magma strongly depends on pressure and temperature
552 conditions, and the chemical composition of the magma (e.g. Dixon *et al.* 1995). In this
553 section, we discuss the storage depth of the mixed-magma based on H₂O concentration.
554 For example, measured volatile concentrations of melt inclusions are considered to be re-
555 equilibrated to a condition of a magma storage. Alternatively, it is also possible to

1
2 556 determine H₂O concentrations estimated from plagioclase rim and groundmass glass pairs
3 557 (geo-hygrometer, Lange *et al.* 2009), likely corresponding to the value of the mixed
4 558 magma during the plagioclase rim growth. The H₂O concentrations of such mixed
5 559 magmas are, ~2 wt.% for NKD14 and KKO, and ~3 wt.% for OJSU, OJSL and KSS
6 560 (Table 4). Here, the hygrometer calibrated for the total fluid pressure is equal to $P(\text{H}_2\text{O})$,
7 561 neglecting the role of CO₂. Yet, these values are comparable to those measured in the
8 562 melt inclusions, and indicate a magma chamber pressures of 0.5 kbar for NKD14 and
9 563 KKO, and 1.0 kbar for OJSU, OJSL, and KSS (*i.e.* 2.1 and 4 km deep, respectively, Fig.
10 564 7, note the depth is calculated using a density of 2200 kg/m³ for the first 1 km and 2700
11 565 kg/m³ for the crust at greater depths (Komazawa 1995), by solving for the depth, h [m],
12 566 $P = g \{2200 (1000) + 2700 (h-1000)\}$. Because CO₂ concentrations in the felsic group
13 567 melt inclusions are notably low (0 - 77 ppm, Table S1), it makes negligible changes to
14 568 the calculated equilibrium pressure (~20 MPa, using RhyoliteMELTS/MagmaSat,
15 569 Ghiorso and Gualda 2015). These pressures correspond to the depths of magma storage
16 570 after mixing, since (1) the last growth rim of plagioclase must have occurred after mixing,
17 571 as both normal and reverse zoning plagioclase have the same rim composition. (2) It is
18 572 less likely that plagioclase rim significantly grew during sub-Plinian and Strombolian
19 573 eruption. Melt inclusion H₂O concentrations range from 0.47 to 2.89 wt. %, indicating
20 574 the minimum equilibrium pressure in agreement with the plagioclase-rim method. Two
21 575 magma chambers, C2 and C1, detected by geophysical studies are also located at similar
22 576 depths, 1 - 4 and 3 - 10 km, respectively (Tsutsui and Sudo 2004; Sudo *et al.* 2006; Hata
23 577 *et al.* 2016; Fig. 7). At the depths, because the solubility of CO₂ is so low, the conclusion
24 578 presented here would remain the same even if the hygrometer calculation does not
25 579 account for CO₂.

26 580 The magma of the mafic endmember is expected to have more than 4.68 wt. %
27 581 H₂O, and it is therefore derived from a greater depth than these C1 and C2 storage depths.
28 582 The corresponding equilibrium pressure is approximately 2.7 kbar (SolEx, Witham *et al.*
29 583 2012; note MagmaSat give 2.3 kbar, Ghiorso and Gualda 2015; with CO₂ of 340 ppm
30 584 reported in a melt inclusion from Nakadake by Saito *et al.* 2018) that is about 10 km deep
31 585 below the edifice. As gas bubbles were seen in melt inclusions, large amounts of CO₂
32 586 incorporated in such shrinkage bubbles significantly increases the entrapment pressure
33 587 estimation (e.g. Moore *et al.* 2015). Therefore, our pressure estimations are minimum and
34 588 true entrapment pressures of the basaltic magma certainly occurred at a depth greater than
35 589 10 km. Recent melt inclusion studies reported more than 40-90 % of the initial CO₂ that
36 590 was dissolved in the melt at the time of entrapment was lost to shrinkage bubbles, with
37 591 an average loss of 75-80 % (Hartley *et al.* 2014; Moore *et al.* 2015; Wallace *et al.* 2015).
38 592 If 90 % of initial CO₂ is present in the shrinkage bubble and a maximum CO₂ value of
39 593 340 ppm is assumed in the melt (from Saito *et al.* 2018), then the expected initial value
40 594 of the melt would reach 3400 ppm. This value is in the same order of magnitude as the
41 595 initial CO₂ concentration in a typical primary arc magma (Aster *et al.* 2016), and in this
42 596 case the saturation pressure would exceed 5 kbar (~19 km depth equivalent). However,

1
2 597 at the time of this study, bubble sizes were not documented with impossibility to go back
3 598 to measuring them *a posteriori* since most are now polished away. In this case, we chose
4 599 not to use the CO₂ data of the melt inclusions. Hata *et al.* (2016) also reported a magma
5 600 pathway from depths deeper than 11 km, feeding the deeper C1 reservoir. Also, the
6 601 presence of a seismic low-velocity layer at 11 - 25 km depth was reported and attributed
7 602 to a magma ponding location beneath the Aso caldera (Abe *et al.* 2010). These
8 603 observations are in good agreement with our petrological implication for the presence of
9 604 volatile-rich basaltic magma beneath C1 magma reservoir at a depth greater than 10 km.
10
11
12
13
14
15

16 607 ***Persistent degassing from a deeper magma reservoir (>10km)***

17
18
19 608 Excess degassing of SO₂ and CO₂ from Nakadake 2014 eruption

20
21 609 Decomposition of magma mixing endmembers and the subsequent
22 610 identification of the primitive magma composition provide critical information for
23 611 investigating volcanic emission of gas and its mass balance. For the 2014 eruption of Aso
24 612 volcano, the mass of erupted magma is insufficient to account for the mass of the observed
25 613 SO₂ gas emissions (Saito *et al.* 2018), which is commonly reported in many active
26 614 volcanoes and is called “excess degassing”. For Aso, approximately 90 – 140 times more
27 615 magma than the erupted tephra mass is needed to account for the observed total SO₂
28 616 emission of $1.4 - 2.2 \times 10^5$ tons for the period of 70 days from Nov. 2014 to Feb. 2015
29 617 (Table 5 and; also Saito *et al.* 2018). As demonstrated in the sections above, NKD magma
30 618 is a mixed magma, so the gas phase must have come from the degassing of mafic and
31 619 felsic endmember magmas. For this reason, we have used the highest volatile element
32 620 concentrations determined for Nakadake samples (*i.e.* mixed magmas) for the sulfur
33 621 budget calculation (Supplementary material S4). This calculation simply demonstrates
34 622 that the mixed magmas are inadequate sources of the observed volcanic gas flux. The
35 623 most commonly proposed explanation for this excess is the existence of a gas/fluid phase
36 624 in the magma, possibly containing C-O-H-S and co-existing with the magma prior to the
37 625 eruption (e.g. Anderson 1973; Wallace 2001; Scaillet and Pichavant 2003; Shinohara
38 626 2008). The magmatic volatile component must originate from the volatile-rich magma
39 627 corresponding to the basaltic/mafic endmember. This magma must degas at a deeper
40 628 depth than that indicated by the equilibrium solubility depth of NKD samples (~2 km at
41 629 the depth of C2). Therefore, the degree of S excess should be re-assessed with a deeper,
42 630 volatile-rich, basaltic magma. It should be noted that the observation of S-excess is
43 631 common (e.g. Wallace and Edmonds 2011) and we simply point out here that the eruption
44 632 of Nakadake edifice of Aso also shows such excess.

45
46
47
48
49
50
51 633 There are geophysical observations indicating that degassing is fed by volcanic
52 634 activities corresponding to depths deeper than ~2 km. The SO₂ gas emission of Aso
53 635 volcano is continuously monitored during the eruptive and the quiescent periods. The
54
55
56
57
58
59
60
61
62
63
64
65

1
2 636 amount of SO₂ emission during the quiescent period (alternatively, “persistent
3 637 degassing”; Shinohara 2008) is more than 100 – 200 tons/day from 1975 to 2006 (Mori
4 638 *et al.* 2013). Ground deformation measurements since 1937 revealed deformation
5 639 (deflation) of the deeper C1 magma reservoir synchronous to gas emission from
6 640 Nakadake cone during the quiescent period (Sudo *et al.* 2006). This C1 deformation,
7 641 located approximately 3 km West of Nakadake, causes no significant deformation on the
8 642 surface around the crater. This degassing is therefore interpreted as open-system
9 643 degassing of the C1 magma reservoir through stable conduit passages to Nakadake crater
10 644 (Yamamoto *et al.* 1999; Sudo *et al.* 2006). Furthermore, deflation of the C1 reservoir was
11 645 seen to slow down from 2008 to early 2014, before acceleration of inflation of the C1
12 646 reservoir from July 2014, shortly before the eruption in November (Ohkura *et al.* 2015;
13 647 JMA 2016). These changes were accompanied by a sudden increase in persistent SO₂ gas
14 648 emission in September 2013, considered as a precursor to the 2014 - 2015 eruptive period
15 649 (JMA 2016). These temporal and spatial relationships of geophysical observation and
16 650 degassing activities strongly indicate the role of the deeper C1 reservoir during degassing.
17 651 However, to sustain replenishment of the C1 reservoir, the magma must be supplied from
18 652 an even deeper depth (greater than 10 km; Sudo *et al.* 2006; Hata *et al.* 2016). For example,
19 653 the slowing down of deflation in 2008 and subsequent inflation in 2014 can be interpreted
20 654 as events relating to magma replenishment of the C1 reservoir (Ohkura *et al.* 2015, 2017).

21 655 We also found excess degassing of CO₂ for this eruption period. Using the
22 656 maximum pre-eruptive CO₂ concentration of 340 ppm measured in a melt inclusion of
23 657 Nakadake eruption products (Saito *et al.* 2018), and assuming there is no pre-eruptive
24 658 vapor phase approximately 1700 – 2700 times more dissolved CO₂ is required to account
25 659 for the observed 0.77 – 1.2 × 10⁶ tons of CO₂ emission (Table 5). In the case of Aso, the
26 660 gas phase must be derived from a depth greater than that of the C1 reservoir.

27 661 Modelling degassing of the deep magma reservoir

28 662 In the sections above, the equilibrium depths of volatile concentration in
29 663 magma were used to indicate magma storage depth, where stagnated-magma and gas
30 664 remain at equilibrium. Equilibrium gas composition at that depth should be the source of
31 665 the gas composition observed at the surface, only if the gas segregated and travelled to
32 666 the surface without precipitating solids or re-dissolving gas in between. In detail, the
33 667 speciation of mixed gas is a function of pressure, temperature, and oxygen fugacity, but
34 668 the gas system composition can be considered closed. With this hypothesis, it is possible
35 669 to determine the depth at which the observed gas composition is in equilibrium with a
36 670 magma (e.g. Burton *et al.* 2007; Allard 2010).

37 671 Fig. 8 is a result of such a calculation using SolEx (Witham *et al.* 2012),
38 672 showing the variations in H₂O/S, CO₂/S, and Cl/S molar ratios of gas in equilibrium with
39 673 a magma as a function of pressure. The observed H₂O/S gas composition of the 2014
40 674 eruption (shown as horizontal dotted red lines) intersects with the equilibrium gas

1
2 675 composition (plain lines Fig. 8) between 2.6 to 3.3 kbars. These pressures correspond to
3 676 10 - 13 km depth below the edifice. The family of curved lines represent the results of the
4 677 model with varying initial CO₂ concentration (400, 750, and 1000 ppm), as the initial CO₂
5 678 concentration was unknown (but for sure higher than 340 ppm). For the range of
6 679 degassing trajectory, the observed Cl/S values (horizontal dotted blue line) intersect with
7 680 the model calculations between 2.6 and 3.8 kbars. H₂O/S and CO₂/S are less sensitive to
8 681 the variation of the initial CO₂ concentration. It should be noted that the closed system
9 682 degassing path here is used to find a unique pressure condition at which the observed high
10 683 temperature gas composition is at the equilibrium with a mafic magma. The systematics
11 684 shows that only CO₂ concentrations between 400 and 750 ppm can produce the observed
12 685 gas composition at pressures between 2.6 to 3.3 kbars, satisfying the observed ranges of
13 686 H₂O/S, CO₂/S, and Cl/S all at once.

14
15
16
17
18
19 687 Therefore, the observed gas composition must have been derived from the
20 688 depth of about 10 to 13 km (~2.6 to 3.3 kb) at which it was in equilibrium with a magma
21 689 with the initial magmatic CO₂ concentration between 400 to 750 ppm (Fig. 8). The
22 690 determination of initial CO₂ is strongly tied to the Cl and S partitioning into H₂O-CO₂
23 691 fluid, and we think that these values may need to be revised once we have a better
24 692 understanding of Cl and S element partitioning. Lastly, this conclusion is highly model
25 693 dependent. Here, we chose to use SolEx for its agreement with the variation of S in the
26 694 melt inclusions. However, one must be cautious with the use of SolEx, because it is shown
27 695 to fail to reproduce degassing trajectories of other volcanoes (e.g., Werner et al. 2020).

28
29
30
31 696 Fig. 9 shows the observed gas composition emitted from Aso volcano in the
32 697 quiescent period and eruptive period. The gas data shown in Fig. 8 correspond to the
33 698 eruptive period data (orange). While Fig. 8 demonstrated the occurrence of deep gas
34 699 segregation, it does not explain the range of gas composition observed before and, even,
35 700 during the eruption of the Nakadake cone. We modelled the variation in gas composition
36 701 using (1) a degassing trend (solid line), the same model as that used in Fig. 8, and it fits
37 702 the data with some scatter and (2) a mixing line (dotted line) between a deep reservoir,
38 703 for example at the storage depth around 10 km, and a shallow reservoir (C2 or top of C1).
39 704 Both explain the data (Fig. 9). Thus, on the one hand, it is possible to consider the
40 705 variation in gas composition as the variation in gas segregation depth. On the other hand,
41 706 the observed gas composition variation potentially represents the different degrees of
42 707 mixing between discharged gas from NKD14 magma at shallow depth and segregated
43 708 gas from a deep reservoir (*i.e.* gas segregation depth at 10 km; Fig. 8 and 10). Case 1 is
44 709 less likely to apply here. Because of the closed-system degassing model (solid line), the
45 710 ascending primitive magma would have been expected to be in equilibrium with gas all
46 711 the time until it reaches near the surface. Therefore, the gas composition representing the
47 712 low pressure must have been in equilibrium with the mafic magmas at the shallowest
48 713 depth. However, no volcanic product of primitive composition was found during the
49 714 eruption of Nakadake cone. Instead, observed volcanic products were all the result of
50 715 mixing. As case 1 is unlikely, we conclude that the mixing of gases (case 2) is the process

1
2 716 explaining the observed compositional variation. The gas mixing could have been
3 717 possible, for example, by bubble accumulation at the roof of a magma chamber (Jaupart
4 718 and Vergnolle 1988, 1989).

7 719 8 720 *Implications for understanding current Aso volcanic activity*

9 721
10 722 This study identified the role of a volatile-rich, primitive magma during
11 723 volcanic degassing (Fig. 10). During ascent, the volatile-rich primitive magma started to
12 724 degas at a depth between 11 and 13 km (2.8 to 3.5 kbars, SolEx) based on the initial
13 725 volatile concentration. The gas and magma reached 10 km depth maintaining equilibrium.
14 726 At that depth, the gas segregated from the magma and moved to the surface without any
15 727 significant modification. The separation of gas from magma was potentially caused by
16 728 stopping of magma ascent, which contributed to overpressuring of C1 observed by the
17 729 deformation of the edifice. The magma then moved upwards and mixed with silicic
18 730 magma in the C1 magma reservoir. While the exact depth of mixing was undetermined,
19 731 the mixed magma was eventually stored at depths of C1 and C2 (for example 2 km (C2)
20 732 for NKD14 and KKO samples, and 4 km (C1) for OJSU, OJSL, and KSS samples).

21 733 The segregated deep gas mixed with the shallow gases upon its ascent at
22 734 shallower levels. We were unable to constrain the exact mechanism of the deep gas
23 735 transport to the shallow depth without significant interaction. One possibility is the
24 736 presence of porosity providing connected gas passages. However, this mechanism implies
25 737 the rigid structure at a temperature lower than magmatic conditions, and this contradicts
26 738 with the observation of the high temperature gas indicating magmatic degassing.
27 739 Alternatively, a convection within C1 and C2 potentially serves a “gas pump”. In this
28 740 scenario, a shallow mixed magma (devoid of volatile elements) descends by convection
29 741 to the bottom of C1 where gas segregation is occurring. Upon the return of such magma
30 742 to shallow depth, it drags the gas component with it. Such parcel of magma may further
31 743 pull gas bubbles from the shallow depth and result in a bulk system of mixed gas. If the
32 744 magma degases completely, the resulting gas composition will be identical to the result
33 745 of the gas mixing. This scenario would fail if some batch of magma do not degas and
34 746 remain in some depth; it requires complete degassing. Shinohara (2018) proposed a model
35 747 which suggested that the observed chemical variation in gases during eruption was caused
36 748 by mixing of gases derived from magmas at different depths. This model is consistent
37 749 with our gas mixing model. Our model furthered understanding of Aso activity, by (1)
38 750 quantifying the volatile concentration of primitive mafic magma, and (2) by determining
39 751 its degassing, segregation, and storage depths.

40 752 **Summary and conclusion**

41 753 Petrological analyses of melt inclusions in basaltic tephra from the late
42 754 Holocene eruption of Aso volcano provided us with insights into the process of the
43 755 persistent degassing in a magma plumbing system.

- 1
2 756 (1) The compositions of melt inclusions in phenocrysts from recent eruption
3 757 products (Nov. 2014) of Nakadake cone were homogeneous, evolved and
4 758 degassed ($S < 434$ ppm), while compositions of melt inclusions in
5 759 phenocrysts from Kishimadake and other related cones (ca. 3.0 – 3.7 ka)
6 760 showed variable compositions with two extreme endmembers. One was
7 761 mafic ($SiO_2 < 55$ wt.%) and volatile-rich, and the other was felsic ($SiO_2 >$
8 762 55 wt.%) and relatively degassed. Mafic melt inclusions were hosted in
9 763 high-Fo olivine and some plagioclase, whereas felsic melt inclusions were
10 764 hosted in plagioclase, clinopyroxene, orthopyroxene and low-Fo olivine.
11 765 (2) Reverse mineral zoning, and highly variable mineral and glass
12 766 compositions indicated a mixing process during which volatile-rich basaltic
13 767 magma was injected in a degassed shallower magma.
14 768 (3) The estimated depths of pre-eruptive magma were approximately 2 km (C2
15 769 magma reservoir) for Strombolian eruption of Nakadake cone (Nov. 27,
16 770 2014) and Kamikomezuka cone (3.0 ka) and approximately 4 km (top of
17 771 C1 magma reservoir) for sub-Plinian eruption of Ojodake and Kishimadake
18 772 cones in 3.5 – 3.7 ka. These depths corresponded to the partially melted
19 773 zones characterized by geophysical investigations (e.g. Hata *et al.* 2016).
20 774 Furthermore, volatile-rich primitive magma originated from a deeper level
21 775 (greater than 10 km) than these two magma reservoirs.
22 776 (4) Even with the highest S concentration of NKD14, it was impossible to
23 777 account for the excess S gas emission. This suggests an addition of gas
24 778 derived from the deep magma reservoir (greater than 10 km depth).
25 779 (5) Initial volatile concentrations of the volatile-rich primitive magma were
26 780 determined from the systematics of melt inclusion, plagioclase
27 781 compositions, and degassing model: >4.68 wt.% H_2O , 3750 ppm S, 716
28 782 ppm Cl and 324 ppm F.
29 783 (6) Emitted gas compositions constrained the initial CO_2 concentration ranges
30 784 in the magma, between 400 and 750 ppm.
31 785 (7) The variation observed in volcanic gas composition was best explained by
32 786 the mixing of the gas segregated at 10 km depth with those from the shallow
33 787 reservoirs.

788 **Acknowledgements**

789 The authors acknowledge the in-depth reviews of K. Iacovino, N. Métrich, and
790 D. Rasmussen. Their comments and challenging questions greatly improved this
791 manuscript. This work received funding from JSPS KAKENHI, Grant Number
792 17K05682 and the Integrated Program for Next Generation Volcano Research and
793 Human Resource Development to TH. MK acknowledges the financial support from the
794 French Embassy in Tokyo, Japan and from the French government through a “Bourse du
795 Gouvernement Français”. Campus France helped MK get settled during his stay in France.
796 MK also extends his thanks to Tadao Nishiyama and Hiroshi Isobe for their assistance

1
2 797 with the electron microprobe at Kumamoto University, and to Akira Yoshiasa for his
3 798 support in this international collaboration. ER-K and KTK acknowledge the financial
4 799 support from Region Auvergne-Rhone-Alpes (program SCUSI) and from the Laboratory
5 800 of Excellence ClerVolc. This is Laboratory of Excellence ClerVolc contribution no xxx.
6
7

8 801 **References**

- 9
10 802 Abe Y, Ohkura T, Shibutani T, Hirahara K, Kato M (2010) Crustal structure beneath Aso
11 803 Caldera, Southwest Japan, as derived from receiver function analysis. *J Volcanol*
12 804 *Geotherm Res* 195:1–12. <https://doi.org/10.1016/j.jvolgeores.2010.05.011>
13 805 Allard P (2010) A CO₂-rich gas trigger of explosive paroxysms at Stromboli basaltic
14 806 volcano, Italy. *J Volcanol Geotherm Res* 189:363–374.
15 807 <https://doi.org/10.1016/j.jvolgeores.2009.11.018>
16 808 Anderson AT (1973) The before-eruption water content of some high-alumina magmas.
17 809 *Bull Volcanol* 37:530–552. <https://doi.org/10.1007/BF02596890>
18 810 Aster EM, Wallace PJ, Moore LR, Watkins J, Gazel E, Bodnar RJ (2016) Reconstructing
19 811 CO₂ concentrations in basaltic melt inclusions using Raman analysis of vapor
20 812 bubbles. *J Volcanol Geotherm Res* 323:148–162.
21 813 <https://doi.org/10.1016/j.jvolgeores.2016.04.028>
22 814 Baker DR, Moretti R (2011) Modeling the solubility of sulfur in magmas: a 50-year old
23 815 geochemical challenge. *Rev Mineral Geochemistry* 73:167–213.
24 816 <https://doi.org/10.2138/rmg.2011.73.7>
25 817 Bucholz CE, Gaetani GA, Behn MD, Shimizu N (2013) Post-entrapment modification of
26 818 volatiles and oxygen fugacity in olivine-hosted melt inclusions. *Earth Planet Sci Lett*
27 819 374:145–155. <https://doi.org/10.1016/j.epsl.2013.05.033>
28 820 Burdo RA, Morrison HG (1971) Table of atomic and molecular lines for spark source
29 821 mass spectrometry of complex sample-graphite mixes. Materials Science Center,
30 822 Cornell University, Ithaca, New York
31 823 Burton MR, Allard P, Muré F, La Spina A (2007) Magmatic gas composition reveals the
32 824 source depth of slug-driven Strombolian explosive activity. *Science* 317:227–230
33 825 Carroll MR, Rutherford MJ (1985) Sulfide and Sulfate Saturation in Hydrous Silicate
34 826 Melts. *J Geophys Res Solid Earth* 90:C601–C612
35 827 Carroll MR, Rutherford MJ (1988) Sulfur speciation in hydrous experimental glasses of
36 828 varying oxidation state: results from measured wavelength shifts of sulfur X-rays.
37 829 *Am J Sci* 73:845–849
38 830 Chen Y, Provost A, Schiano P, Cluzel N (2011) The rate of water loss from olivine-hosted
39 831 melt inclusions. *Contrib to Mineral Petrol* 162:625–636.
40 832 <https://doi.org/10.1007/s00410-011-0616-5>
41 833 Costa F, Dohmen R, Chakraborty S (2008) Time scales of magmatic processes from
42 834 modeling the zoning patterns of crystals. *Rev Mineral Geochemistry* 69:545–594.
43 835 <https://doi.org/10.2138/rmg.2008.69.14>
44 836 Danyushevsky L V., Della-Pasqua FN, Sokolov S (2000) Re-equilibration of melt
45 837 inclusions trapped by magnesian olivine phenocrysts from subduction-related
46 838 magmas: petrological implications. *Contrib to Mineral Petrol* 138:68–83.
47 839 <https://doi.org/10.1007/PL00007664>
48 840 Danyushevsky L V., Sokolov S, Falloon TJ (2002) Melt inclusions in olivine phenocrysts:
49 841 using diffusive re-equilibration to determine the cooling history of a crystal, with
50 842 implications for the origin of olivine-phyric volcanic rocks. *J Petrol* 43:1651–1671.
51
52
53
54
55
56
57
58
59
60
61
62
63
64
65

- 1
2 843 <https://doi.org/10.1093/petrology/43.9.1651>
3
4 844 de Moor JM, Kern C, Avaré G, Muller C, Aiuppa A, Saballos A, Ibarra M, LaFemina P,
5 845 Protti M, Fischer TP (2017) A new sulfur and carbon degassing inventory for the
6 846 Southern Central American Volcanic Arc: the importance of accurate time-series
7 847 data sets and possible tectonic processes responsible for temporal variations in arc-
8 848 scale volatile emissions. *Geochemistry, Geophys Geosystems* 18:4437–4468.
9 849 <https://doi.org/10.1002/2017GC007141>
10
11 850 Dixon JE, Stolper EM, Holloway JR (1995) An experimental study of water and carbon
12 851 dioxide solubilities in mid-ocean ridge basaltic liquids. Part I: calibration and
13 852 solubility models. *J Petrol* 36:1607–1631
14
15 853 Edmonds M, Wallace PJ (2017) Volatiles and exsolved vapor in volcanic systems.
16 854 *Elements* 13:29–34. <https://doi.org/10.2113/gselements.13.1.29>
17
18 855 Ferriss E, Plank T, Walker D (2016) Site-specific hydrogen diffusion rates during
19 856 clinopyroxene dehydration. *Contrib to Mineral Petrol* 171:1–24.
20 857 <https://doi.org/10.1007/s00410-016-1262-8>
21
22 858 Fortin M-A, Riddle J, Desjardins-Langlais Y, Baker DR (2015) The effect of water on
23 859 the sulfur concentration at sulfide saturation (SCSS) in natural melts. *Geochim*
24 860 *Cosmochim Acta* 160:100–116. <https://doi.org/10.1016/j.gca.2015.03.022>
25
26 861 Gaetani GA, O’Leary JA, Shimizu N, Bucholz CE, Newville M (2012) Rapid
27 862 reequilibration of H₂O and oxygen fugacity in olivine-hosted melt inclusions.
28 863 *Geology* 40:915–918. <https://doi.org/10.1130/G32992.1>
29
30 864 Gardner JE, Rutherford M, Carey S, Sigurdsson H (1995) Experimental constraints on
31 865 pre-eruptive water contents and changing magma storage prior to explosive
32 866 eruptions of Mount St Helens volcano. *Bull Volcanol* 57:1–17.
33 867 <https://doi.org/10.1007/BF00298703>
34
35 868 Ghiorso MS, Gualda GAR (2015) An H₂O–CO₂ mixed fluid saturation model compatible
36 869 with rhyolite-MELTS. *Contrib to Mineral Petrol* 169:1–30.
37 870 <https://doi.org/10.1007/s00410-015-1141-8>
38
39 871 Hartley ME, Bali E, Maclennan J, Neave DA, Halldórsson SA (2018) Melt inclusion
40 872 constraints on petrogenesis of the 2014–2015 Holuhraun eruption, Iceland. *Contrib*
41 873 *to Mineral Petrol* 173:10. <https://doi.org/10.1007/s00410-017-1435-0>
42
43 874 Hartley ME, Maclennan J, Edmonds M, Thordarson T (2014) Reconstructing the deep
44 875 CO₂ degassing behaviour of large basaltic fissure eruptions. *Earth Planet Sci Lett*
45 876 393:120–131. <https://doi.org/10.1016/j.epsl.2014.02.031>
46
47 877 Hata M, Takakura S, Matsushima N, Hashimoto T, Utsugi M (2016) Crustal magma
48 878 pathway beneath Aso caldera inferred from three-dimensional electrical resistivity
49 879 structure. *Geophys Res Lett* 43:10720–10727.
50 880 <https://doi.org/10.1002/2016GL070315>
51
52 881 Hauri E, Wang J, Dixon JE, King PL, Mandeville C, Newman S (2002) SIMS analysis of
53 882 volatiles in silicate glasses 1. Calibration, matrix effects and comparisons with FTIR.
54 883 *Chem Geol* 183:99–114. [https://doi.org/10.1016/S0009-2541\(01\)00375-8](https://doi.org/10.1016/S0009-2541(01)00375-8)
55
56 884 Helo C, Longpré M-A, Shimizu N, Clague DA, Stix J (2011) Explosive eruptions at mid-
57 885 ocean ridges driven by CO₂-rich magmas. *Nat Geosci* 4:260–263.
58 886 <https://doi.org/10.1038/geo1104>
59
60 887 Hirata Y, Ueta K, Miyawaki R, Iemura K, Yokoyama T, Miyawaki A (2020) Tephra
61 888 stratigraphy and an about 4000-year-old slope failure on Janoo volcano, NW Aso
62 889 caldera. *Trans Japanese Geomorphological Union* 41:27–47 (in Japanese with

- 1
2 890 English abstract)
3
4 891 Ikebe S, Watanabe K, Miyabuchi Y (2008) The sequence and style of the 1988-1955
5 892 eruption of Nakadake Aso volcano, Kyushu, Japan. *Bull Volcanol Soc Japan* 53:15-
6 893 33 (in Japanese with English abstract)
7 894 Japan Meteorological Agency (2020) Results of volcanic gas observation at Aso volcano.
8 895 [http://www.data.jma.go.jp/svd/vois/data/fukuoka/rovdm/Asosan_rovdm.html](http://www.data.jma.go.jp/svd/vois/data/fukuoka/rovdm/Asosan_rovdm/Asosan_rovdm.html). Accessed 20 Apr 2020
9 896
10 897 Japan Meteorological Agency (2016) Volcanic activity of Asosan volcano —October
11 898 2014–February 2015—. *Rep Coord Com Predict Volcan Erupt* 120:166-186 (in
12 899 Japanese).
13 900 [http://www.data.jma.go.jp/svd/vois/data/tokyo/STOCK/kaisetsu/CCPVE/Report/1](http://www.data.jma.go.jp/svd/vois/data/tokyo/STOCK/kaisetsu/CCPVE/Report/120/kaiho_120_23.pdf)
14 901 [20/kaiho_120_23.pdf](http://www.data.jma.go.jp/svd/vois/data/tokyo/STOCK/kaisetsu/CCPVE/Report/120/kaiho_120_23.pdf)
15
16 902 Jaupart C, Vergnolle S (1988) Laboratory models of Hawaiian and Strombolian
17 903 eruptions. *Nature* 331:58–60
18 904 Jaupart C, Vergnolle S (1989) The generation and collapse of a foam layer at the roof of
19 905 a basaltic magma chamber. *J Fluid Mech* 203:347–380.
20 906 <https://doi.org/10.1017/S0022112089001497>
21 907 Jugo PJ, Wilke M, Botcharnikov RE (2010) Sulfur K-edge XANES analysis of natural
22 908 and synthetic basaltic glasses: implications for S speciation and S content as function
23 909 of oxygen fugacity. *Geochim Cosmochim Acta* 74:5926–5938.
24 910 <https://doi.org/10.1016/j.gca.2010.07.022>
25 911 Kamata H (1998) Quaternary volcanic front at the junction of the South-west Japan Arc
26 912 and the Ryukyu Arc. *J Asian Earth Sci* 16:67–75. [https://doi.org/10.1016/S0743-](https://doi.org/10.1016/S0743-9547(97)00044-5)
27 913 [9547\(97\)00044-5](https://doi.org/10.1016/S0743-9547(97)00044-5)
28 914 Kelley KA, Cottrell E (2009) Water and the oxidation state of subduction zone magmas.
29 915 *Science* 325:605–607. <https://doi.org/10.1126/science.1174156>
30 916 Kilinc A, Carmichael ISE, Rivers ML, Sack RO (1983) The ferric-ferrous ratio of natural
31 917 silicate liquids equilibrated in air. *Contrib to Mineral Petrol* 83:136–140.
32 918 <https://doi.org/10.1007/BF00373086>
33 919 Komazawa M (1995) Gravimetric analysis of Aso volcano and its interpretation. *J Geod*
34 920 *Soc Japan* 41:17–45. <https://doi.org/10.11366/sokuchi1954.41.17>
35 921 Kuno H (1960) High-alumina basalt. *J Petrol* 1:121–145.
36 922 <https://doi.org/10.1093/petrology/1.1.121>
37 923 Lange RA, Frey HM, Hector J (2009) A thermodynamic model for the plagioclase-liquid
38 924 hygrometer/thermometer. *Am Mineral* 94:494–506.
39 925 <https://doi.org/10.2138/am.2009.3011>
40 926 Le Voyer M, Cottrell E, Kelley KA, Brounce M, Hauri EH (2015) The effect of primary
41 927 versus secondary processes on the volatile content of MORB glasses: an example
42 928 from the equatorial Mid-Atlantic Ridge (5°N–3°S). *J Geophys Res Solid Earth*
43 929 120:125–144. <https://doi.org/10.1002/2014JB011160>
44 930 Le Voyer M, Kelley KA, Cottrell E, Hauri EH (2017) Heterogeneity in mantle carbon
45 931 content from CO₂-undersaturated basalts. *Nat Commun* 8:1–8.
46 932 <https://doi.org/10.1038/ncomms14062>
47 933 Le Voyer M, Rose-Koga EF, Shimizu N, Grove TL, Schiano P (2010) Two contrasting
48 934 H₂O-rich components in primary melt inclusions from Mount Shasta. *J Petrol*
49 935 51:1571–1595. <https://doi.org/10.1093/petrology/egq030>
50 936 Li C, Ripley EM (2009) Sulfur contents at sulfide-liquid or anhydrite saturation in silicate

1
2 937 melts: empirical equations and example applications. *Econ Geol* 104:405–412.
3 938 <https://doi.org/10.2113/gsecongeo.104.3.405>
4
5 939 Lloyd AS, Plank T, Ruprecht P, Hauri EH, Rose W (2013) Volatile loss from melt
6 940 inclusions in pyroclasts of differing sizes. *Contrib to Mineral Petrol* 165:129–153.
7 941 <https://doi.org/10.1007/s00410-012-0800-2>
8 942 Médard E, Grove TL (2008) The effect of H₂O on the olivine liquidus of basaltic melts:
9 943 Experiments and thermodynamic models. *Contrib to Mineral Petrol* 155:417–432.
10 944 <https://doi.org/10.1007/s00410-007-0250-4>
11 945 Melekhova E, Blundy J, Martin R, Arculus R, Pichavant M (2017) Petrological and
12 946 experimental evidence for differentiation of water-rich magmas beneath St. Kitts,
13 947 Lesser Antilles. *Contrib to Mineral Petrol* 172:98. [https://doi.org/10.1007/s00410-](https://doi.org/10.1007/s00410-017-1416-3)
14 948 [017-1416-3](https://doi.org/10.1007/s00410-017-1416-3)
15
16 949 Métrich N, Wallace PJ (2008) Volatile abundances in basaltic magmas and their
17 950 degassing paths tracked by melt inclusions. *Rev Mineral Geochemistry* 69:363–402.
18 951 <https://doi.org/10.2138/rmg.2008.69.10>
19
20 952 Miyabuchi Y (2009) A 90,000-year tephrostratigraphic framework of Aso volcano, Japan.
21 953 *Sediment Geol* 220:169–189. <https://doi.org/10.1016/j.sedgeo.2009.04.018>
22 954 Miyabuchi Y (2010) Eruption age of Komezuka at Aso volcano, Japan. *Bull Volcanol*
23 955 *Soc Japan* 55:219–225 (in Japanese with English abstract)
24 956 Miyabuchi Y (2017) Eruption history of Janoo volcano in the Northwestern part of Aso
25 957 caldera, Japan. *Bull Volcanol Soc Japan* 62:1–12 (in Japanese with English abstract)
26 958 Miyabuchi Y, Watanabe K (1997) Eruption ages of Holocene tephras from Aso volcano,
27 959 southwestern Japan, inferred from ¹⁴C ages of buried andisols. *Bull Volcanol Soc*
28 960 *Japan* 42:403–408 (in Japanese with English abstract)
29 961 Miyoshi M, Fukuoka T, Sano T, Hasenaka T (2008a) Subduction influence of Philippine
30 962 Sea plate on the mantle beneath northern Kyushu, SW Japan: an examination of
31 963 boron contents in basaltic rocks. *J Volcanol Geotherm Res* 171:73–87.
32 964 <https://doi.org/10.1016/j.jvolgeores.2007.10.016>
33 965 Miyoshi M, Hasenaka T, Sano T (2005) Genetic relationship of the compositionally
34 966 diverse magmas from Aso post-caldera volcanism. *Bull Volcanol Soc Japan* 50:269–
35 967 283 (in Japanese with English abstract)
36 968 Miyoshi M, Shimono M, Hasenaka T, Sano T, Fukuoka T (2008b) Determination of
37 969 boron and other elements in volcanic rocks by prompt gamma-ray analysis: an
38 970 application to magma genesis in Kyushu island, SW-Japan. *J Radioanal Nucl Chem*
39 971 278:343–347. <https://doi.org/10.1007/s10967-008-9607-z>
40 972 Moore G, Vennemann T, Carmichael ISE (1998) An empirical model for the solubility
41 973 of H₂O in magmas to 3 kilobars. *Am Mineral* 83:36–42
42 974 Moore LR, Gazel E, Tuohy R, Lloyd AS, Esposito R, Steele-MacInnis M, Hauri EH,
43 975 Wallace PJ, Plank T, Bodnar RJ (2015) Bubbles matter: an assessment of the
44 976 contribution of vapor bubbles to melt inclusion volatile budgets. *Am Mineral*
45 977 100:806–823. <https://doi.org/10.2138/am-2015-5036>
46 978 Mori T, Shinohara H, Kazahaya K, Hirabayashi J, Matsushima T, Mori T, Ohwada M,
47 979 Odai M, Iino H, Miyashita M (2013) Time-averaged SO₂ fluxes of subduction-zone
48 980 volcanoes: example of a 32-year exhaustive survey for Japanese volcanoes. *J*
49 981 *Geophys Res Atmos* 118:8662–8674. <https://doi.org/10.1002/jgrd.50591>
50 982 Mori Y, Mashima H (2005) X-ray fluorescence analysis of major and trace elements in
51 983 silicate rocks using 1:5 dilution glass beads. *Bull Kitakyushu Museum Nat Hist Hum*

1
2 984 Hist Ser A 3:1–12
3
4 985 Nakada S, Kamata H (1991) Temporal change in chemistry of magma source under
5 986 Central Kyushu, Southwest Japan: progressive contamination of mantle wedge. *Bull*
6 987 *Volcanol* 53:182–194
7 988 Narvaez DF, Rose-Koga EF, Samaniego P, Koga KT, Hidalgo S (2018) Constraining
8 989 magma sources using primitive olivine-hosted melt inclusions from Puñalica and
9 990 Sangay volcanoes (Ecuador). *Contrib to Mineral Petrol* 173:80.
10 991 <https://doi.org/10.1007/s00410-018-1508-8>
11 992 Neave DA, Hartley ME, MacLennan J, Edmonds M, Thordarson T (2017) Volatile and
12 993 light lithophile elements in high-anorthite plagioclase-hosted melt inclusions from
13 994 Iceland. *Geochim Cosmochim Acta* 205:100–118.
14 995 <https://doi.org/10.1016/j.gca.2017.02.009>
15 996 Ohkura T, Utsugi M, Yokoo A, Yoshikawa S, Inoue H, Kagiya T (2015) Eruptive
16 997 activities of Aso volcano, 2014–2015. *Japan Geosci Union Meet 2015 SVC45-04*
17 998 Ohkura T, Utsugi M, Yokoo A, Yoshikawa S, Inoue H, Kagiya T, Yamamoto M,
18 999 Oikawa J (2017) Eruptive activities of Aso Volcano, 2014–2016. *Program Abstr*
19 1000 *Volcanol Soc Japan 2017 fall Meet A3-20* (in Japanese)
20 1001 Ono K, Watanabe K (1985) Geological map of Aso volcano, 1:50,000. Geological Survey
21 1002 of Japan (in Japanese with English abstract)
22 1003 Pioli L, Azzopardi BJ, Cashman K V. (2009) Controls on the explosivity of scoria cone
23 1004 eruptions: magma segregation at conduit junctions. *J Volcanol Geotherm Res*
24 1005 186:407–415. <https://doi.org/10.1016/j.jvolgeores.2009.07.014>
25 1006 Portnyagin M, Almeev R, Matveev S, Holtz F (2008) Experimental evidence for rapid
26 1007 water exchange between melt inclusions in olivine and host magma. *Earth Planet Sci*
27 1008 *Lett* 272:541–552. <https://doi.org/10.1016/j.epsl.2008.05.020>
28 1009 Putirka KD (2008) Thermometers and barometers for volcanic systems. *Rev Mineral*
29 1010 *Geochemistry* 69:61–120. <https://doi.org/10.2138/rmg.2008.69.3>
30 1011 Roberge J, Delgado-Granados H, Wallace PJ (2009) Mafic magma recharge supplies high
31 1012 CO₂ and SO₂ gas fluxes from Popocatepetl volcano, Mexico. *Geology* 37:107–110.
32 1013 <https://doi.org/10.1130/G25242A.1>
33 1014 Roggensack K (2001) Unraveling the 1974 eruption of Fuego volcano (Guatemala) with
34 1015 small crystals and their young melt inclusions. *Geology* 29:911–914.
35 1016 [https://doi.org/10.1130/0091-7613\(2001\)029<0911:UTEOFV>2.0.CO;2](https://doi.org/10.1130/0091-7613(2001)029<0911:UTEOFV>2.0.CO;2)
36 1017 Roggensack K, Hervig RL, McKnight SB, Williams SN (1997) Explosive basaltic
37 1018 volcanism from Cerro Negro volcano: influence of volatiles on eruptive style.
38 1019 *Science* 277:1639–1642. <https://doi.org/10.1126/science.277.5332.1639>
39 1020 Rose-Koga EF, Koga KT, Devidal JL, Shimizu N, Voyer M Le, Dalou C, Döbeli M
40 1021 (2020) In-situ measurements of magmatic volatile elements, F, S, and Cl, by electron
41 1022 microprobe, secondary ion mass spectrometry, and heavy ion elastic recoil detection
42 1023 analysis. *Am Mineral* 105:616–626. <https://doi.org/10.2138/am-2020-7221>
43 1024 Rose-Koga EF, Koga KT, Hamada M, HéLouis T, Whitehouse MJ, Shimizu N (2014)
44 1025 Volatile (F and Cl) concentrations in Iwate olivine-hosted melt inclusions indicating
45 1026 low-temperature subduction. *Earth, Planets Sp* 66:81. [https://doi.org/10.1186/1880-](https://doi.org/10.1186/1880-5981-66-81)
46 1027 [5981-66-81](https://doi.org/10.1186/1880-5981-66-81)
47 1028 Rose-Koga EF, Koga KT, Schiano P, Le Voyer M, Shimizu N, Whitehouse MJ,
48 1029 Clocchiatti R (2012) Mantle source heterogeneity for South Tyrrhenian magmas
49 1030 revealed by Pb isotopes and halogen contents of olivine-hosted melt inclusions.

- 1
2 1031 Chem Geol 334:266–279. <https://doi.org/10.1016/j.chemgeo.2012.10.033>
3 1032 Rowe MC, Kent AJR, Nielsen RL (2007) Determination of sulfur speciation and
4 1033 oxidation state of olivine hosted melt inclusions. *Chem Geol* 236:303–322.
5 1034 <https://doi.org/10.1016/j.chemgeo.2006.10.007>
6 1035 Saal AE, Hauri EH, Langmuir CH, Perfit MR (2002) Vapour undersaturation in primitive
7 1036 mid-ocean-ridge basalt and the volatile content of earth's upper mantle. *Nature*
8 1037 419:451–455. <https://doi.org/10.1038/nature01073>
9 1038 Saito G, Ishizuka O, Ishizuka Y, Hoshizumi H, Miyagi I (2018) Petrological
10 1039 characteristics and volatile content of magma of the 1979, 1989, and 2014 eruptions
11 1040 of Nakadake, Aso volcano, Japan. *Earth, Planets Sp* 70:197.
12 1041 <https://doi.org/10.1186/s40623-018-0970-x>
13 1042 Sakuyama M (1979) Evidence of magma mixing: petrological study of Shirouma-Oike
14 1043 calc-alkaline andesite volcano, Japan. *J Volcanol Geotherm Res* 5:179–208.
15 1044 [https://doi.org/10.1016/0377-0273\(79\)90040-4](https://doi.org/10.1016/0377-0273(79)90040-4)
16 1045 Sakuyama T, Nakai S, Yoshikawa M, Shibata T, Ozawa K (2014) Progressive interaction
17 1046 between dry and wet mantle during high-temperature diapiric upwelling: constraints
18 1047 from cenozoic Kita-Matsuura intraplate basalt province, Northwestern Kyushu,
19 1048 Japan. *J Petrol* 55:1083–1128. <https://doi.org/10.1093/petrology/egu020>
20 1049 Scaillet B, Pichavant M (2003) Experimental constraints on volatile abundances in arc
21 1050 magmas and their implications for degassing processes. *Geol Soc London, Spec Publ*
22 1051 *Spec Publ* 213:23–52. <https://doi.org/10.1144/GSL.SP.2003.213.01.03>
23 1052 Shibata T, Yoshikawa M, Itoh J, Ujike O, Miyoshi M, Takemura K (2014) Along-arc
24 1053 geochemical variations in Quaternary magmas of northern Kyushu Island, Japan.
25 1054 *Geol Soc Spec Publ* 385:15–29. <https://doi.org/10.1144/SP385.13>
26 1055 Shimizu K, Saal AE, Hauri EH, Perfit MR, Hékinian R (2019) Evaluating the roles of
27 1056 melt-rock interaction and partial degassing on the CO₂/Ba ratios of MORB:
28 1057 implications for the CO₂ budget in the Earth's depleted upper mantle. *Geochim*
29 1058 *Cosmochim Acta* 260:29–48. <https://doi.org/10.1016/j.gca.2019.06.013>
30 1059 Shimizu K, Ushikubo T, Hamada M, Itoh S, Higashi Y, Takahashi E, Ito M (2017) H₂O,
31 1060 CO₂, F, S, Cl, and P₂O₅ analyses of silicate glasses using SIMS: report of volatile
32 1061 standard glasses. *Geochem J* 51:299–313. <https://doi.org/10.2343/geochemj.2.0470>
33 1062 Shinohara H (2008) Excess degassing from volcanoes and its role on eruptive and
34 1063 intrusive activity. *Rev Geophys* 46:RG4005.
35 1064 <https://doi.org/10.1029/2007RG000244>
36 1065 Shinohara H (2013) Volatile flux from subduction zone volcanoes: insights from a
37 1066 detailed evaluation of the fluxes from volcanoes in Japan. *J Volcanol Geotherm Res*
38 1067 268:46–63. <https://doi.org/10.1016/j.jvolgeores.2013.10.007>
39 1068 Shinohara H, Kazahaya K, Saito G, Fukui K, Odai M (2003) Variation of CO₂/SO₂ ratio
40 1069 in volcanic plumes of Miyakejima: stable degassing deduced from heliborne
41 1070 measurements. *Geophys Res Lett* 30. <https://doi.org/10.1029/2002gl016105>
42 1071 Shinohara H, Yokoo A, Kazahaya R (2018) Variation of volcanic gas composition during
43 1072 the eruptive period in 2014–2015 at Nakadake crater, Aso volcano, Japan. *Earth,*
44 1073 *Planets Sp* 70:151. <https://doi.org/10.1186/s40623-018-0919-0>
45 1074 Sisson TW, Grove TL (1993) Temperatures and H₂O contents of low-MgO high-alumina
46 1075 basalts. *Contrib to Mineral Petrol* 113:167–184
47 1076 Sisson TW, Layne GD (1993) H₂O in basalt and basaltic andesite glass inclusions from
48 1077 four subduction-related volcanoes. *Earth Planet Sci Lett* 117:619–635.

- 1
2 1078 [https://doi.org/10.1016/0012-821X\(93\)90107-K](https://doi.org/10.1016/0012-821X(93)90107-K)
3
4 1079 Spilliaert N, Métrich N, Allard P (2006) S-Cl-F degassing pattern of water-rich alkali
5 1080 basalt: modelling and relationship with eruption styles on Mount Etna volcano. *Earth*
6 1081 *Planet Sci Lett* 248:772–786. <https://doi.org/10.1016/j.epsl.2006.06.031>
7 1082 Straub SM, Layne GD (2003) The systematics of chlorine, fluorine, and water in Izu arc
8 1083 front volcanic rocks: implications for volatile recycling in subduction zones.
9 1084 *Geochim Cosmochim Acta* 67:4179–4203. [https://doi.org/10.1016/S0016-](https://doi.org/10.1016/S0016-7037(03)00307-7)
10 1085 [7037\(03\)00307-7](https://doi.org/10.1016/S0016-7037(03)00307-7)
11 1086 Sudo Y, Kong LSL (2001) Three-dimensional seismic velocity structure beneath Aso
12 1087 volcano, Kyushu, Japan. *Bull Volcanol* 63:326–344.
13 1088 <https://doi.org/10.1007/s004450100145>
14 1089 Sudo Y, Tsutsui T, Nakaboh M, Yoshikawa M, Yoshikawa S, Inoue H (2006) Ground
15 1090 deformation and magma reservoir at Aso volcano: location of deflation source
16 1091 derived from long-term geodetic surveys. *Bull Volcanol Soc Japan* 51:291-309 (in
17 1092 Japanese with English abstract)
18 1093 Sugawara T (2000) Empirical relationships between temperature, pressure, and MgO
19 1094 content in olivine and pyroxene saturated liquid. *J Geophys Res Solid Earth*
20 1095 105:8457–8472. <https://doi.org/10.1029/2000jb900010>
21 1096 Takada H (1989) Preliminary report on tephra from Aso central cones. *J Kumamoto*
22 1097 *Geosci Assoc* 90:8-11 (in Japanese)
23 1098 Teplow W, Marsh B, Hulen J, Spielman P, Kaleikini M, Fitch D, Rickard W (2009)
24 1099 Dacite melt at the Puna Geothermal Venture wellfield, Big Island of Hawaii.
25 1100 *Geotherm Resour Counc Trans* 33:989–994
26 1101 Toplis MJ (2005) The thermodynamics of iron and magnesium partitioning between
27 1102 olivine and liquid: criteria for assessing and predicting equilibrium in natural and
28 1103 experimental systems. *Contrib to Mineral Petrol* 149:22–39.
29 1104 <https://doi.org/10.1007/s00410-004-0629-4>
30 1105 Tsuchiyama A (1985) Dissolution kinetics of plagioclase in the melt of the system
31 1106 diopside-albite-anorthite, and origin of dusty plagioclase in andesites. *Contrib to*
32 1107 *Mineral Petrol* 89:1–16
33 1108 Tsutsui T, Sudo Y (2004) Seismic reflectors beneath the central cones of Aso Volcano,
34 1109 Kyushu, Japan. *J Volcanol Geotherm Res* 131:33–58.
35 1110 [https://doi.org/10.1016/S0377-0273\(03\)00315-9](https://doi.org/10.1016/S0377-0273(03)00315-9)
36 1111 Tucker JM, Hauri EH, Pietruszka AJ, Garcia MO, Marske JP, Trusdell FA (2019) A high
37 1112 carbon content of the Hawaiian mantle from olivine-hosted melt inclusions.
38 1113 *Geochim Cosmochim Acta* 254:156–172. <https://doi.org/10.1016/j.gca.2019.04.001>
39 1114 Van den Bleeken G, Koga KT (2015) Experimentally determined distribution of fluorine
40 1115 and chlorine upon hydrous slab melting, and implications for F-Cl cycling through
41 1116 subduction zones. *Geochim Cosmochim Acta* 171:353–373.
42 1117 <https://doi.org/10.1016/j.gca.2015.09.030>
43 1118 Wallace PJ (2005) Volatiles in subduction zone magmas: concentrations and fluxes based
44 1119 on melt inclusion and volcanic gas data. *J Volcanol Geotherm Res* 140:217–240.
45 1120 <https://doi.org/10.1016/j.jvolgeores.2004.07.023>
46 1121 Wallace PJ (2001) Volcanic SO₂ emissions and the abundance and distribution of
47 1122 exsolved gas in magma bodies. *J Volcanol Geotherm Res* 108:85–106.
48 1123 [https://doi.org/10.1016/S0377-0273\(00\)00279-1](https://doi.org/10.1016/S0377-0273(00)00279-1)
49 1124 Wallace PJ, Carmichael ISE (1994) S speciation in submarine basaltic glasses as
50
51
52
53
54
55
56
57
58
59
60
61
62
63
64
65

- 1
2 1125 determined by measurements of $SK\alpha$ X-ray wavelength shifts. *Am Mineral* 79:161–
3 1126 167
4
5 1127 Wallace PJ, Edmonds M (2011) The sulfur budget in magmas: evidence from melt
6 1128 inclusions, submarine glasses, and volcanic gas emissions. *Rev Mineral*
7 1129 *Geochemistry* 73:215–246. <https://doi.org/10.2138/rmg.2011.73.8>
8
9 1130 Wallace PJ, Kamenetsky VS, Cervantes P (2015) Melt inclusion CO₂ contents, pressures
10 1131 of olivine crystallization, and the problem of shrinkage bubbles. *Am Mineral*
11 1132 100:787–794. <https://doi.org/10.2138/am-2015-5029>
12 1133 Wanless VD, Behn MD, Shaw AM, Plank T (2014) Variations in melting dynamics and
13 1134 mantle compositions along the Eastern Volcanic Zone of the Gakkel Ridge: insights
14 1135 from olivine-hosted melt inclusions. *Contrib to Mineral Petrol* 167:1005.
15 1136 <https://doi.org/10.1007/s00410-014-1005-7>
16 1137 Wanless VD, Shaw AM (2012) Lower crustal crystallization and melt evolution at mid-
17 1138 ocean ridges. *Nat Geosci* 5:651–655. <https://doi.org/10.1038/ngeo1552>
18 1139 Wanless VD, Shaw AM, Behn MD, Soule SA, Escartín J, Hamelin C (2015) Magmatic
19 1140 plumbing at Lucky Strike volcano based on olivine-hosted melt inclusion
20 1141 compositions. *Geochemistry Geophys Geosystems* 16:126–147.
21 1142 <https://doi.org/10.1002/2014GC005517>
22 1143 Watanabe K (2001) History and activity of Aso volcano (Japanese title “Aso kasan no
23 1144 oitachi”). Ichinomiya-cho, Japan (in Japanese)
24 1145 Watanabe K (1991) Volcanic activity of Nakadake, Aso volcano. *J Kumamoto Geosci*
25 1146 *Assoc* 98:2-13 (in Japanese)
26 1147 Watanabe K, Itaya T, Ono K, takada (1989) K-Ar ages of dike rocks in the Southwestern
27 1148 region of Aso caldera, Kyushu, Japan. *Bull Volcanol Soc Japan* 34:189-195 (in
28 1149 Japanese with English abstract)
29 1150 Webster JD, Mandeville CW, Goldoff B, Coombs ML, Tappen C (2010) Augustine
30 1151 Volcano—The influence of volatile components in magmas erupted A.D. 2006
31 1152 to 2,100 years before present. In: Power JA, Coombs ML, Freymueller JT (eds) *The*
32 1153 *2006 eruption of Augustine Volcano, Alaska: U.S. Geological Survey Professional*
33 1154 *Paper* 1769
34 1155 Witham F, Blundy J, Kohn SC, Lesne P, Dixon J, Churakov S V., Botcharnikov R (2012)
35 1156 SolEx: a model for mixed COHSCI-volatile solubilities and exsolved gas
36 1157 compositions in basalt. *Comput Geosci* 45:87–97.
37 1158 <https://doi.org/10.1016/j.cageo.2011.09.021>
38 1159 Yamamoto M, Kawakatsu H, Kaneshima S, Mori T, Tsutsui T, Sudo Y, Morita Y (1999)
39 1160 Detection of a crack-like conduit beneath the active crater at Aso volcano. *Geophys*
40 1161 *Res Lett* 26:3677–3680
41 1162 Yasuda A (2014) A new technique using FT-IR micro-reflectance spectroscopy for
42 1163 measurement of water concentrations in melt inclusions. *Earth, Planets Sp* 66:34.
43 1164 <https://doi.org/10.1186/1880-5981-66-34>
44 1165 Yasuda A, Nakada S, Fujii T (2001) Sulfur abundance and redox state of melt inclusions
45 1166 from Miyake-jima 2000 eruption products. *Bull Volcanol Soc Japan* 46:165-173 (in
46 1167 Japanese with English abstract)
47 1168 Yokoo A, Miyabuchi Y (2015) Eruption at the Nakadake 1st crater of Aso volcano started
48 1169 in November 2014. *Bull Volcanol Soc Japan* 60:275-278 (in Japanese)
49 1170
50
51
52
53
54
55
56
57
58
59
60
61
62
63
64
65

1
2
3 **1171 Figure caption**
4

5 **1173 Fig. 1** Locations of volcanic cones and sampling sites of the study. Main map shows
6 **1174** topography of Aso volcano with a 50 m contour interval. Volcanic cones are indicated by
7 **1175** solid triangles. Sampling sites are indicated by solid circles. Location of Aso volcano is
8 **1176** indicated in an inset in the top left corner, showing Japanese islands with plate boundaries:
9 **1177** solid line, active subduction plate boundary, and dashed line, diffused plate boundary.
10 **1178** Stratigraphic log shows corresponding eruption stages and nature of volcanic deposits in
11 **1179** A9418 site (Miyabuchi and Watanabe 1997). Kishimadake scoria (KSS) and Ojodake
12 **1180** scoria (OJSL and OJSU) were collected at the indicated units. Kamikomezuka scoria
13 **1181** (KKO) and Nakadake scoria (NKD14) were collected at the location indicated by field
14 **1182** symbols. KKO in parenthesis indicates the relative eruption age (top of N4 stage).
15 **1183**

16 **1184 Fig. 2** Microscope photographs (a-d) and backscatter electron images (e, f) of
17 **1185** representative phenocrysts and textures from Holocene basaltic tephra products in Aso
18 **1186** central cones. (a) Plagioclase (Pl) phenocrysts with honeycomb texture in KKO, under
19 **1187** cross-polarized light. Clinopyroxene (Cpx) and olivine (Ol) phenocrysts also present. (b)
20 **1188** An orthopyroxene (Opx) phenocryst with reaction rim consisted of clinopyroxene and
21 **1189** olivine in KSS, under cross-polarized light. (c) An aggregate of phenocryst consisted of
22 **1190** plagioclase, clinopyroxene and olivine in KSS, under cross-polarized light. (d) A
23 **1191** microlite-rich part of groundmass in KSS with abundant crystals, under plain-polarized
24 **1192** light. (e) High-Fo olivine phenocryst and its melt inclusions observed in KSS. (f) A
25 **1193** texture of plagioclase phenocryst with (optically) dusty zone, in the middle part of the
26 **1194** crystal, observed in NKD14.
27 **1195**

28 **1196 Fig. 3** Major element and volatile concentrations in melt inclusions from Holocene
29 **1197** basaltic tephra products in Aso central cones. Melt inclusion data from minerals other
30 **1198** than olivine are shown as open symbols. The melt inclusion data are compared to bulk
31 **1199** tephra and average groundmass glass compositions, solid circles, and solid squares,
32 **1200** respectively. The distribution of Fo content in all olivine cores is shown as a relative
33 **1201** density function on the left side of (a). The dashed line in Figure 3a and 3b indicates the
34 **1202** value Fo72. Bulk lava compositions of late-Holocene volcanic products, reported
35 **1203** previously, are also shown as solid grey circles in (c) (Miyoshi *et al.* 2005; Miyabuchi
36 **1204** 2010, 2017; Saito *et al.* 2018). All oxide concentrations were normalized to 100 wt. %,
37 **1205** excluding volatile element abundance.
38 **1206**

39 **1207 Fig. 4** Ratios of volatiles/K₂O vs. K₂O in melt inclusions and groundmass glasses (the
40 **1208** same symbols as Fig. 3). All volatile elements showed a systematic decrease (a,
41 **1209** H₂O/K₂O; b, S/K₂O; c, Cl/K₂O) with respect to increasing K₂O. High volatile/K₂O
42 **1210** corresponds to high volatile concentration as well as low K₂O.
43 **1211**

1
2 1212 **Fig. 5** (a) Variations in S and total FeO concentrations of melt inclusions and groundmass
3 1213 glasses. Symbols are the same as Fig. 3. Melt inclusions hosted in olivine show abrupt
4 1214 decrease in S content, and the change lacks correlation with FeO. (b) Measured S
5 1215 concentration in olivine-hosted melt inclusions as a function of sulfur concentration at
6 1216 sulfide saturation (SCSS). In this figure, the samples at the saturation can be seen on the
7 1217 solid grey line (1:1 line). The dashed line shows the SCSS corrected for abundance of S²⁻,
8 1218 which was 0.85, the maximum value. All data plots below the corrected SCSS. SCSS is
9 1219 calculated according to Fortin *et al.* (2015) using the trapping temperature (T_{trap}) of the
10 1220 melt inclusion (Table S1) at 0.05 GPa (for NKD14) and 0.1 GPa (for KKO, OJSU, OJSL,
11 1221 and KSS) based on estimated volatile saturation pressure of the pre-eruptive magma
12 1222 reservoir. For melt inclusions without measured H₂O concentration, we attributed average
13 1223 H₂O concentrations (by SIMS) of NKD14 and KSS.
14 1224

15 1225 **Fig. 6** Variations in Cl and F concentrations of melt inclusions (KSS and NKD14) plotted
16 1226 in decadic log scale. The KSS and NKD14 data are compared with the volatile rich mafic
17 1227 primitive magma, represented by a large blue diamond. The two areas are indicated to
18 1228 show the Cl and F concentrations in primitive arc basalt and MORB, which were
19 1229 measured in olivine-hosted melt inclusions (taken from Van den Bleeken and Koga 2015).
20 1230 MORB melt inclusions were plotted as solid light-grey circles (Saal *et al.* 2002; Wanless
21 1231 and Shaw 2012; Wanless *et al.* 2014, 2015; Le Voyer *et al.* 2017; Shimizu *et al.* 2019)
22 1232 including Cl-rich data of assimilated MORB samples by seawater derived component.
23 1233 Melt inclusions from Iwate volcanoes, one of low F concentration arc lava from Japan
24 1234 arc, is shown as an example of a cold subduction zone (red plus sign, Rose-Koga *et al.*
25 1235 2014). The lines show the constant Cl/F values, and the values are indicated above the
26 1236 line.
27 1237

28 1238 **Fig. 7** Pre-eruptive temperatures and water concentrations calculated from the
29 1239 compositions of plagioclase rim and groundmass glass. The squares represent the
30 1240 estimated range of temperature and H₂O concentration. The calculation was based on a
31 1241 combination of a plagioclase-olivine-liquid hygrometer (Lange *et al.* 2009) and olivine-
32 1242 saturated liquid geothermometer (Sugawara 2000; Médard and Grove 2008) according to
33 1243 Sakuyama *et al.* (2014), assuming the crustal conditions (0.1 – 0.5 GPa). Standard
34 1244 deviations (1σ) of the difference in temperature and H₂O concentration between
35 1245 estimation and expectations using this method were 23 °C and 0.6 wt. %, respectively.
36 1246 The dashed lines represent water saturation isobars for groundmass glass composition of
37 1247 KSS calculated according to Moore *et al.* (1998); the corresponding pressures (kbar) and
38 1248 the depths (km) are indicated to the left of the line. The depth in the crust was calculated
39 1249 assuming a density of 2200 kg/m³ for less than 1 km depth and a density of 2700 kg/m³
40 1250 for depth greater than 1 km (Komazawa 1995). The red and blue colors show the range
41 1251 of the magma storage depths: red, C1 from 3 to 10 km depth, and blue, C2 from 1 to 4
42 1252 km depth beneath Nakadake's first crater (Sudo and Kong 2001; Sudo *et al.* 2006; Hata

1
2 1253 *et al.* 2016).

3
4 1254

5 **Fig. 8** Evolution of H₂O/S, CO₂/S, and Cl/S molar ratios of magmatic gases in equilibrium
6 with the primitive basaltic melt plotted against pressure. Horizontal dotted lines indicate
7 measured gas compositions of H₂O/S = 22.5, CO₂/S = 6, and Cl/S = 0.07 (S as total sulfur)
8 with the variation observed with propagated measurement uncertainties shown by shaded
9 regions. The values correspond to high-pressure gas component A reported in previous
10 studies (Shinohara 2013; Shinohara *et al.* 2018). SO₂ and H₂S components were added to
11 calculate the total S. Horizontal colored bars at the top of the panel show pressure ranges
12 corresponding to the C1, C2, and LVL. To evaluate the evolution of the gas composition
13 of the basaltic magma from a great depth, we modelled the equilibrium compositions of
14 gas and magma for a closed system magma ascent using SolEx (Witham *et al.* 2012).
15 Grey field indicates the pressure range of 2.3 – 2.9 kbars, at which conditions the modeled
16 gas compositions (solid and dashed curves) intersect with measured gas ratios. Thus, the
17 observed gas composition potentially originated at these depths. We chose the primitive
18 magma composition (discussed in the text) with values of FMQ+1.4 and 1090 °C based
19 on the individual melt analyses. We tested initial CO₂ contents of 400, 750 and 1000 ppm
20 for the calculation, as the CO₂ concentration was unknown to us. In combination with
21 H₂O/S and Cl/S, the initial CO₂ concentration from 400 to 750 ppm produced the gas
22 composition evolution curves that agree at a similar depth.
23
24
25
26
27
28
29
30

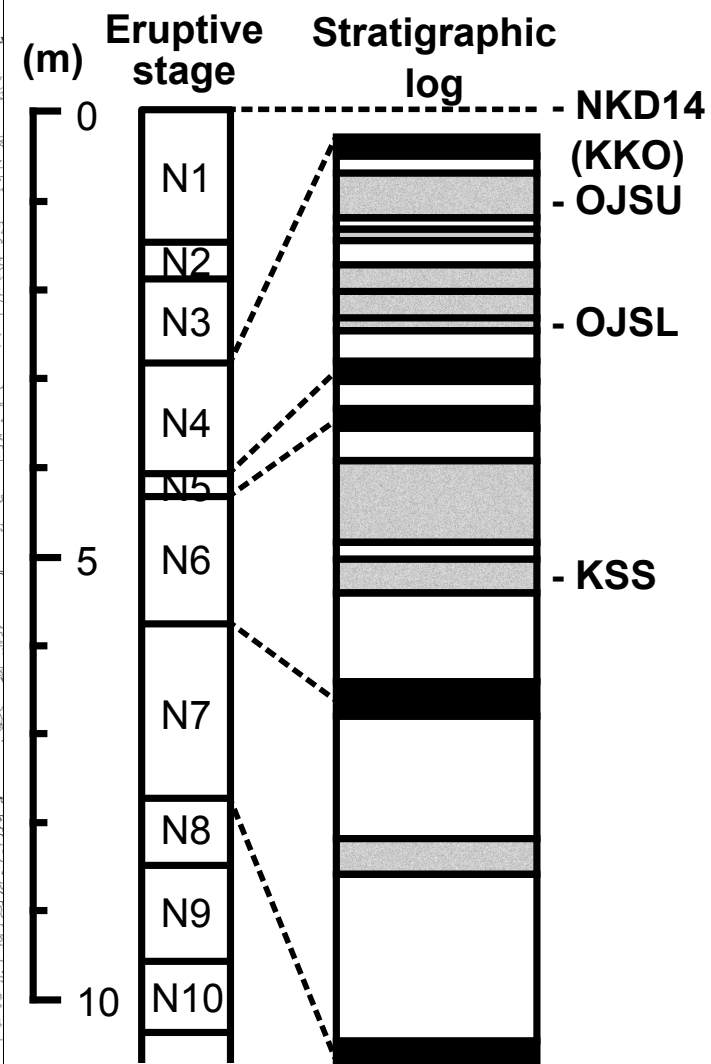
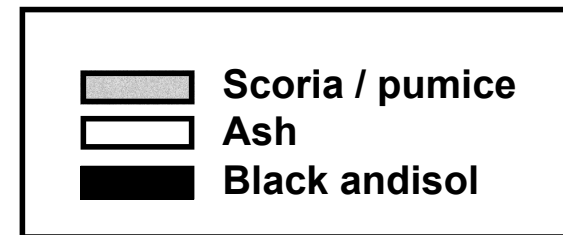
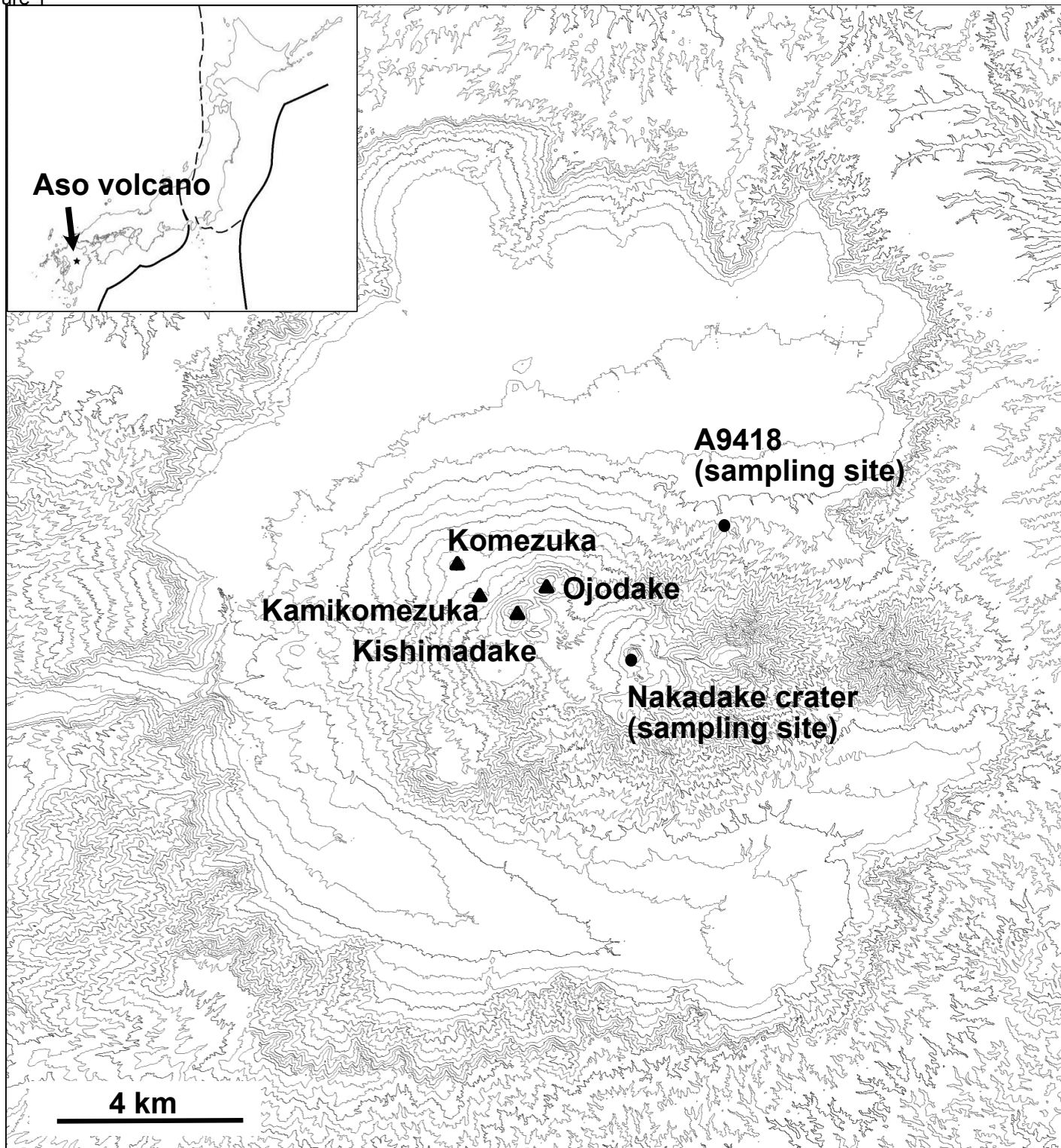
31
32 **Fig. 9** Observed volcanic gas compositions emitted from Aso volcano compared with
33 modelled variation in CO₂/SO₂ and H₂O/CO₂ molar ratios. Observed gas compositions
34 are those during quiescent periods (fumarole and lake gases) and during eruptive periods
35 (Shinohara *et al.* 2018). Some data points were reported as poor quality observations due
36 to atmospheric H₂O, and they are plotted as smaller symbols. Solid curve is a modeled
37 gas composition of closed-system ascent of primitive magma with 750 ppm initial CO₂
38 concentration, which is the same as that used in Fig. 8. The gas compositions on the curve
39 indicate the different depths of gas segregation, and thus, the variation among
40 observations can be attributed to a variation in segregation depths. Dashed curve shows a
41 mixing curve between a CO₂-rich gas in equilibrium with the deep primitive magma at
42 2.6 kbar (crossed circle) and a gas discharged from NKD14 magma at shallow depth
43 (asterisk) representing the gas stored at the shallow reservoir. The shallow gas component
44 was calculated from the difference in volatile concentrations between pre-eruptive melt
45 and groundmass glass.
46
47
48
49
50
51

52
53 **Fig. 10** Schematic summary of the magma and gas evolution in the Aso plumbing system.
54 Magma passage is indicated by the color ranging red-orange-yellow. The gas is white,
55 and the grey zone corresponds to the conductivity anomaly (Hata *et al.* 2016). C1, C2,
56 and LVL (black thick bars) are the zones of magma stagnations determined by
57 geophysical methods (Yamamoto *et al.* 1999; Sudo and Kong 2001; Tsutsui and Sudo
58
59
60

1
2
3
4
5
6
7
8
9
10
11
12
13
14
15
16
17
18
19
20
21
22
23
24
25
26
27
28
29
30
31
32
33
34
35
36
37
38
39
40
41
42
43
44
45
46
47
48
49
50
51
52
53
54
55
56
57
58
59
60
61
62
63
64
65

1294 2004; Sudo *et al.* 2006; Abe *et al.* 2010; Hata *et al.* 2016).

Figure 1



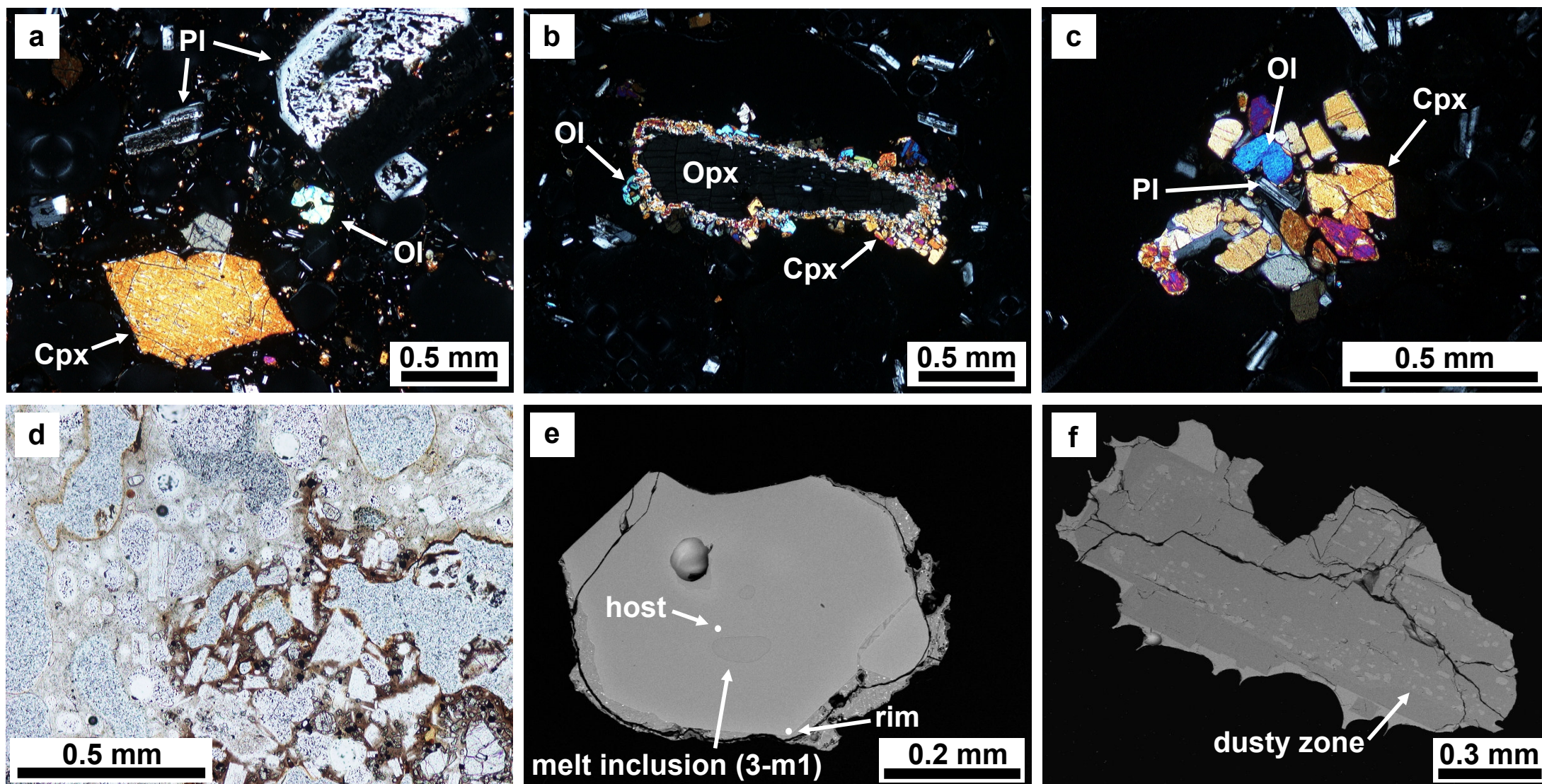
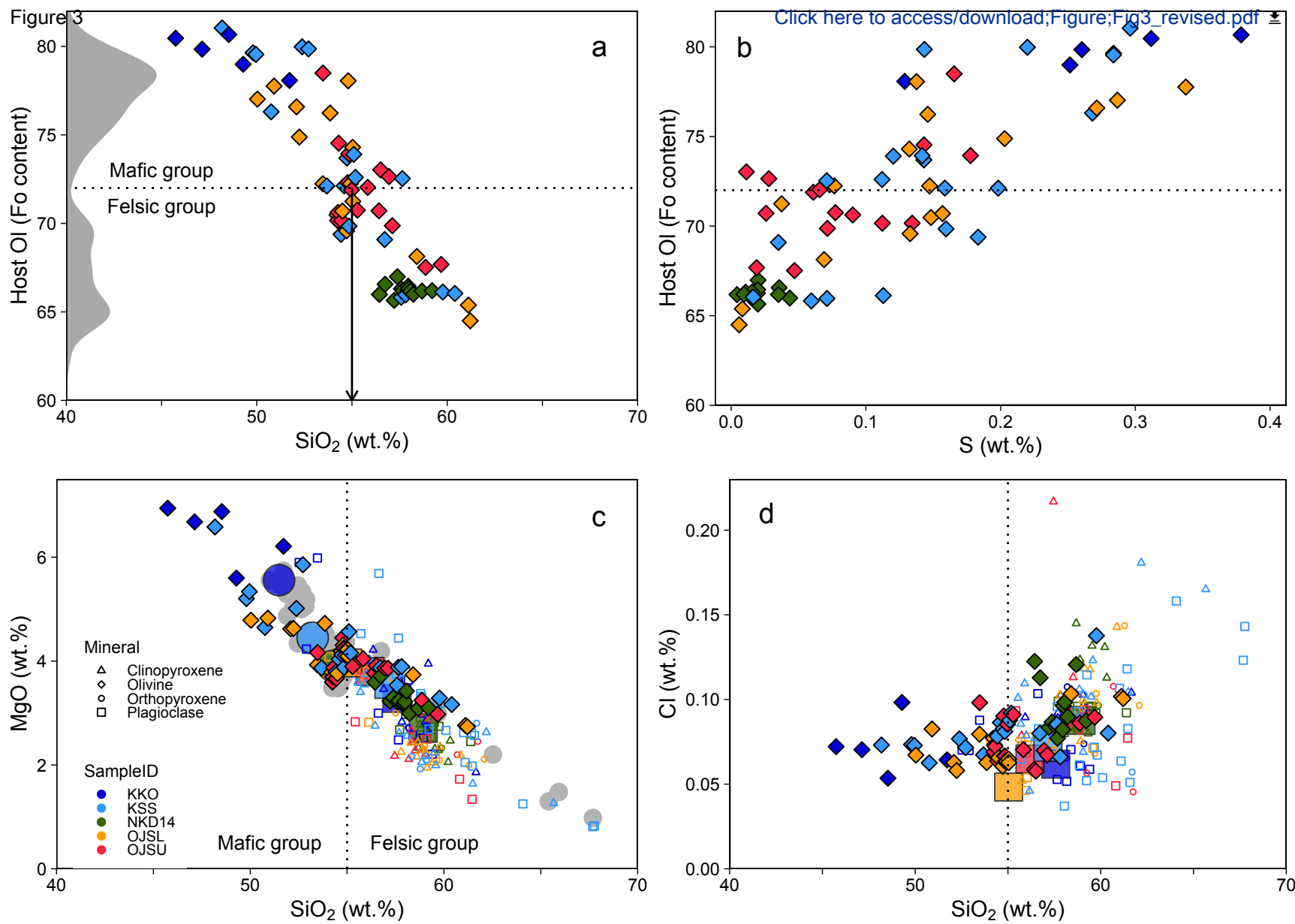


Figure 3



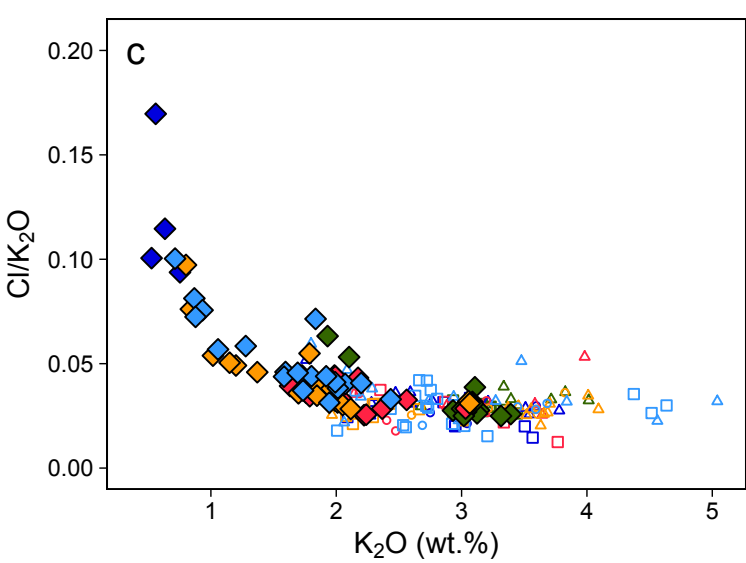
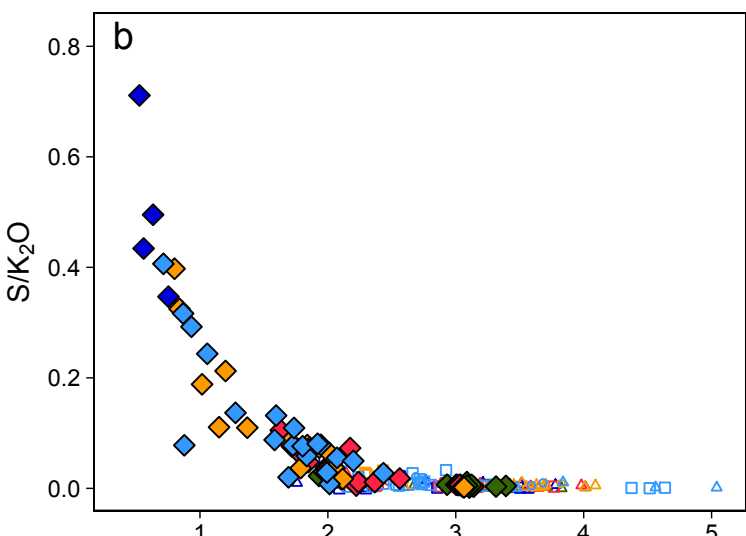
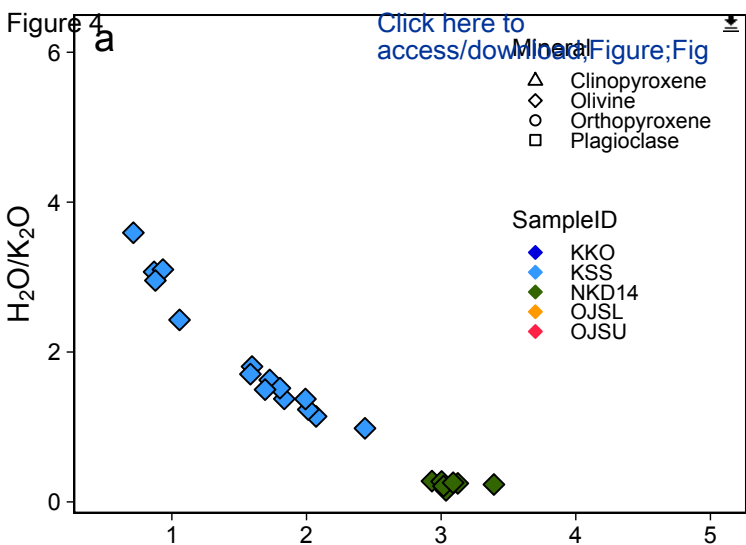


Figure 5

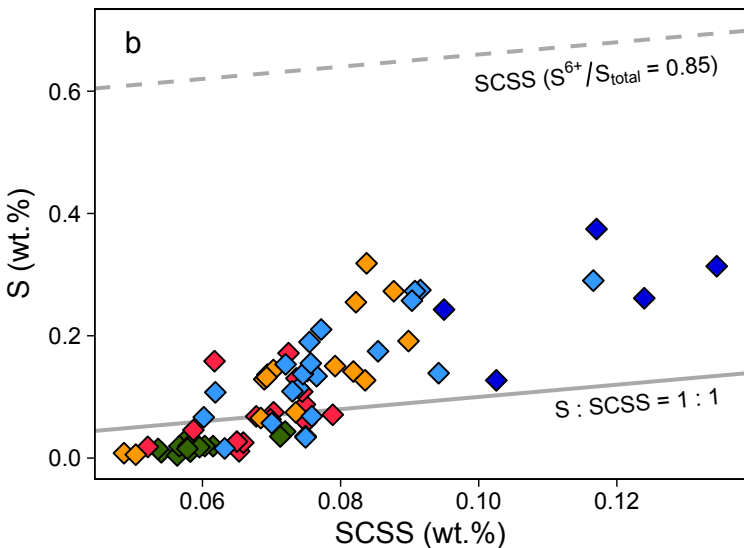
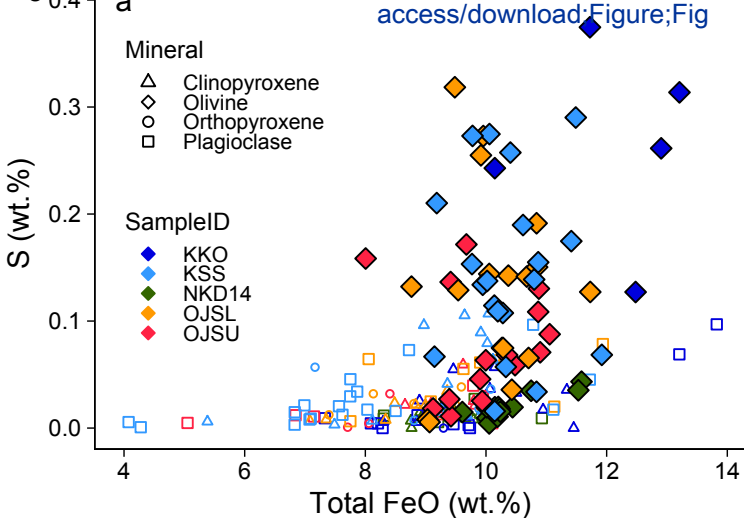


Figure 6

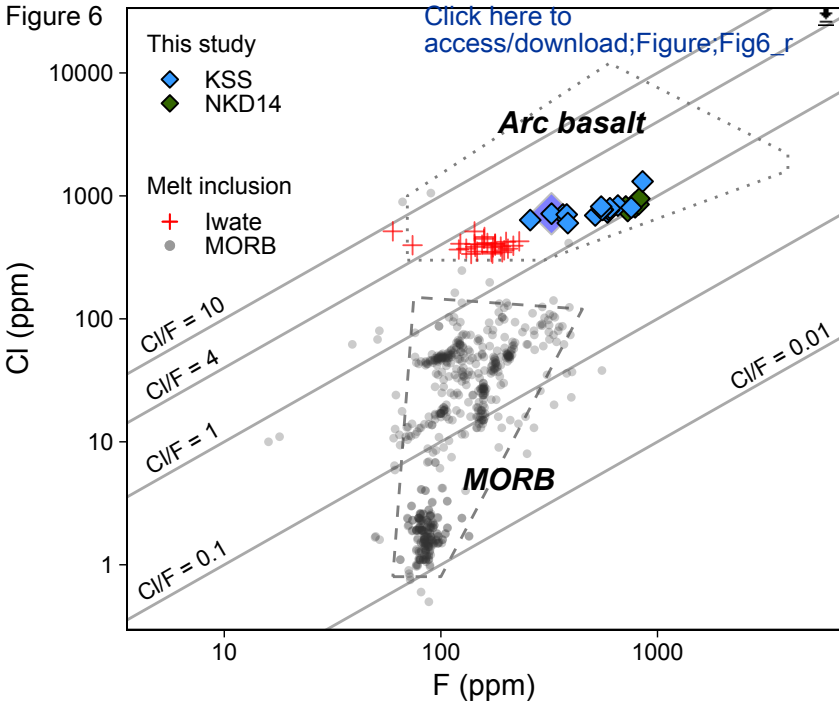


Figure 7

[Click here to access/download;Figure;Fig7_revised.p](#)

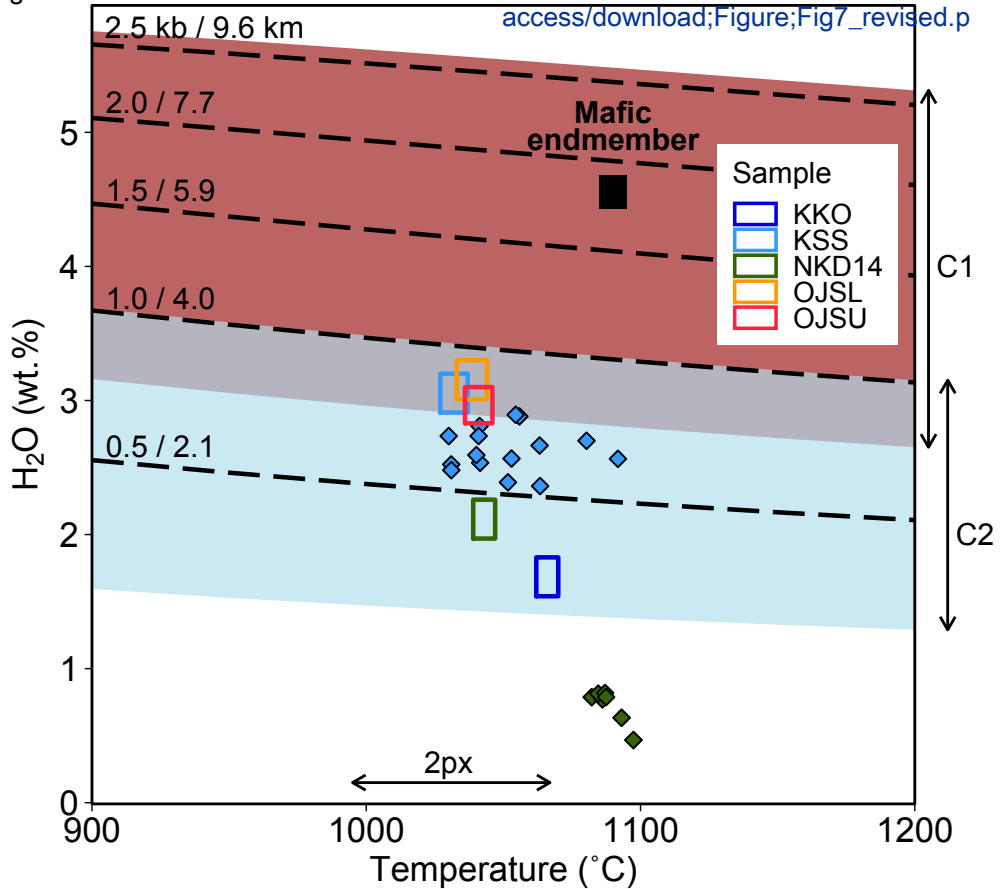


Figure 8

[Click here to access/download;Figure;Fig8_r](#)

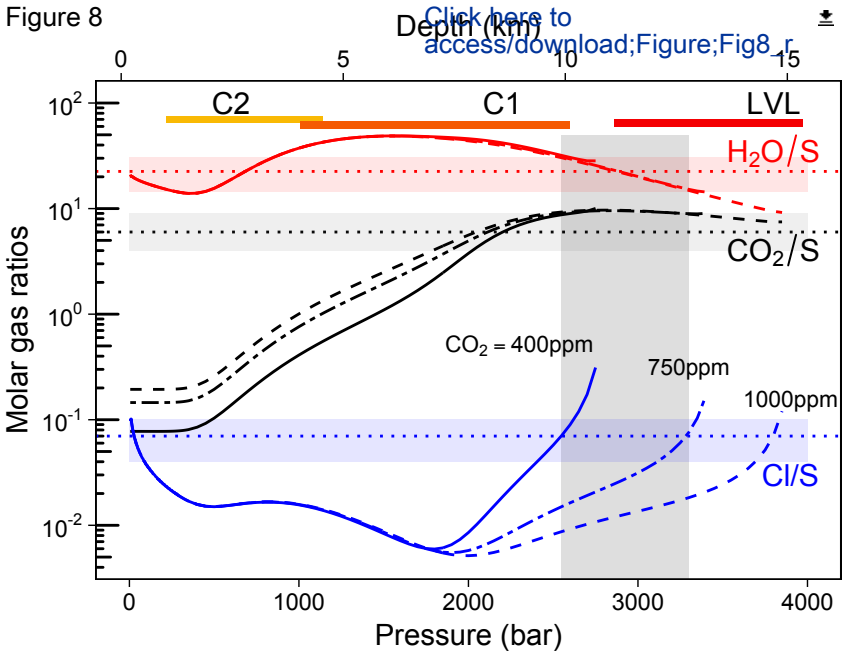


Figure 9

[Click here to access/download/Gas_and_magma/Gas_and_magma.pdf](#)

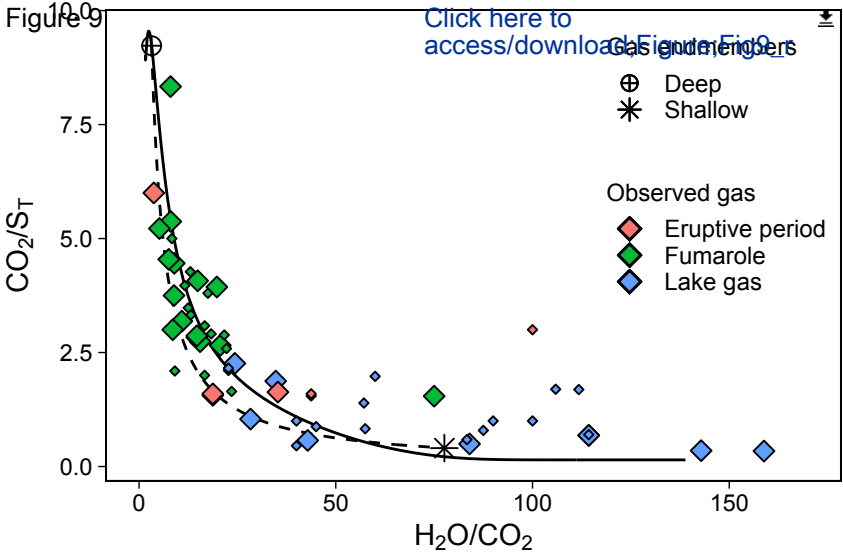


Figure 10

[Click here to access/download;Figure;Fig10_new.pdf](#)

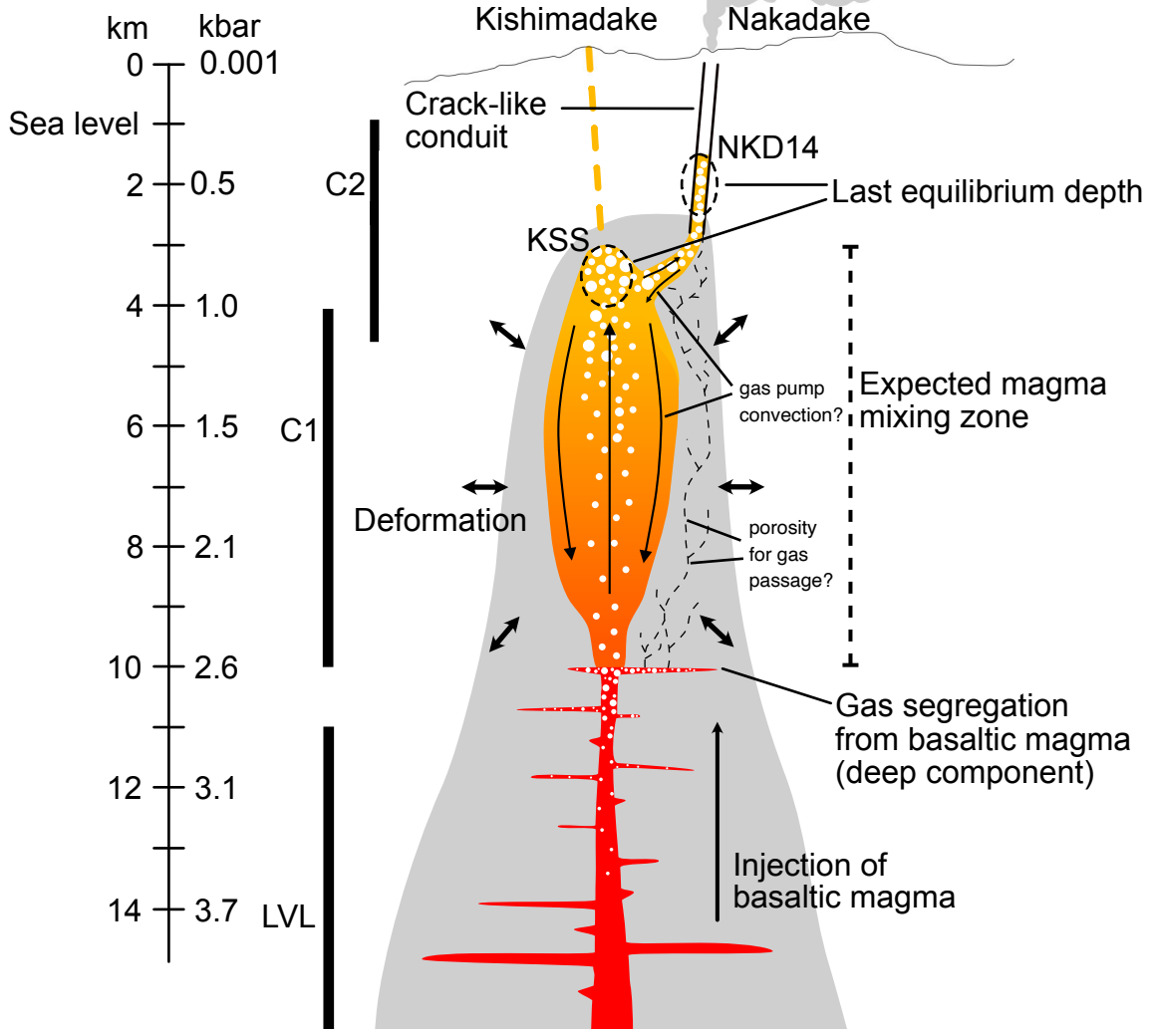


Table 1 Major and trace element compositions of bulk tephra samples.

Volcanic cone	Nakadake	Kamikomezuka	Kishimadake		
Sample	NKD14	KKO	KSS	RSTD (%) ^b	Detection limit
<i>Major elements (wt.%)^a</i>					
SiO ₂	54.26	51.49	53.22	0.1	
TiO ₂	0.94	0.94	1.00	0.3	
Al ₂ O ₃	17.84	18.52	18.48	0.1	
FeO*	8.78	10.07	9.62	0.1	
MnO	0.16	0.18	0.17	0.3	
MgO	3.91	5.56	4.45	0.1	
CaO	8.77	9.38	8.71	0.1	
Na ₂ O	3.05	2.49	2.61	0.2	
K ₂ O	2.00	1.16	1.51	0.3	
P ₂ O ₅	0.28	0.21	0.22	0.4	
Total**	99.75	99.93	99.50		
<i>Trace elements (ppm)</i>					
Sc	26	31	30	2.4	4.6
V	260	320	283	0.5	5.4
Cr	n.d.	11	12	8.9	3.7
Ni	n.d.	21	18	6.2	5.1
Cu	209	202	131	0.7	5.3
Zn	81	88	81	0.7	2.9
Rb	58	31	45	0.7	1.4
Sr	566	588	598	0.2	2.7
Y	26	21	23	2.3	2.5
Zr	139	88	121	0.6	2.4
Nb	7	5	7	6.3	1.5
Ba	369	277	328	0.7	9.8
La	18	13	15	11.2	6.1
Ce	82	33	33	4.2	5.4
Nd	25	16	18	7.3	5.5
Pb	13	7	18	3.8	2.4

^a All oxides were normalized to 100 wt.%.

^b Relative standard deviation (RSTD) of major elements were from Mori and Mashima (2005). RSTD of trace elements were calculated for KSS using the relationship between RSTD and concentration reported in Mori and Mashima (2005).

* Total iron as FeO calculated by following equation: $\text{FeO} = 0.8998 \cdot \text{Fe}_2\text{O}_3$.

** Total of the raw data.

Table 2: PEC corrected and normalized to 100%, major element and volatile concentrations in representative melt inclusions.

Sample Host mineral ^a Melt ID	NKD14			KKO								OJSU					
	OL 1-m1	OL 2-m1	OL 4-m4	PL a3-m1	CPX c5-m1	OPX 4-m6	OL 2-m1	OL 3-m3	PL a2-m1	PL Cb3-m1	CPX d2-m1	OPX 1-m2	OL 1-m5	OL 1-m13	PL 1-m1	PL 1-m4	CPX 1-m2
SiO ₂ (wt.%) ^v	59.21	56.44	57.22	57.71	60.22	59.88	48.53	49.29	57.65	52.53	61.65	59.09	59.68	54.30	59.11	55.74	57.45
TiO ₂	1.33	1.01	1.35	1.48	1.45	1.25	0.86	1.07	1.15	1.25	1.39	1.36	0.97	1.15	1.10	1.33	1.60
Al ₂ O ₃	14.43	14.82	14.33	14.61	14.23	14.37	18.08	19.52	17.10	13.35	13.69	14.90	14.42	16.77	16.91	15.34	15.47
FeO ^{100%}	10.08	11.63	10.63	11.16	10.06	9.45	11.85	10.50	8.34	13.85	9.31	9.24	9.45	9.88	7.39	10.14	10.04
MnO	0.23	0.22	0.21	0.23	0.18	0.24	0.13	0.19	0.15	0.28	0.21	0.19	0.19	0.17	0.14	0.21	0.19
MgO	3.10	3.59	3.23	2.68	2.05	2.33	6.88	5.60	2.48	5.90	1.86	2.76	2.98	3.87	2.50	3.84	2.17
CaO	5.13	6.50	6.38	5.83	4.90	5.24	10.37	10.60	6.86	8.85	4.71	5.87	5.72	8.50	5.92	7.51	5.27
Na ₂ O	2.86	3.49	3.03	2.55	2.97	3.63	2.61	2.48	2.44	1.81	3.16	3.40	3.02	3.10	3.49	3.11	3.09
K ₂ O	3.16	1.94	3.09	3.23	3.36	3.35	0.53	0.58	3.62	1.98	3.78	2.78	3.14	1.95	2.97	2.46	4.07
P ₂ O ₅	0.48	0.37	0.53	0.52	0.57	0.26	0.16	0.17	0.21	0.20	0.23	0.40	0.44	0.31	0.46	0.31	0.64
S (EPMA)	0.010	0.044	0.022	0.009	0.013	0.019	0.378	0.251	0.004	0.097	0.022	0.014	0.019	0.143	0.011	0.041	0.021
Cl (EPMA)	0.087	0.122	0.085	0.099	0.131	0.096	0.054	0.098	0.053	0.070	0.104	0.074	0.090	0.072	0.094	0.073	0.217
H ₂ O (SIMS)	-	-	0.48	-	-	-	-	-	-	-	-	-	-	-	-	-	-
S ppm (SIMS)	-	-	199	-	-	-	-	-	-	-	-	-	-	-	-	-	-
Cl ppm (SIMS)	-	-	835	-	-	-	-	-	-	-	-	-	-	-	-	-	-
F ppm (SIMS)	-	-	727	-	-	-	-	-	-	-	-	-	-	-	-	-	-
P ₂ O ₅ (SIMS)	-	-	0.49	-	-	-	-	-	-	-	-	-	-	-	-	-	-
H ₂ O/K ₂ O	-	-	0.154	-	-	-	-	-	-	-	-	-	-	-	-	-	-
S/K ₂ O	0.003	0.022	0.006	0.003	0.004	0.006	0.711	0.434	0.001	0.049	0.006	0.005	0.006	0.073	0.004	0.017	0.005
Cl/K ₂ O	0.028	0.063	0.027	0.031	0.039	0.029	0.101	0.170	0.015	0.035	0.028	0.027	0.028	0.037	0.032	0.029	0.053
F/K ₂ O	-	-	0.024	-	-	-	-	-	-	-	-	-	-	-	-	-	-
PEC% ^c	1.3	1.6	1.4	-	-	-	5.6	0.1	-	-	-	-	0.7	0.1	-	-	-
Host Mg#/An ^u	66.2	66.0	65.6	66.8	69.6	69.2	80.7	79.0	66.7	89.6	69.2	68.9	67.7	74.5	65.7	80.8	69.6

Table 2 (continued)

Sample Host mineral ^a Melt ID	OJSL						KSS									
	OPX 1-m2	OL 1-m2	OL 1-m3	PL 1-m1	PL 1-m6	CPX 1-m6	CPX O1-m7	OPX 1-m8	OL 2-m1	OL 3-m4	OL 4-m6	PL c1-m1	PL d2-m1	CPX a2-m1	CPX b5-m1	OPX 3-m2
SiO ₂ (wt.%) ^v	61.75	52.24	61.21	56.12	59.57	58.65	60.87	62.08	48.18	56.92	60.40	59.81	67.77	55.90	59.58	58.78
TiO ₂	0.76	1.08	0.79	1.48	1.19	1.24	1.27	1.21	0.99	0.56	1.25	0.98	1.01	1.37	1.41	1.36
Al ₂ O ₃	14.16	16.91	13.34	16.56	16.37	15.31	15.22	14.53	17.89	13.04	12.71	16.61	15.89	16.09	14.99	14.51
FeO ^{100%}	8.68	11.50	9.60	9.41	8.01	9.66	7.55	7.67	11.72	10.28	10.56	7.31	4.20	10.25	9.44	10.48
MnO	0.16	0.16	0.20	0.20	0.13	0.18	0.16	0.16	0.18	0.17	0.27	0.20	0.10	0.23	0.24	0.17
MgO	2.45	4.63	2.74	2.82	2.13	2.44	2.18	2.11	6.58	3.13	3.16	3.19	0.83	3.55	1.99	1.92
CaO	5.45	9.35	5.49	7.01	5.78	5.50	4.59	4.68	10.99	6.14	5.97	6.94	2.99	7.28	5.09	5.27
Na ₂ O	3.91	2.77	2.89	2.78	3.36	2.96	3.58	3.40	2.50	2.81	3.15	2.24	2.04	3.16	2.79	3.08
K ₂ O	2.55	1.08	3.25	2.76	3.11	3.50	4.12	3.74	0.73	1.84	2.10	2.42	4.77	1.84	3.87	3.83
P ₂ O ₅	0.12	0.29	0.49	0.86	0.36	0.56	0.45	0.41	0.23	0.35	0.43	0.30	0.41	0.34	0.60	0.60
S (EPMA)	0.033	0.203	0.006	0.026	0.007	0.021	0.008	0.013	0.180	0.068	0.017	0.008	0.006	0.081	0.042	0.038
Cl (EPMA)	0.045	0.058	0.101	0.078	0.071	0.103	0.143	0.096	0.071	0.153	0.085	0.067	0.143	0.109	0.123	0.118
H ₂ O (SIMS)	-	-	-	-	-	-	-	-	2.62	2.52	2.58	-	-	-	-	-
S ppm (SIMS)	-	-	-	-	-	-	-	-	2962	1075	164	-	-	-	-	-
Cl ppm (SIMS)	-	-	-	-	-	-	-	-	731	1311	801	-	-	-	-	-
F ppm (SIMS)	-	-	-	-	-	-	-	-	331	853	578	-	-	-	-	-
P ₂ O ₅ (SIMS)	-	-	-	-	-	-	-	-	0.22	0.40	0.50	-	-	-	-	-
H ₂ O/K ₂ O	-	-	-	-	-	-	-	-	3.591	1.375	1.232	-	-	-	-	-
S/K ₂ O	0.013	0.188	0.002	0.009	0.002	0.006	0.002	0.003	0.406	0.059	0.008	0.003	0.001	0.044	0.011	0.010
Cl/K ₂ O	0.018	0.054	0.031	0.028	0.023	0.030	0.035	0.026	0.100	0.071	0.038	0.028	0.030	0.059	0.032	0.031
F/K ₂ O	-	-	-	-	-	-	-	-	0.045	0.047	0.028	-	-	-	-	-
PEC% ^c	-	2.3	0.1	-	-	-	-	-	8.7	1.3	0.3	-	-	-	-	-
Host Mg#/An ^u	70.4	74.9	64.5	81.8	66.4	71.1	69.2	66.7	81.0	66.1	66.0	76.7	56.8	76.4	69.4	66.2

^a OL: olivine, PL: plagioclase, CPX: clinopyroxene, OPX: orthopyroxene. ^b All major oxides were normalized to 100 wt.% as volatile-free. ^c Degree of post-entrapment crystallization (wt.%) based on the addition of equilibrium olivine. Oxide concentrations presented in this table were corrected values. ^d Mg# = Mg/(Fe+Mg), An = Ca/(Ca+Na), in mole%.

Table 3 Major element and volatile contents in groundmass glasses.

Sample	Volcanic cone Nakadake		Kamikomezuka Ojodake				Kishimadake			
	NKD14		KKO		OJSU		OJSL		KSS	
	Avr.	Std.	Avr.	Std.	Avr.	Std.	Avr.	Std.	Avr.	Std.
N = ^a	17		8		14		13		18	
SiO ₂ (wt.%) ^v	58.94	0.30	57.58	0.46	56.19	0.95	55.03	0.33	57.15	0.63
TiO ₂	1.39	0.05	1.56	0.06	1.32	0.06	1.30	0.05	1.24	0.05
Al ₂ O ₃	14.66	0.35	14.14	0.23	15.01	0.43	15.40	0.55	15.77	0.32
FeO ^{total}	9.60	0.26	12.11	0.43	10.36	0.35	10.87	0.42	9.40	0.36
MnO	0.21	0.02	0.23	0.02	0.21	0.02	0.22	0.02	0.21	0.02
MgO	2.70	0.15	3.28	0.15	3.80	0.19	3.96	0.22	3.55	0.17
CaO	6.05	0.23	6.67	1.12	7.29	0.34	7.84	0.28	7.29	0.36
Na ₂ O	2.87	0.23	2.15	0.66	3.33	0.18	3.28	0.31	2.73	0.22
K ₂ O	3.09	0.09	2.01	0.45	2.22	0.10	1.86	0.29	2.30	0.15
P ₂ O ₅	0.48	0.04	0.28	0.05	0.26	0.04	0.23	0.03	0.36	0.05
S	0.008	0.011	0.003	0.005	0.012	0.018	0.006	0.008	0.006	0.006
Cl	0.088	0.013	0.062	0.016	0.065	0.014	0.048	0.008	0.072	0.012

^a Number of analyses.^v All major oxides were normalized to 100 wt.% excluding S and Cl.

Table 4 Results of thermo-barometric calculation for mixed magma

Volcanic cone	Nakadake	Kamikomezuka	Ojodake		Kishimadake
Sample	NKD14	KKO	OJSU	OJSL	KSS
An content (Pl-rim)	63	70	77	79	78
Temperature (°C) ^b	1039 - 1047	1062 - 1070	1036 - 1046	1033 - 1044	1027 - 1037
H ₂ O in melt (wt.%)	1.97 - 2.26	1.54 - 1.83	2.83 - 3.10	3.01 - 3.30	2.91 - 3.20

^a Mode of plagioclase-rim composition

^b Temperature and H₂O content are estimated based on groundmass glasses and plagioclase compositions after Sakuyama et al. (2014). Ranges of estimated values correspond with the range of assuming crustal condition (0.1 - 0.5 GPa).

Table 5 Comparison of the measured volatile emission with petrological estimation for Nakadake 2014 eruption

	H ₂ O	CO ₂	SO ₂	HCl
Total emitted mass (ton) ^a	1.2×10^9	7.7×10^7	1.4×10^7	5.6×10^7
Pre-eruptive concentration in melt (wt%)	1.08	0.034	0.069*	0.196*
Exsolved volatile from magma (ton)	14000	440	1600	1400

^a Total mass of each volatile species were computed from observed gas composition of CO₂/SO₂ = 8, H₂O/SO₂ = 30 and HCl/SO₂ = 0.07 in mole (Shinohara 2013, 2018) assuming observed average SO₂ emission rate of 2000 - 3100 ton/day from November 18, 2014 to January 9, 2015 (JMA 2016, 2020) for 70 days.

^b Pre-eruptive volatile concentrations were estimated for an average K₂O concentration of groundmass glass times the maximum volatiles/K₂O ratios of NKD14 melt inclusions. For pre-eruptive CO₂ concentration, we chose the highest reported value (340 ppm) of Nakadake eruption products (Saito et al. 2018).

^c Total masses of exsolved volatiles from erupted magma were calculated using the total mass of erupted products of 2.0×10^6 ton during the eruption of 2014 - 2015 (Yokoo and Miyabuchi 2015) assuming all S degassed as SO₂.

*Values with asterisk are shown as S and Cl.

[Click here to view linked References](#)

Reply to reviewer's comments

First of all, we thank the reviewers for detailed and insightful comments. We carefully read the comments and answered to all in this reply summary. To distinguish the comments from replies, we quoted the comment as an indented paragraph or in double quotation marks in italic. Please note that the reviewer comments refer to the page and line numbers of our initial submitted document, while our replies refer to line numbers of the newly revised document. The modified text as it reads now in the revised manuscript is quoted in blue.

Our manuscript got three reviews and four major points were raised by all the reviewers so we are making a common response to the three issues that were:

- 1) Regarding the choice of magma degassing model, some reviewers were skeptical about the accuracy of SolEx. They have asked if we can explain, provide arguments in favor of, the choice of SolEx? Why not D-Compress?
- 2) The term felsic and mafic correspond to two groups of samples that are not well defined. This makes the text hard to follow and consequently some parts of discussion appear *ad hoc*.
- 3) The concentration of volatile elements in the volatile-rich end-member is re-assessed in the middle section of the discussion. The reason for the re-calculation of the volatile concentration in mafic endmember is not clear, especially for H₂O concentration.
- 4) The authors have measured CO₂ by SIMS and although they argue it could be contaminated by prior carbon coating for EMPA analysis, yet the authors claim they are low in the text. These values should be reported in the tables.

In addition to these points, we realized that our discussion may have been unclear. Because of this, we have added a new figure (Fig. 10), summarizing the conclusion derived from the discussion. We sincerely hope that the paper improved the clarity.

Response to (1): In this paper, we compared published Aso volcanic gas composition with modelled gas composition at depths. Here, we used the SolEx model to achieve such comparison. As pointed out by all reviewers, S behavior during magmatic degassing is a complex process and it appears that there is no one model applicable for all volcanic degassing, and accuracy of some models were questioned as well. It is possible that our approach to apply an existing model may be premature and misleading. In this revision, we investigated further and came to a conclusion that SolEx still suits our situation best. “[Lastly, this conclusion is highly model dependent. Here, we chose to use SolEx for its agreement with the variation of S in melt inclusions. However, one must be cautious with the use of SolEx, because it is shown to fail to reproduce degassing trajectories in other volcanoes \(e.g., Werner et al. 2020\)](#)” [[see Line 692-695](#)].

As suggested by the reviewers, we now have calculated the compositional variations modelled by the model D-compress (Burgisser et al. 2015), and compared the results with the observed compositional trend (the figure shown below). The degassing paths modelled by D-compress (red lines) show moderate decrease of S with a decrease of H₂O (left panel), whereas the paths of SolEx (black lines) show dramatic depression of sulfur with the initial decrease of H₂O, and fits globally with the observed trend. The SolEx results indicate negligible degassing of Cl (right panel), which is also consistent with our observation. However, some previous studies reported the inconsistency between SolEx paths and observed melt compositions (e.g. Werner et al. 2020). Furthermore, unlike D-compress, which accounts for chemical potential of gas species, SolEx treats the behavior of S with variable partition coefficient with pressure while not accounting for other parameters, such as oxygen fugacity change with decompression. Lastly, because the compositional trend of volatile elements in the melt inclusions is a result of degassing, mixing, and probably crystal fractionation, the disparity of melt composition from the degassing path is likely due to such processes. On top of this, diffusive H-loss of melt inclusion can reduce H₂O while keeping S concentration. Similarly, many Cl points are shifted to a higher value

compared to the SolEx path, which can be explained by mixing and crystal fractionation as Cl is incompatible in minerals. Here, our point is that the trend of the volatile element depletion is better explained by SolEx than D-compress, while it is far from a perfect fit.

An ideal case, would be to use the method for predicting gas evolution using pressure-dependent bulk partitioning coefficients derived from the observed trend (Werner et al. 2020; Johnson et al. 2010; Sisson and Layne 1993; Spilliaert et al. 2006). However, this method requires a well-documented sample set representing the degassing and crystallization, but without mixing. In our case, the variation of major and some volatile elements is clearly controlled by mixing, while H₂O and CO₂ are degassed. It was not possible to separate these processes, and derive degassing controlled S partition coefficient, like in those studies. Thus, we did not pursue this approach, and accepted to use SolEx for the degassing modelling of our sample.

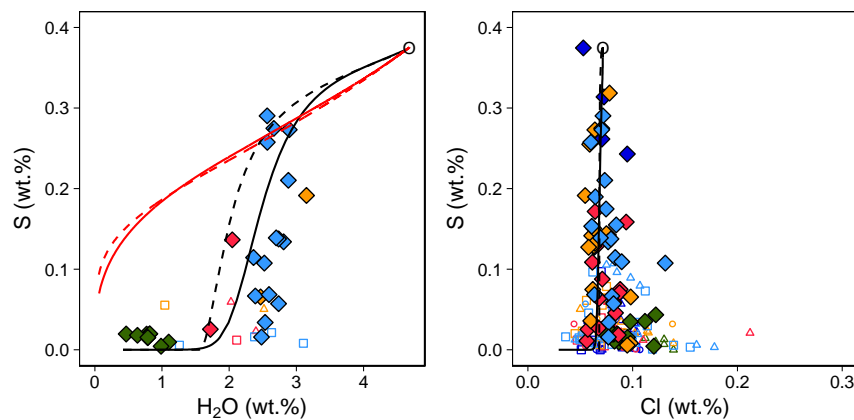
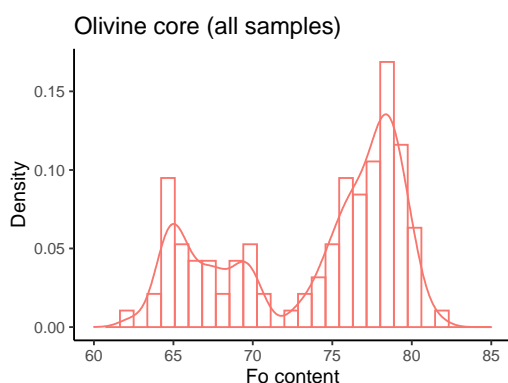


Figure caption: Red and black lines correspond to the modelled degassing paths of D-compress and SolEx, respectively. Solid and dashed line indicates the closed-system and the open-system degassing, respectively. Initial volatile concentration used for the degassing model is plotted as an open circle, with H₂O=4.68 %, S = 3750 ppm, Cl = 716 ppm (Our mafic endmember composition before degassing). The paths shown in the figures is the case with 650 ppm initial CO₂. Changing the initial CO₂ concentration did not change the paths significantly. Measured volatile concentrations of individual melt inclusion and average values of groundmass glasses are plotted as the same symbols as in Figure 3. H₂O concentrations of groundmass glasses are assumed to be 0.01wt.%.

Response to (2): The definition of the two groups, mafic and felsic, is based on their host olivine composition. In our sample set, the core composition of the host olivines are clearly divided into two groups with Fo72 representing the divide (see the histogram below). We interpreted that olivines are grown from two distinctively different lavas, which we called mafic and felsic. Based on the anti-correlation of SiO₂ concentration in olivine-hosted melt inclusions with host Fo content, we concluded that magma composition can be divided into two groups above and below 55 wt.% SiO₂. The high SiO₂ corresponds to low-Fo olivine and low SiO₂ corresponds to high-Fo olivine. Thus, we grouped all melt inclusions lower than 55 wt.% SiO₂ in a mafic group, and others in a felsic group.



Thank you for pointing out the cut-off value of Fo74 as being unclear. While we mention the value in the text that was misquoted (as Fo74), the correct value is Fo72. We corrected the Fo value in the main texts to “...as low-Fo (62 to 72) and high-Fo (72 to 82)...” [Line 328]. In addition, we modified Figure 3a to include the relative density distribution of olivine core composition. On top of it, a dashed line representing Fo72 is added to Figure 3a and 3b to indicate the separation between the two MI groups. In the caption of Figure 3, we added the sentence, “The distribution of Fo content in all olivine cores is shown as a relative density function on the left side of (a). The dashed line in Figure 3a and 3b indicates the value Fo72.”

To clarify the definition of the groups, we added a new passage in the manuscript. The new text now reads [L 351-358], “In our sample set, the core composition of host olivines were clearly divided into two groups with Fo72 representing the divide (Fig. 3a). We interpreted that olivines have grown from two distinctively different lavas, which we called mafic and felsic. Based on the anti-correlation of SiO₂ concentration in olivine-hosted melt inclusions with host Fo content, we concluded that magma composition can be divided into two groups above and below 55 wt.% SiO₂. The high SiO₂ corresponded to low-Fo olivine and low SiO₂ corresponded to high-Fo olivine. Thus, in the following we grouped all the melt inclusions lower than 55 wt.% SiO₂ in a mafic group, and others in a felsic group.”

Response to (3): The volatile concentration of the mafic endmember is defined based on the hygrometer of the plagioclase – melt – olivine equilibrium. This is necessary because MI data are influenced by magma degassing as H₂O concentration in melt inclusion is easily modified by diffusion of H⁺ through host olivine (Portnyagin et al. 2008, Chen et al. 2011, Gaetani et al. 2012, Bucholz et al. 2013). Thus, water content in MI is re-equilibrated to a degassed magma after entrapment. The measured water content in melt inclusions does not represent the water concentration at the depth of the deep magma chamber. To clarify, we rearranged the section “Characterization of mixing endmembers” and added sentences to better express what we meant. The exact changes are as follow:

- First these comments made us realise that the source of confusion originates from the mixing calculation applied to H₂O concentration while we were clearly aware of the post-entrapment loss. In retrospect, the mixing model does not need to include H₂O. In the revised manuscript, we suppressed all the discussions concerning the H₂O in the context of mixing. Furthermore, to clarify the definition of the mafic endmember, we change the order of sections. Now “Characterization of mixing endmembers” is followed by “volatile concentrations of the primitive magma” then “storage depth of magma mixture”
- We also addressed the issue by re-organizing a section of the discussion, “Characterization of mixing endmembers”, by separating the discussion concerning the endmember compositions in major elements and volatile elements. Then, in the paragraphs discussing the characterization of the end-member of volatile elements, we explicitly discussed the effect of degassing in melt inclusions and why MI volatile data are not used.
- In the section “Characterization of mixing endmembers” in the discussion, “former” page 10 line 15 – 17, the sentences “For volatile elements, during/after magma mixing.” are deleted from the paragraph and moved to the end of this section. This separates the discussion of major elements from volatile elements. The new paragraph now reads: “The mixing trend among

volatile elements is present and generally consistent with the trend of major elements. However, in detail, there are systematic disparities from the mixing curve (Supplementary document S4). Notably, abundances of H₂O, S, and Cl for NKD14 samples are depleted compared to the mixing trend traced by KSS melt inclusions (Fig. S4-5). This is best explained by significant degassing occurring during/after magma mixing. Furthermore, there is no single melt inclusion uniquely representing suitable mafic endmember volatile concentrations. The sample KSS-2-m1 is selected as the major element endmember, but its H₂O contents are not the highest values. From the inspection of the trend, we inferred that mafic endmember must have higher volatile content thus most likely lost water after its entrapment. If melt inclusions formed at a deeper depth were stored in a shallower magma chamber, it is expected that H⁺ diffusion through olivine equilibrates melt inclusion with surrounding magma (Portnyagin et al. 2008, Chen et al. 2011, Gaetani et al. 2012, Bucholz et al. 2013, Ferris et al., 2016). Complete re-equilibration of the melt inclusions would have erased the mixing trend. However, we have found suitable endmember volatile element concentrations that satisfy the general trend. Because the mafic endmember magma is expected to be volatile-rich, its H₂O concentration has to be higher than the H₂O of the mixed magma (e.g. melt inclusions). The maximum estimated H₂O concentration (4.68 wt. %) based on the hygrometer discussed above is therefore taken as the concentration for the volatile-rich mafic endmember. This value of 4.68 wt.% H₂O is higher, by about 2 wt. %, than the highest H₂O concentration measured in the melt inclusion. Sakuyama's method implicitly ignores the CO₂ activity in magma, and predict lower H₂O content when considering CO₂-bearing system (by 0.9 wt. % less, assessed from an experimental result of Melekhova et al., 2017). Furthermore, this volatile content is the value at the condition of olivine - plagioclase crystallization, most likely of the cooling magma in the crust. At this point we have no other constraint on the H₂O concentration of the mafic endmember and the primary magma could have an even higher H₂O content.” [Line 448-475].

- The discussion concerning the volatile element concentration in the mafic endmember appears in two other sections, “Storage depth of the magma mixture”, and “Volatile concentrations of primitive basaltic melt”. We carefully examined redundancy, paid extra attention to improve the clarity of our interpretation.
- Lastly, we added a sentence in the supplementary material S4 “H₂O concentration of mafic endmember was taken from the maximum plagioclase-olivine-liquid hygrometer-estimated value (4.68 wt.%) rather than from the measured melt inclusion because of possible diffusive H-loss (e.g. Portnyagin et al. 2008).”

Response to (4): the CO₂ measurements by SIMS were added to Table 2 and S1. The CO₂ concentrations measured in the melt inclusions vary from 10 to 411 ppm. Although we wrote that these concentrations are generally low, we have doubts on the higher CO₂ values. We advise for caution interpreting the values in the range of a few hundreds ppm because of possible carbon contamination, since the EMP analyses (therefore carbon coating) were performed prior to volatile measurements by SIMS. In any case we did not use the melt inclusion measured CO₂ data in the discussion.

Specific replies to reviewer's comments:

Reviewer #1: Kayla Iacovino

K. Iacovino review of “Persistent gas emission originating from a deep basaltic magma reservoir of an active volcano: the case of Aso volcano, Japan” by Kawaguchi et al. for Contributions to Mineralogy and Petrology.

Dear Editor,

This manuscript represents an increasingly important approach to understanding volcanic degassing; that is, it is one of a growing number of studies to look in depth at both the petrology of erupted products (petrography; compositional analysis of matrix glass and phenocrysts; and major and volatile element compositional analysis of melt inclusions) as well as modeling of the surface gas data. The data collected in this work seem to be of top quality, and I have no qualms with the results of chemical analyses (including the descriptions of the analyses performed). However, I find that key sections of this paper are complicated in ways that make it impossible to understand the use of these data. For example, while melt inclusion volatile concentrations are measured, key volatile concentrations of various magma reservoirs are also calculated in multiple ways. It is unclear why the authors have calculated so many of these values, instead of relying more heavily on their hard-won and quite thorough dataset.

Below I detail specific areas of concern where I think the manuscript could be improved with additional clarity in both a.) what samples are being referred to when; and b) why certain choices were made by the authors. Overall, the body of work is impressive, and I find the final analyses intriguing. But, I cannot comment intelligently on whether I am convinced with the final argument, since I am so confused by key details along the way. I recommend that this manuscript be accepted pending major revisions to the text. Some new calculations may be required OR the authors must better justify the values they chose for various modeling exercises.

Response: We thank you very much for the support of the paper and the model. We took your comment carefully into account, and revised the discussion section as detailed in the following replies, especially examining what we have stated what is referred to and why certain choices are made.

Specific comments

Volatile concentrations: which are which?

*The authors present a large number of values for H₂O, CO₂, S, F, and Cl concentrations in various magma reservoirs. Some of these are based on measured values in melt inclusions, while others are based on various calculated values. It is unclear to me throughout the text which reservoir is being referred to at any given time. I *think* there are three main reservoirs: a shallow region which contains a mixed magma created by the mixing of a mafic end-member and a silicic end-member plus a deeper region which is referred to as either a primitive or primary source region. I attempted to keep a running tally of the values ascribed to each of these magma bodies as I read the text but was unable to accurately do so. I think a table AND a figure showing the values broken down based on these three reservoirs with symbols for measured (MI) and calculated (hygrometer, K₂O ratio modeling...) values would be very helpful.*

The different “sets” of values that I encountered include:

- 1. Measured melt inclusion values for various subsets of the data (although it is never made clear which samples within each sample number are grouped into which of the three reservoirs listed above)*
- 2. Primitive reservoir values modeled using the plagioclase hygrometer (some of which are discounted by the authors)*
- 3. Primitive reservoir values modeled using the ratio of volatiles to K₂O concentration*
- 4. Values from another paper (Saito et al., 2018) that show up and which are used in the final analysis despite new values presented in this paper*

Response: The reason why we constantly mention different sets of values, volatile concentration in particular, is the reflection of the complexity of the processes. On the one hand, we have the measured

values, yet these are the results of modifications due to magma transport and storage. As we develop the discussion to distinguish processes (mixing, deep and shallow storages), inevitably we need to introduce other geochemical indications that may be the reflections of our model hypothesis.

We acknowledge that our discussion was not organized enough to present our idea clearly. Especially since the issues mentioned here were also pointed out by other reviewers. We addressed it as one of the four points listed at the beginning of this summary.

Introduction and methods sections

These sections are fantastic and well written, and I suggest no changes here.

Results section

Section on host mineral compositions: *Here is where my confusion begins. The MI-bearing olivines (e.g., those shown in figure 3) come from 5 different sampled locations (the five sample numbers) and are grouped into two groups: high Fo_olivine with low SiO₂_MI and low Fo_olivine with high SiO₂_MI. These groups are separated at Fo=74. However, figure 3a does not seem to indicate that there are two distinct groups of ol, and it makes me wonder why the authors chose this seemingly arbitrary Fo value to define their groups.*

Response: We wrote a common reply for the three reviewers at the beginning of the document. This is addressed in “Response to (2)” of the list.

Section on major and volatile elements in melt inclusions: *As with the previous section, this one details volatile concentrations in two “groups”: mafic and felsic. It is not immediately clear to me which samples in Fig 3 fall into which groups. Specific volatile concentrations are called out here, but for example, which sample in Fig 3 represents the “felsic volatile-poor magma” with S<1069 ppm? Since the distinction between these groups seems arbitrary to me, I lose the meaning of the most volatile-rich sample from the felsic group.*

Response: As we have revised the presentation of the mafic and felsic groups (see “Response to (2)), we hope the discussion on volatile elements is clearer. We also modified figure 3, adding a background color to identify immediately the mafic and felsic groups.

Section on storage depth of magma mixture: *Here it is very unclear as to which samples are being referred to at any given time.*

Response: we revised the text carefully to be more specific about what sample we were talking about. We hope that the section now reads well. Also, we switched the position of two sections, “***Volatile concentrations of primitive basaltic melt***” now comes before “***Storage depth of the magma mixture***” for clarity of discussion.

A plagioclase hygrometer is used here to calculate the H₂O concentration of the mixed magma (I think?). I think I understand the rationale for this, although it should be more clearly stated. E.g., MI measured values give H₂O in end-member magmas, so the hygrometer calculated values using feldspar rims and matrix glass should correspond to the mixed value.

Response: Measurements of H₂O in melt inclusions are not used for determining the H₂O concentrations of the endmembers. Instead, the H₂O determined by the hygrometer is the H₂O concentration of the mixed magma, because plagioclase rim - melt are equilibrated after mixing. The H₂O concentration of the endmember has to be higher than the H₂O of the mixed magma, therefore higher than the H₂O-determined by the hygrometer. The H₂O concentration of the volatile-rich endmember is 4.68 wt.% (and this is still a minimum value) corresponding to the highest calculated value with the hygrometer determined from the plagioclase core. To clarify the significance of the results of the hygrometers, we

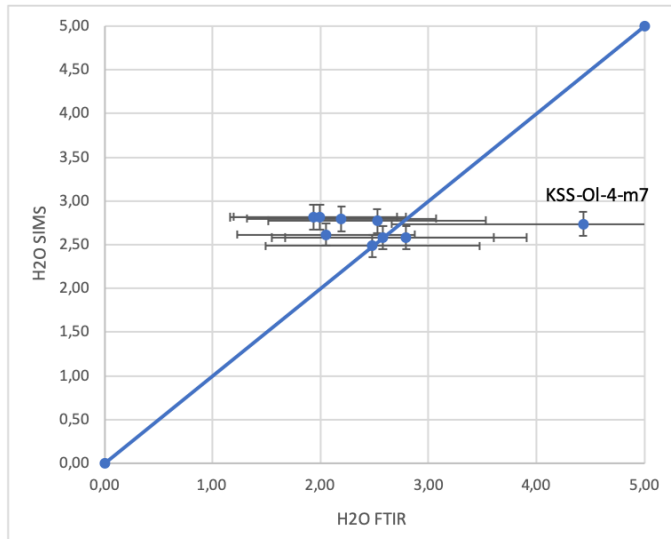
added a sentence in (former) page 11, line 13. It reads: “For example, measured volatile concentrations of melt inclusions are considered to be re-equilibrated to a condition of a magma storage. Alternatively, it is also possible to determine H₂O concentrations estimated from plagioclase rim and groundmass glass pairs (geo-hygrometer, Lange et al. 2009), likely corresponding to the value of the mixed magma during the plagioclase rim growth. The H₂O concentration of such mixed magmas are, ~2 wt.% for NKD14 and KKO, and ~3 wt.% for OJSU, OJSL and KSS (Table 4).” [Line 554-560]

H₂O concentrations are converted to storage depths. VERY IMPORTANT: which model was used to calculate saturation pressures?

Response: The conversion from H₂O concentrations to saturation pressure was based on the water solubility model of Moore et al. (1998). Estimated H₂O concentrations and temperatures were plotted in Figure 4, then saturation pressures were read from solubility contours. The corresponding depths of these pressures were calculated based on the reported crustal density structure in the Aso area (2200 kg/m³ for depths <1km and 2700 kg/m³ for greater depths; Komazawa, 1995). We have revised and made sure that all the information is explicitly cited in the text.

Line 22-23 on this page: 1) “Melt inclusion H₂O measurements ranged from 0.47 to 2.97 wt% (SIMS)” For which samples? 2) In table 2, measured H₂O in MI goes up to 4.57 (measured by FTIR). Do you discount this FTIR value? 3) Also noteworthy that I think the authors should decide how to compare FTIR and SIMS data. Currently, both are presented, but it is unclear if one method is favored over another?

Response: (1) The sample names are NKD14-Olivine-4-m4 corresponding to 0.47 wt. % H₂O and KSS-Olivine-4-m11 corresponding to 2.89 wt. %. Sample names are added to the sentence [Line 369]. (2) The comparison of H₂O measurements by FTIR and SIMS data: although we reported H₂O concentrations done with both methods, FTIR by reflectance is prone to overestimation of H₂O concentration due to the baseline correction of spectra. Therefore, in the entire manuscript only the SIMS H₂O measurements are used for discussion and considered reliable. As some inclusions are only measured by FTIR, we couldn't compare them with SIMS measurements and we do not have a concrete reason to discard the data neither. So we decided to report the data with a caution of potentially large uncertainty close to a factor of 2. We added the following sentence as a footnote to the Table S1 “In this study, we did not find satisfactory agreement between H₂O determined by FTIR and by SIMS (uncertainty of FTIR measurements is close to 40%) so in the following, we only consider H₂O concentrations measured by SIMS, based on the better detection limit and precision of the method.” [Line 262-265]. (3) Regarding the measurements of H₂O concentration, FTIR and SIMS measurements are unusually in weak agreement (within 40%, see first figure below), with one obvious outlier (KSS-OL-4-m7). As already written in (2), one explanation to this disagreement is overestimation of H₂O in reflectance FTIR analysis due to the contamination of reflective components derived from the host minerals. Again in response to this, we only consider SIMS H₂O measurements in the entire manuscript, for the sake of consistency, and the range of H₂O cited everywhere in the text is always that of SIMS measurements.



Lines 26-28 on this page: I don't understand why the CO₂ concentration in the matrix glass has any meaning here. The matrix glasses are completely degassed. If anything, the CO₂ concentration in the MI should be considered (even given the presence of vapor bubbles). By the way, how is CO₂ measured in glasses? It seems like it is not measured, but here it is reported that matrix glasses have very low CO₂.

Response: Yes, your remark is absolutely correct. It was our error. We deleted the text referring to CO₂ measurements in the matrix. The section of “Storage depth and . . . “ is completely re-written, suppressing such incoherence.

Second paragraph in this section: 1) Why is H₂O concentration calculated using the plagioclase hygrometer for the mafic end-member? Surely it makes more sense to rely on measured MI concentrations here? 2) Also, why is a CO₂ value of 200 ppm used to model the saturation pressure? 3) What is the rationale for the crustal densities of 2400 kg/m³ and 2700 kg/m³?

Response:

1) The reason that we calculated using the plagioclase-olivine-melt hygrometer is to have the H₂O concentration of the mixed magma. The risk with H₂O measurements in olivine-hosted melt inclusion as we already explained, is that melt inclusions could have suffered H₂O loss by proton diffusion (e.g. Portnyagin et al. 2008). We modified the text accordingly to explain this. Considering that olivine-plagioclase crystallization comes after olivine-only crystallization, the value from the plagioclase hygrometer cannot be the primary concentration (at most its maximum value represents a minimum H₂O of the endmember). It represents a deep magma saturation value but not the H₂O concentration before crystallization.

2) In the revised text, we have changed completely how we refer to measured CO₂ data. This is mainly due to the fact that our measurements are potentially influenced by carbon contamination of the EMP carbon coating and we do not have any good way to discriminate the bad data. While we incorporated CO₂ data in the supplementary data, in the text we only mention them as the indication of low CO₂ abundance. The concentration referred to here, is suppressed.

3) Both crustal densities of 2200 kg/m³ and 2700 kg/m³ were the reported values based on the gravimetric analysis of Aso volcano by Komazawa (1995). To avoid any confusion, we have explicitly cited the source and provided a complete description how we converted the entrapment pressure to depth. “note the depth is calculated using a density of 2200 kg/m³ for the first 1 km and 2700 kg/m³ for the crust at greater depths (Komazawa, 1995), by solving for the depth, h [m], $P = g \{2200 (1000) + 2700 (h-1000)\}$.” [Line 564-566]

Section on volatile concentrations of primitive basaltic melt: (1) It is unclear to me why new volatile concentrations are calculated here, since some of the language here makes it seem like

the most mafic MI are used as representative of this primitive reservoir. Did I misunderstand? (2) Please provide a rationale for why K₂O is used as the index of fractionation. In calculating the volatile contents of this primitive reservoir, why is a value of 0.71 wt% K₂O used? This seems random. (3) Further, H₂O is calculated here to be only 2.55 wt%, a value which is discounted immediately since some MI have up to 4.5 wt%. If this value is so wrong, how can you trust the calculations for other volatiles? More discussion is needed here.

Response: (1) The H₂O and CO₂ measurements in the melt inclusions from the mafic group are not interpreted as representing the volatile composition of the mafic endmember, after the revision, because melt inclusions have been affected by degassing. We hope the message is clear now that we reorganized this section.

(2) The choice of K₂O concentration was on the basis of the lowest concentration. However, such estimates create significant disparities with F and Cl concentration measured. We chose to simplify the discussion regarding the determination of mafic endmember composition, during the revision. We now tie the endmember composition of S, Cl, and F to the melt inclusion values.

(3) H₂O was measured by 2 methods FTIR (reflectance) and SIMS. We reported both in the table but the agreement between the 2 methods is poor because the FTIR method overestimates H₂O concentrations. To remain conservative, we only trust and consider the H₂O measurements that were obtained by SIMS.

Second paragraph in this section and Figure 6: the calculation of SCSS is very confusing to me. Based on the text, it seems like the first calculation (at a reduced condition?) was incorrectly calculated. If fO₂ is known, why are curves for two different fO₂ values plotted? Then, I don't understand how these data are plotted; were SCSS values calculated independently for each MI sample? Finally, why are the S concentrations in "undersaturated oxidized melt" considered to represent primary concentrations? What does "primary" mean in this context? The deepest primitive reservoir? Which S concentrations correspond this "undersaturated oxidized melt"?

Response: SCSS equation of Fortin et al. (2015) does not include the term of fO₂ explicitly. Rather, the author specifies he determines FeO abundance from the total FeO with the correct redox state while the sulfur concentration in the melt is as S²⁻. As commented here, we could calculate the fO₂ corrected line but it would be a deviation from Fortin's equation. For the clarity, we decided to develop the discussion in this manner. We revised the figure 5 caption to include more detail about these points. SCSS can be calculated with melt composition, P, and T. This allows us to plot SCSS vs. measured S content. The grey line on the figure thus indicates the 1:1 line. When measured S is equal to SCSS, such melt inclusion would plot on the line. The word primary is used to state that magma did not experience sulfur phase saturation and fractionation since the formation of the magma.

Figure 4: *This might be a good place to plot all of the various H₂O concentrations (measured and calculated).*

Response: Figure 4 was modified accordingly with plotting individual measured melt inclusions and calculated H₂O concentrations. FTIR data is excluded.

Section on persistent degassing from a deeper magma reservoir (>10km): *Here, some new volatile concentrations are introduced, but I'm not sure where they are from. An "initial S concentration" of 690 ppm and a "maximum pre-eruptive CO₂ concentration" of 340 ppm are given. Are both of these values from Saito et al., (2018)? I can understand using CO₂ values from this work, as it appears those were not measured in this study (although this should be explicitly stated earlier in the manuscript), but why use that value for S? What reservoir does it correspond to? The deep primitive reservoir? Odd, since the S concentrations measured in this study are much greater than 690 ppm.*

Response: Reading the comment, we realised that our organization of the discussion was too meandering. In this revision, we simply tied CO₂ budget to a result from a previous study (Saito et al., 2018), as our measurements of CO₂ content is only reliably concluded as low (0-77 ppm) among the mixed magmas (inclusions with intermediate compositions).

In line 357-379, we have a revised paragraph discussing CO₂ concentration mafic endmember. Now, we state clearly here that we do not know the exact value, and consider 340 ppm as the observed high value, probably indicating the depth of equilibration. Later in the section “Modelling degassing of the deep magma reservoir”, we make further advances on possible source CO₂ contents by comparing with the gas observation. In this paper, one of our goals is to demonstrate the possible CO₂ constraints in such a complex system.

There is another passage (line 381, section “Excess degassing of SO₂ and CO₂ from Nakadake 2014 eruption”) where we introduce a different volatile content (Table 5). The point of this discussion simply illustrates the occurrence of excess degassing by investigating recent 2014 eruption with its magmatic product and observed gas output. The magma of the 2014 eruption is the mixed magma. Therefore, the corresponding possible source composition is independently assessed (supplementary S4). As we considered this part as a passage to support the needs of deep gas sources, we did not see the importance of developing a full discussion, and in consequence caused confusion. As it is mentioned in the footnote of Table 5, the value of 690 ppm S was calculated for NKD14 based on their maximum S/K₂O ratios and average K₂O concentration of the groundmass glass because we explained the excess degassing of NKD14 magma in this first section “Excess degassing of SO₂ and CO₂ from Nakadake 2014 eruption” in “Persistent degassing from a deeper magma reservoir (>10 km)”.

One of the reasons making confusion is the usage of the term “initial volatile concentration”. To distinguish from the “initial” meaning volatile concentrations in primary magma, we changed to use “pre-eruptive” for volatile concentration at the pre-eruptive magma reservoir and modified the text accordingly.

Section on modelling degassing of the deep magma reservoir: It is never stated here which model is used to perform these calculations, which is paramount. DCOMPRESS?

Response: Indeed, thank you, we forgot to specify the model we used. The modified text now reads: “Fig. 8 is the result of such a calculation using SolEx (Witham et al. 2012), showing the variations in H₂O/S, CO₂/S and Cl/S molar ratios of gas in equilibrium with a magma as a function of pressure.” [Line 671-673]

“Equilibrium gas composition at depth should be the same as the gas composition observed at the surface, if the gas segregated and travelled to the surface without any modification in between.” Senso stricto, this is not true. Due to P-dependent fugacity coefficients, the speciation of a gas will change from depth to surface (even at constant fO₂). This does not matter for this study if and only if surface gas measurements were made in terms of total S. Based on the information in the supplement, it appears that S may have been measured as SO₂. Technically, if total C in the gas was measured as CO₂, this also presents a problem as a gas will speciate between (primarily) CO₂ and CO (plus other probably minor C species). However, the amount of CO is usually quite low, so I am okay with this approximation for carbon. For sulfur, however, the fO₂ of the system can have a big effect on SO₂ concentration, since S is split primarily between SO₂ and H₂S (plus other probably minor S species). I can't say off the top of my head whether the bulk gas composition will be significantly affected, but this felt worthy of pointing out.

Response: Absolutely. We have completely overseen the changes of gas speciation between the depth and the surface, and indeed Shinohara et al. (2018) reports measurements of SO₂/H₂S, but not CO₂/CO. We revised and made sure to calculate the gas ratios as molar H₂O/(total S), CO₂/(total S), and Cl/(total S), and rewrote the discussions, and modified Fig. 8, and 9 where gas compositions were compared with magmatic sulfur input.

Overall, I find it difficult to comment on the conclusions drawn in this section, since I am unclear as to which dissolved volatile concentrations were used to represent which magma reservoirs. I think an additional table AND a figure showing the various volatile concentrations measured or calculated for these reservoirs will help alleviate this, PLUS some necessary clarification in the text. Other than this confusion, the manuscript was well written. I think that some more thought into how to organize and present the volatile data can go a long way toward strengthening the manuscript.

This work is very interesting to me, and I am available to re-review this manuscript should that be desired.

Response: We thank the reviewer again for the positive encouragement. In conclusion, we have added a figure (Fig10) summarising the discoveries made in this study using a schematic diagram. We hope this would improve the readability of the paper.

Reviewer #2: Daniel Rasmussen

1. Summary

Kawaguchi et al. provide a detailed study of melt inclusions from Aso volcano. They evaluate compositions of melt inclusions, host crystals, and bulk tephras, as well as phenocryst textures. They find that melt inclusion major elements give evidence of magma mixing as the primary means of variation in melt composition. Volatile elements were used to investigate magma storage depths, and the authors argue for shallow, pre-eruptive storage at depths of 2 and 4 km, and they suggest that mafic magmas feeding the system originate at depths >10 km. They use SolEx to model magma degassing paths, and a comparison of their model results with observed gas emissions indicates that mixing of shallow and deep gases occurs.

This paper was a pleasure to read, and it will be an important contribution. The authors have conducted a careful, thorough study. The dataset presented here represents a monumental effort (200 melt inclusions!). The data are robust. The writing is very clear, and I was amazed by the level of polish. Broadly, the authors have been careful in their interpretation of the data. However, I have identified some areas that need improvement or further clarification below. Specifically, the main findings of the paper relate to magma mixing, magma storage depth, and origins of gas emissions. In all three of these areas, there are weaknesses in some aspects of the arguments.

2. Major comments

- 1. The authors rely heavily on a model of magma mixing (“liquid”-“liquid” mixing) to describe the chemical compositions and textures of minerals, and the major-element trends in melt inclusions. No consideration is given for alternative scenarios (magma-crystal mixing, crystallization). The paper would benefit from the authors making a stronger case for the mixing scenario they consider and/or describing some of the alternatives. More information on my concerns can be found in my specific comments on Pages 8 and 9 of the manuscript.*

Response: This was the point we contemplated for the organization of the paper. We absolutely agree that magma evolution is complex and it is rarely controlled only by a single process. With this in mind, our choice to place mixing as a central process to explain the magma transport may have appeared too simplistic. However, we maintain the idea that the major compositional variation reflects that of mixing, while crystallization contributes to a minor dispersion. The mixing might have been a mixing process of magma crystal mixture, certainly, but melt inclusion is expected to represent magma only. Even if magma-crystal mixtures had been present, inclusions probably record only the mixing of magma. In the revision, we paid attention to discuss competing magmatic processes, while insisting on why we prefer the magma-magma mixing model.

- 2. There are weak arguments that surround the suggested shallow region of magma storage. The authors discuss saturation pressures that are relevant for a pure-H₂O system when the system in question is a mixed-volatile (i.e., H₂O and CO₂) system. Pressures derived using assuming the melt and vapor only had H₂O are minimums. If CO₂ is added to the melt (and coexisting vapor), the saturation-pressure estimates increase. The authors state that there was no CO₂ in the systems when the crystals formed because at the depths of the imaged reservoirs, CO₂ solubility is low (Page 11, lines 26-28). That may be true. However, then the petrological data are not being used as an independent confirmation of the geophysically determined magma storage depths. Rather, the interpretation of the petrological data relies on the assumption that the depths recorded by the samples are the same as the geophysical depths. Their data could be used as an independent constraint on magma depth if they can convincingly argue that the magma did not have much CO₂ in it at the time the crystals in question formed without relying on the geophysical data.*

Response: First of all, we insist that the abundance of CO₂ in the melt inclusions were low especially for the felsic group melt inclusion (0 - 77 ppm). While we agree with all the points raised here by the reviewer, because of the low CO₂ in the melt inclusions, the change of the pressure of equilibration is minor. As with the presence of bubbles in the inclusions, the concentration of volatile element in melt is equilibrated with the pressure condition just before the eruption, thus the shallow storage in this case, and as it is not the discussion of the entrapment pressure, it is unnecessary to account for the CO₂ in the bubble.

Ultimately, as commented here, the weakness of our argument was rooted in lack of independent evidence showing low CO₂. In this revision, we decided to include SIMS CO₂ data, with a cautionary note for high concentration measurements for potential C contamination. However, it is clearly shown that the mixed magmas are low in CO₂. We added a sentence stating “[Because CO₂ concentrations in the felsic group melt inclusions are notably low \(0 - 77 ppm, Table S1\), it makes negligible changes to the calculated equilibrium pressure.](#)” [Line 566-568].

- 3. The authors base several of their interpretations on modeling that was performed using melt inclusion H₂O contents without adequately exploring the potential role of diffusive exchange of H⁺ (i.e., water loss or gain) between the melt inclusion and exterior melt. The authors indicate that they selected samples to minimize the effects of this process during quench, and they indicate the possibility of water loss in page 11. However, there are ample opportunities for the process to have occurred prior to quench. Are the measured H₂O contents consistent with their mixing model? Or could they be described by a model of ascent, degassing, and crystallization? Diffusive exchange of H⁺ is a widely*

known and understand challenge when working with melt inclusion data which must be very clearly addressed.

Response: This point was raised by all reviewers. We addressed this at the beginning of this reply letter, point (3).

- 4. The authors argue that the “initial” CO₂ contents of the magma is 250-500 ppm. This is very low for an arc magma. The basis for this argument is the comparison of observed gas emissions with the results of SolEx modeling. Degassing model predictions are highly dependent on the model, the parameters, and the scenario. The authors do not adequately justify their modeling. For further information, see my comments on page 15.*

Response: Again, we can only accept this comment. The discussion surrounding CO₂ strongly depends on the choice model as pointed out here. As for the reply to this, we examined the alternative model available at this moment (see the beginning of this reply document, point 1). As we found that SolEx after all, appears to follow our compositional trend better, we decided to keep the original interpretation. However, we revised the section of “degassing” and carefully described the limit of our interpretation.

- 5. If the paper goes back to review, it would be helpful for the authors to make the line numbers continuous (i.e., not start over at the beginning of each page).*

Response: We apologize for the inconvenience caused by the line numbering and our revised manuscript now has continuous line numbering

3. Line comments

Abstract: The authors have been very consistent with their use of verb tense. From what I can tell, the entire paper is written in past tense. I do not recommend the authors change any of the tenses in this paper. However, for future papers, the authors should consider using other tenses. Here is a general guideline from Nature: “In your scientific paper, use verb tenses (past, present, and future) exactly as you would in ordinary writing. Use the past tense to report what happened in the past: what you did, what someone reported, what happened in an experiment, and so on. Use the present tense to express general truths, such as conclusions (drawn by you or by others) and atemporal facts (including information about what the paper does or covers). Reserve the future tense for perspectives: what you will do in the coming months or years. Typically, most of your sentences will be in the past tense, some will be in the present tense, and very few, if any, will be in the future tense.”
(<https://www.nature.com/scitable/topicpage/effective-writing-13815989/>)

Response: We appreciate very much the advice here. In fact, correct usage of verb tense is difficult to master.

Page 2, Line 11: Melt inclusions.

Response: Corrected, thank you. [new line, Line 45] Also we have re-examined the singular-plural usage carefully throughout the manuscript.

Page 2, Line 12: Phenocrysts. What was their Fo?

Response: Corrected thank you. [Line 46]

Page 2, Line 34: Suggest replacing “characterized” with “governed”.

Response: Corrected thank you. [Line 69]

Page 2, Line 38: Suggest replacing “melt inclusion” with “the study of melt inclusions”.

Response: Corrected thank you. [Line 73]

Pages 2-3, Lines 37-1: Today, it is very well known that melt inclusions are not completely isolated from chemical interaction with their host crystal and the external melt. The authors should make a brief comment of this here with one or two references.

Response: Yes indeed, we added the following sentence and references in the text [Line 76-80] : “In fact, melt inclusions are not perfectly isolated from surrounding magmas since H⁺ can diffuse through the host olivine (e.g. Gaetani et al., 2012) and CO₂ can be redistributed in shrinkage bubbles (e.g. Tucker et al., 2019). Therefore, H₂O and CO₂ measurements in melt inclusions are regarded as minimum values indicating the conditions of last equilibration.”

Page 3, Lines 1-6: The excess sulfur problem has been known for a long time, and several studies have given explanations to explain the observation. Some should be cited here.

Response: We agree and we cited more references for example: Métrich and Wallace 2008, Wallace and Edmonds 2011, de Moor et al. 2017 [Line 83-84]

Page 3, Line 20: Suggest replacing “magma” with “glass”.

Response: Corrected thank you. [Line 100]

Page 4, Lines 27-29: It is great that you have made note of your consideration for post-eruptive cooling. It is also important that you describe the clast size of the tephra samples you worked with. Did you focus on loose crystals in the ash size fraction of tephra samples?

Response: Yes, indeed. The clast size of the tephra sample is written in the following paragraph [Line 160 - 181]. We only used lapilli-size scoria (up to 6 cm) [Line 185-186].

Page 4, Lines 32-33: Do you have a sense of the relative abundance of each of these phases?

Response: We have no data about the relative abundance of these minerals in our samples. However, Miyoshi et al. (2005) reported the phenocryst mode of basalt – basaltic andesite lava (<54 wt.% SiO₂) erupted from Kishimadake, Ojodake, Komezuka, and Nakadake volcanoes: 32 – 39 vol.% plagioclase, 7 – 9 vol.% clinopyroxene, <1 vol.% orthopyroxene, 1 – 2 vol.% olivine, 1 – 2 vol.% opaque minerals. To point the reader to the right information, we added “Detailed descriptions of these tephra are found in Miyabuchi et al. (2005).” [Line 158 - 159]

Page 4, Line 36 (and throughout): In some cases, the authors use the Oxford comma. In others, they do not. Its use should be systematic. I would recommend using it.

Response: Thank you for pointing out the inconsistency. We have revised all the occurrences and corrected accordingly.

Page 5, Line 5: Suggest changing “was not identified today” to “has not been identified presently.”

Response: Corrected thank you.

Page 5, Lines 34-35: It would be better to express the accuracies as percent errors. An uncertainty of 5-25 ppm may be a lot more significant for an element like Nb than it is for something like Sr.

In the text we cited the range to indicate the standard deviations. The detailed variations are in fact in Table 1. For this revision, we decided to report relative standard deviations.

Page 6, Lines 19-27: Do you have a sense of the detection limit for the reflectance technique? It probably depends somewhat on the specifics of the sample, but a rough estimate would be helpful to include here.

Response: Our understanding of the reflectance technique for FTIR made us realise how difficult and how user-dependent the estimation of the baseline of FTIR spectra is. As already explained, we therefore took the conservative decision to only trust the SIMS data for H₂O measurements. We nonetheless reported the FTIR H₂O measurement in the supplementary material. [While the detection limit of the method strongly depends on the sample, we estimated detection limits as 0.14 wt. % \[Line 233-235\].](#)

Page 6, Lines 19-27: It appears that you performed SIMS on some of the same melt inclusions that you obtained water content measurements using FTIR. It is important to describe how the two measurements compare. It appears that, in some cases, the agreement is good, while in others is pretty poor.

Response: Like we replied to the reviewer 1, we adopted SIMS H₂O values rather than FTIR. Similarly, we systematically favored SIMS volatile data to EMPA measurements, SIMS being more precise.

Pages 6-7, Lines 28-6: Did you measure secondary (check) standards? Do you have a sense of the precision and accuracy of the SIMS analyses?

Response: Yes, we measured a secondary standard, EPR-G3 an aphyric basalt from the East Pacific Rise. We added the sentence [“Repeated analysis of a secondary basaltic glass standard from East Pacific Rise EPR-G3 \(Shimizu et al., 2017\) yielded a relative standard deviation for H₂O, CO₂, F, Cl, and S of 1.4, 3.2, 1.5, 2.5, and 0.9%, respectively”.](#) [\[Line 252-255\].](#)

Page 7, Lines 34-37: Are the FeO concentrations significantly elevated about the bulk rock?

Response: We realised our writing raised this question. In fact, FeO in the inclusions is mostly the same as the bulk rock or higher. High FeO melt inclusions were also lower in SiO₂ consistent with magma evolution. As it was not our aim to develop the discussion regarding the precision of FeO content in the melt inclusion, we did not elaborate more information here. Instead, we changed the sentence to [“The melt inclusions were not corrected for post-entrapment diffusive Fe-loss \(Danyushevsky et al. 2000\), as total FeO concentrations in melt inclusions are either the same or higher than those in bulk rocks.”](#) [\[Line 294-296\]](#)

Page 8, Lines 5-6: How was equilibrium with the host tested?

Response: The melt inclusions that are in equilibrium with their host were identified by filtering our data. Specifically, the melt inclusion - host pair must satisfy an expected range of K_d, typical for basaltic compositions. The modified text now reads: [“Among these samples, only the melt inclusions in equilibrium with host minerals were used for the magmatic temperature calculation, in which the](#)

exchange coefficients were within expected range of basaltic composition: $KD(Fe-Mg)_{cpx-liq} = 0.28 \pm 0.08$, $KD(Fe-Mg)_{opx-liq} = 0.29 \pm 0.06$, and $KD(An-Ab)_{pl-liq} = 0.27 \pm 0.01$ or 0.1 ± 0.05 (depending on the calculated temperature; Putirka 2008).” [Line 303-307]

Page 8, Lines 9-10: Suggest changing wording to “major and volatile element concentrations”.

Response: Corrected thank you.

Page 9, Line 16: Here and elsewhere “olivine-hosted” should be hyphenated.

Response: Corrected thank you.

Page 9, Line 30: Normally zoned olivine phenocrysts are not described in the “Host mineral compositions section”. Are these common? Does normal zoning occur in the high-Fo olivine only?

Response: Yes, all high-Fo olivine observed in KKO, OJSU, OJSL, and KSS are normally zoned and common. As described in former page 8 line 37, some plagioclase phenocrysts were also normally zoned. In conclusion, normal zoning occurred in the high-Fo olivine and high-An plagioclase only. We added the sentence into former page 8 line 30: “All high-Fo olivine phenocrysts were normally zoned.” [Line 333]

Page 9, Lines 29-34: I wonder if describing the mixing as something that occurs between two “liquids” is too reductive. (1) Does the mixing need to be between two liquids? Could you have one magma carrying some crystals interact with xenocrysts or antecrysts? In other words, could you explain the observations listed in lines 31-34 with a mafic magma bearing crystals interacting with a more evolved pile of crystals? Also, if the “liquids” are suggested to be bearing crystals (and/or other phases), I would recommend calling them “magmas”.

Response: Yes indeed, it is better to use “magma” and we changed the text accordingly. In fact, we don’t have a clear evidence to judge if mixing was just between “liquids”. As the reviewer said, we can not exclude the incorporation of xenocrysts or antecrysts into the ascending magma. However, given the presence of banded pumice in ACP-1 (e.g. Miyabuchi 2017) erupted prior KSS eruption, it seems conceivable that melt would have been present. Even if the silicic endmember magma was the remnant of such mixed ACP-1, the mixing of two distinct extreme magmas is not geochemically wrong. Furthermore, considering the high temperature of the silicic endmember and the fact inclusion traps the liquid only, we stand by our choice of mixing liquids. Thanks to the reviewer’s comment we leave this possibility open for food for thoughts without having any good argument here to constrain it. In any case, for the flow of discussion it is not the right place to state “liquid” here [Line 372-384]. Reference to liquid-liquid mixing is suppressed here and moved further down in the discussion.

We modified the text to clarify our interpretation in this discussion, “It is important to note that there is a surface expression of this silicic endmember in the Aso eruption products, while the mixing endmember is set by a melt inclusion. Major element compositions of ACP1 dacitic pumice (Miyabuchi 2017), the only Holocene felsic product erupted three hundred years before that of KSS, are similar to the felsic endmember, and this indicates the presence of the silicic magma. Furthermore, the presence of a banded pumice was reported in ACP1 prior to KSS (Miyabuchi 2017). This banded texture is evidence of magma mingling and therefore the mixing trend is unlikely a result of assimilation and crystal fractionation of single parental magma.” [Line 408-415]

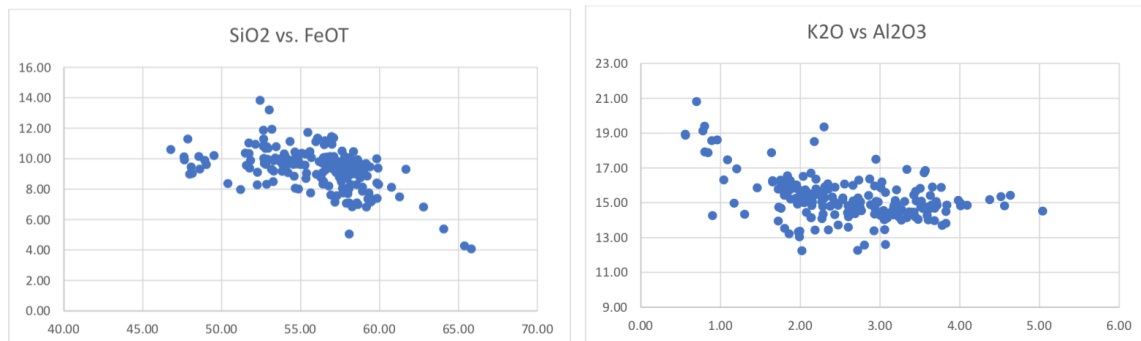
Page 10, Lines 4-6: Perhaps you could make a brief statement why the two types of magmas that mix are proposed to not be derived from a single parent. It is easy to imagine a scenario where magma mixing occurs between two magmas that have a similar parent.

Response: Certainly. We modified the first paragraph of the discussion expanding to mention the point raised here. “While the major variance of concentration variations was explained by a simple mixing process, in close inspection of trends, it is likely that crystal fractionation contributed to the dispersion from the mixing model. It should also be noted that the mixing model required the presence of independent mixing endmembers, it does not constrain their origin.” [Line 403-407]

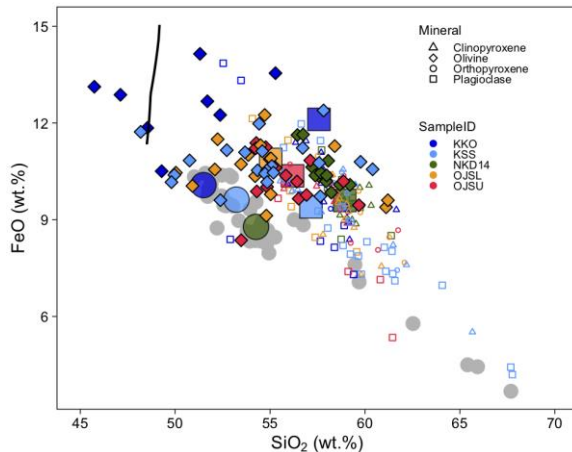
Page 10, Lines 16-17: Some of the variation in water could be due to diffusive equilibration of H⁺, right?

Response: Yes for example most MI from KSS have H₂O concentrations between 2.36 and 2.89 wt.%, with the exception of one Mi (KSS 3-m3) which has probably suffered diffusive equilibration of proton and has a lower H₂O concentration (1.52 wt.%). For this reason, we did not include H₂O in the mixing model.

Page 10, Lines 9-17: Can the major elements be described by a crystallization model? In the major element data alone, is mixing required? Mixing requires linear trends on major element plots. Some major element plots (see below, note these were made using the uncorrected major element data of melt inclusions) do not seem to show linear trends. Rather, there is some evidence of “kinked” paths, which are commonly attributed to crystallization.



Response: Thank you. We tested the idea of a fractional crystallization on the figure the reviewer produced but with the corrected MI data and we added the fractional crystallization model. The trend in corrected major element FeO vs SiO₂ is closer to linear now (no kink, figure below). However, a simple crystallisation trend (produced by Rhyolite MELTS, fractional crystallization from 1150 °C) disagrees with the composition variation here. So maybe fractional crystallization happens but it is not the main process justifying the composition variation. Therefore, we maintain our mixing model to explain the melt inclusion variations but we now mention the fractional crystallization because we can not rule it out entirely, but we add that it does not play an essential role in this variation.



Page 10, Line 21: It appears that the stated uncertainty is the standard deviation of your temperature estimates? Does the thermometer have an associated uncertainty (i.e., standard error of the estimate)? What is that?

Response: Yes, indeed. The cited uncertainty is of the sample variations. The standard error of Putirka's two pyroxene thermometer is ± 38 °C. The text is modified as "... are 1010-1025°C for KKO, OJSU, OJSL, and KSS (± 13 °C 1σ of samples, while standard error of the thermometer is ± 38 °C; Table 4)". [Line 419-421]

Page 10, Lines 22-27: Do you have a possible explanation for your high temperatures? Is there a big difference in the water content of your magmas relative to the low-temperature dacites?

Response: Yes, the low temperature (770 – 915 °C) found for the dacitic magma from Mount St Helens might have been due to higher H₂O contents (4 to 5 wt.%) compared to H₂O range that we have in this study (0.5 to 2.9wt.%). Actually, our temperature estimates (1010-1025°C) are in between that found for this previous hydrous dacite (Mount St Helens) and that found for an anhydrous dacite (Puna Geothermal Venture Wellfield, Hawaii; Teplow *et al.* 2009; 1050°C). We modified the text accordingly. [Line 422-428]

For volcanological sense, we do not have a concrete explanation on what would cause the production of the high temperature magmas. We just report here that it does exist beneath Aso.

Pages 10-11, Lines 32-8: The thermometry is highly dependent on water contents. The authors have not discussed diffusive water exchange. What is the evidence that the basaltic melt inclusions have retained their original water contents throughout the course of mixing, ascent, and cooling in the plume? At high temperatures (i.e., >1000 or 1100 C), melt inclusions hosted in olivine will likely loose some water while cooling in an eruptive plume if they are in lapilli clasts (although, this does depend on several factors). I imagine the eruptive temperature of these magmas is lower?

Response: Yes, this was certainly our point as well. First, we discussed the diffusive water exchange of olivine-hosted melt inclusion and stressed that melt inclusions have lost water. In the revision, we wrote more statements recognising this. Furthermore, Sakuyama's method exactly recognizes the issue and is based on the major element composition of melt inclusion and plagioclase. Using the latter method, temperature and H₂O concentration are calculated simultaneously. Lastly, we also applied a simple olivine thermometer to the melt inclusion with the highest water content to have a comparable value to Sakuyama's method. We think that the convergence of these two methods is an indication of the successful determination of magma temperature.

Page 11, Lines 11-28: The saturation pressures presented are the pressure of saturation of a pure- H₂O vapor. However, this is a mixing volatile system. If you start to add CO₂ to the melt (and coexisting vapor), the pressures presented become minimums. The authors argue that if magma storage occurs at 2 and 4 km, then it is unlikely that the system contained much CO₂ because the saturation pressures calculated for an H₂O-only system are consistent with those depths. That may be true. However, that means that the petrological data are not being used as an independent constraint on those depths. Rather, the authors are just arguing that their data can be consistent with it if no (or very little) CO₂ existed in the melt (and coexisting vapor) that the samples record. This problem could be resolved by presenting measurements of CO₂, which the authors say they performed using SIMS, yet there is no mention of the results of these analyses.

Response: The SIMS CO₂ measurements were done after the EMP analyses, and we conservatively thought that the carbon coating contamination could have ruined the data. However, the CO₂ we measured in the melt inclusions is low (<450ppm; mostly 10-30 ppm for mixed felsic magmas). We decided to follow the reviewers' request and reported the CO₂ SIMS measurements in the supplementary material. Table S1 is modified to include CO₂.

Page 11, Lines 27-28: The CO₂ content of the groundmass is irrelevant. Clearly, the groundmass has degassed its CO₂. What is more important is determining the CO₂ that existed in the melt at the conditions of the entrapment of your melt inclusions (or formation of plagioclase).

Response: yes absolutely, we agree. We deleted this erroneous sentence from our text.

Page 12, Line 22: The first clear demonstration of rapid water equilibration in olivine-hosted melt inclusions is Portnyagin et al. (2008). The most up-to-date reference on the diffusivity of H⁺ in olivine is Ferriss et al. (2016). Both references should be cited here.

Response: Yes thank you, we added the references.

Page 12, Lines 29-31: SCSS was calculated using the pressures of the shallow reservoir, but the high S contents are observed in melt inclusions hosted in high-Fo olivine (i.e., Fo~80) that I thought were entrapped at much greater depths? The depth of the "pre-eruptive magma reservoir" is not important here. The depth of melt inclusion entrapment is key.

Response: There can be a pressure effect but here we think the higher S concentrations in melt inclusions reflects mainly a change in redox conditions. The pressure change does not affect S solubility as much as the oxidation change. The melt are oxidised and have more dissolved S.

We added a sentence to clarify such limitations: "The elevated S concentrations in the undersaturated oxidized melt are therefore considered to represent, less-degassed, non-sulfide-fractionated, S concentrations, at least at the condition of the shallow storage depth." [Line 513-516]

Page 13, Lines 2-3: The authors are considering the sulfur contents of the melt inclusions relative to saturation of an S-bearing phase. It is not clear to me how they are arguing that their S contents are primary. If you are below SCAS (or SCSS), S can still degas. S partitions strongly into vapor. What is the evidence that S has not degassed from the high-S melt inclusions?

Response: We have no counter argument against this point. We were too eager to extend the interpretation. We dropped the claim that we demonstrated the undegassed S content. The value was rather the best we could find.

Page 14, Lines 13-14: I thought the authors were arguing that their least-degassed melt inclusions recorded primary S contents (e.g., page 13, lines 2-3)? Here they indicate that they need a “deeper, volatile-rich basaltic magma” to assess the S excess. Can this be assessed using their deep, volatile-rich melt inclusions?

Response: As pointed here, that is exactly how we would like to develop our discussion. In the paragraph in question, we are just establishing S-excess to illustrate the necessity of the deep source.

Pages 13-15, Lines 37-7: The discussion here is very interesting. I think it would benefit from further discussion of possible mechanisms of degassing (e.g., second boiling, magma ascent and decompression) and the relationship of observed SO₂ and CO₂ emissions.

Response: At this point of the discussion, our goal was to establish the observation of excess degassing. Instead, we introduced the mechanism of degassing in the revised conclusion.

Page 15, Lines 16-31: SolEx is often inaccurate and unreliable (e.g., Werner et al., 2020). The issue is that SolEx uses an extremely limited range of experimental data to model the degassing of S, which is a complex function of melt composition, fO₂, temperature, pressure, etc. The authors need to justify their use of SolEx. One way the authors could do this would be by comparing SolEx predictions for volatile contents of the melt with their observations (i.e., melt inclusions). Have the authors considered using D-compress? There are a lot more knobs to turn when performing modeling with D-compress, but I think many would consider that model capable of producing results that are more accurate.

Response: Refer to the answers at the beginning of the reply.

Figure 8: The authors model degassing as “closed system”, yet they suggest excess sulfur is derived from a deeper magma. This would mean that the gas that exsolved from the deep melt become decoupled from its melt. The authors acknowledge this when they discuss the segregation of a deep gas (e.g., page 15, line 35). Later (page 16, lines 18-20) the authors suggest that at 9 km, the system changes from open to closed. Therefore, their modeled degassing path does not apply at depths of <9 km. Regardless, the authors have not justified the assumption that degassing occurs in a closed system at depths >9 km.

Response: Based on our idea of Fig. 8, the closed system model is used to find a unique condition at which observed gas compositions agree with the prediction of the model. Chemically, we envisioned the scenario to decouple the deep gas from the magma at depth, and thus the system became open. Because our intention was to find thermodynamic equilibrium, we did not justify why degassing should be closed below 9 km. Rather we consider that even if magma might have gone through some kind of open system degassing below 9 km, if the gas became stagnant at 9 km and re-equilibrated with magma, we can still argue for the condition of equilibrium.

Figure 8: Perhaps the authors could add a second x-axis that indicates depth? It would be helpful for the reader.

Response: Fig. 8 was modified and the depth tick marks are added.

Page 15, Lines 27-29: By “initial magmatic CO₂ concentration”, do the authors mean the primary CO₂ contents (i.e., CO₂ concentration of the melt when it entered the lower crust)? If so, this would be very low for an arc magma. Most would argue that, in general, primary arc magmas have at least 1000s of ppm CO₂. The modeling the authors present here does not seem robust enough to make such a bold claim. The results of the degassing model are highly sensitive to several factors, such as choice of model (e.g., SolEx vs. D-compress), style of degassing (e.g., open, closed), degassing scenario (e.g., second-boiling, ascent), whether or not the gas emitted at the surface reflects gas derived from a single depth or if it is a mix of gases from multiple depths, etc. Most of these factors are not discussed with relation to the estimate of initial CO₂ contents.

Response: It seems we did not express ourselves better here. First, CO₂ content should be considered as an estimate highly dependent on the model. We think our deduction is correct as long as the model works. In the revision, we stress this point. As for low CO₂ in Aso, we think it is possible as total CO₂ flux of Aso appears to be lower than other arc volcanoes. Certainly, this maybe a transient, only contemporary, observation. Again, we agree that we do not have a constraint to say anything definitive about primitive CO₂ content, contrary to what we stated initially. We have revised the point: “Therefore, the observed gas composition must have been derived from the depth of about 9 km (~2.4 kb) at which it was in equilibrium with a magma with the initial magmatic CO₂ concentration between 400 to 750 ppm (Fig. 8). The total CO₂ flux of Aso is described to be lower than of other arc volcanoes, and this may be an indication why our estimated CO₂ content in Aso magma is lower than those of many other arcs (e.g. 1000 - 2000 ppm; Wallace 2005). The determination of initial CO₂ is strongly tied to the Cl and S partitioning into H₂O-CO₂ fluid, and we think that these values may need to be revised once we have a better understanding of Cl and S element partitioning. Lastly, this conclusion is highly model dependent. Here, we chose to use SolEx for its agreement with the variation of S in the melt inclusions. However, we must be careful with the use of SolEx, because it is shown to fail to reproduce degassing trajectories in other volcanoes (e.g., Werner et al. 2020).” [Line 687-695]

Page 16, Lines 9-12: If gas mixing occurred, how does this impact the interpretations of Figure 8?

Response: We think the conclusion of Fig. 9 holds independently of Fig. 8. The key is to explain the mechanism at which the deep gas travels to the surface without experiencing significant modifications. Such discussion is added to the end. [Line 733-751]

Pages 16-17, Lines 35-3: It would be helpful to use ranges of chemical compositions to elaborate on terms like “mafic” and “felsic”. Also, it would be helpful to show the ranges of crystal endmember mole fractions for the olivine, plag, cpx, and opx hosts.

Response: A lack of explicit definition of mafic and felsic was pointed out by other reviewers, and addressed in the beginning of this reply (point 2).

Figure 8: The authors indicate that the observed gas component they investigate is “high-pressure gas component A”. Was there also a low-pressure gas component identified in the Shinohara studies?

Response: Yes, Shinohara et al. (2018) reported low-pressure gas component B and C having low CO₂/SO₂ molar ratio of 1.6 observed during eruption. All these gas components were also plotted in Figure 9.

Reviewer #3: Nicole Métrich

Comments on the manuscript entitled “Persistent gas emission originating from a deep basaltic magma reservoir of an active volcano: the case of Aso volcano, Japan”, submitted to Contributions to Mineralogy and Petrology by Masataka Kawaguchi and co-authors.

The authors have conducted a standard study of the mineralogy and melt inclusions for modelling the magma differentiation and degassing at Aso, a very active volcano. The tephra samples which have been studied cover a span of time from ~ 4 ka to present-day.

Major elements, S and Cl were analyzed with electron microprobe and H₂O by FTIR in melt inclusions hosted in olivine, cpx and plagioclase. Water, S, Cl and F were also analyzed by SIMS in a subset of MIs hosted in olivine. Magma mixing well explains the evolution trends recorded by MIs and the mineral zoning. The possible depths of magma storage at Aso have been assessed from the dissolved H₂O amounts (P_{H_2O} is calculated using Volatilecalc), and from literature data for CO₂. The petrological results are discussed and compared to the seismic records. Both support Aso magma ponding at various levels in the crust beneath Aso. The last part of the manuscript is dedicated to the modelling of the gas emissions. This paper deserves to be published in Contributions to Mineralogy and Petrology and fits well with the objectives of the journal. The data are of high quality and the target volcano of interest. My main comments are related to the sulfur degassing, the modelling of the magma mixing, and the pressure determinations. In my point of view the manuscript could be improved in its form, and some references could be added that would strengthen the discussion.

My comments are detailed hereafter. I suggest moderate revisions.

Comments

P3, 11. Excess degassing is known at open -vent systems (i.e., Stromboli, Etna, Villarica, Popo..) and the approach using melt inclusions to describe and quantify the degassing path of magmas is widely discussed as reviewed, as an example by Métrich and Wallace (2008, RiMG69), and Wallace and Edmonds (2011; RiMG 73). There is also a nice paper on sulfur degassing (gas and MIs measurements) at Erta Ale and Masaya by de Moor et al., (2017, Gcubed).

Response: The reviewer is correct, we added the proposed citations in the introduction to this well-known “sulfur excess degassing” question. We hadn’t given enough credit to previous work.

P7. “SIMS analysis was conducted after EPMA analysis”. Could H₂O have been lost and the SIMS analyses of H₂O biased to some extents? It could explain the low concentrations measured in olivine KSS-4-m7: 4.4 wt% (FTIR) vs 2.74 (SIMS) as an example.

Response: To our knowledge it has never been reported that H₂O analysis by SIMS is affected by prior EPMA measurements. We take notes of beam position in the melt inclusion and are careful not to reposition the beam of the SIMS on or near the EPMA beam spot. Therefore, we do not think this is the right argument to explain the FTIR vs SIMS measurement discrepancy for some of the samples. However, it is true that in this study, we heavily rely on the SIMS measurements due to the disappointing correlation between EMP and SIMS (within 25%) and basically the no correlation between FTIR and SIMS. We now have clearly stated our position regarding our analytical preference in the “analytical methods” section, “major and volatile elements in melt inclusions”.

P8, 127. Remove Fo before 62-74

Response: Thank you, we have suppressed Fo.

P9. Section major and volatile elements.

-1. A few words to describe how H₂O and halogens are evolving as written for sulfur could be informative.

Response: Thank you for the suggestion. We added the following text, “F and Cl correlates with SiO₂ and K₂O and anti-correlate with host Fo content.” [Line 367-368]

-2. “The tephra samples of this study were basaltic to basaltic andesite with SiO₂ .. (large circles in Fig. 3c). Melt composition in inclusions varied significantly more than that of the bulk tephra composition...”. This sentence could be easily re-arranged in order to present Figure 3 first. This Figure 3 is very important for the understanding of the paper. Adding two plots with Cl, and H₂O vs MgO could be worth.

Response: we added in figure 3, Cl and S versus SiO₂ and Fo of host olivine, respectively.

-3. It is written, in the description of the mixing model (ESM2), that MIs in plagioclase and cpx were not considered in the modelling of mixing. However, in Fig.3b most MIs in olivine, plagioclase and cpx form a cluster. For the NKD 14 sample these MIs and the matrix glasses have similar compositions. It means that the post-entrapment evolution is minimum and that these mineral phases crystallized in the same magma batch or in closely similar magma batches. It is fully consistent with the NKD 14 sample which would result from the mixing between basalt and dacite and in which the crystals are in equilibrium with the residual melt.

Response: We apologize for the confusing story. Actually, we tested all melt inclusions including those hosted in plagioclase and pyroxenes, and we now wrote “All melt inclusions (even those hosted in other crystals than olivine), whole rocks, groundmass glasses and everything plots along the linear trend of olivine-hosted melt inclusions (Fig. S4-3).” Figures were just showing the results of olivine hosted melt inclusion only. However, the sentence we were using might have been unclear. Therefore, we modified text and figures to include the results of melt inclusions hosted in other minerals.

We replaced the text in the second paragraph “It should be noted that the model was verified by the melt compositions of melt inclusions hosted in olivine and hosted in other minerals. However only olivine hosted melt inclusions have an established procedure for the correction of the post-entrapment

crystallization.“, and now reads: “The major element variation was well reproduced with the mixing model for melt inclusions of all host minerals (Fig. S4-5)” [Line 402-403] Furthermore, we exchanged captions of Fig. S4-3 and Fig. S4-4 because it was inverted.

-4. From Fig. 3d MIs in KSS olivine record a significant depletion in sulfur (from ~ 0.3 wt% down to <0.05 wt% @ nearly constant MgO that is not due to mixing (at least in my point of view). I am wondering if KSS-MIs recording such a trend are fully enclosed. Could they be instead embayments?

Response: thank you, yes indeed after your comment we double checked the “melt inclusion” and found that there were three embayments (KSS-OL-3-m3, KKO-OL-3-m1, and KKO-OL-OP2-m2) We verified visually that they were indeed embayments. We now signal that all embayment data are suppressed from the Table S1 of the supp. material.

In this figure there are two trends of evolution: one is due but most likely to degassing since sulfide immiscibility is not observed, without crystallization and the other to mixing of magma batches differing by their composition and extent of degassing. Adding a transmitted light photomicrograph of a typical olivine-hosted melt inclusion would be important.

Response: As we have acknowledged in the reply to the reviewer 2, we were too assertive about the mixing process without carefully evaluating other processes. In the revision, for the simplicity of the discussion we decided not to discuss the mixing process for H₂O and CO₂. For S, Cl, and F, we retained the presence of the mixing trend, however we also mentioned the role of degassing, and crystallisation.

Three images of olivine hosted-melt inclusions are added to the supplementary documents S4.

Fig .2e shows that the olivine and its MI have been carefully prepared but does provide any information on the MI itself (bubble size, morphology..). Moreover looking at the Table S1, the analysis of this olivine (KSS 3-m1) is not so good (total = 96.5%), MgO is most likely underestimated.

Response: Unfortunately, the textural information of melt inclusions were not recorded during the preparation. This work started during the second year Master of the first author Kawaguchi and was done in Kumamoto University. It is now *a posteriori* not possible to provide information regarding bubble size. The form of inclusions were consistent with the type of primary inclusions, meaning not align in a plane with many other melt inclusions.

Olivine host composition is measured by EPMA with WDS mode. In fact, we see the total is generally poor. Here, we accepted the data with the total more than 98 % and less than 102 %. Since stoichiometry is good, we now reported only cation for poor total olivine data set and only used Fo content for PEC correction. The table does not include the other worse totals now.

-5. For clarity it could be written that the volatile (at least S) concentrations that are considered are the SIMS data (even if in the Table only the SIMS data are reported after PEC correction).

Response: As we replied in previous question of reviewer 1, we added the sentence in the main text to clarify that we adopted SIMS values because of high analytical precision.

What could justify the difference between SIMS and EMP analyses of sulfur whereas for SIMS and EMP data for Cl are in good agreement? As an example the S content of the MI (KSS-2m1) chosen as the basaltic end-member is 0.31 wt% (SIMS) and <0.2 wt% (EMPA).

Response: As we already answered, the measured values for S between EPMA and SIMS analysis agree within 25%. When melt inclusions are measured by both method EMP and SIMS, we favored SIMS data because of high analytical precision.

What about H₂O?

Response: we adopted SIMS H₂O values because of high precision of analysis, they are the only H₂O measurements we trust here.

P9. Discussion: evidence of magma mixing. What is the significance of the MIs compositions (major and volatile elements) in reversely zoned crystals? A short description of the MIs in the dedicated section should be inserted to describe a little bit better these MIs. Is there any evidence of cracks and overpressure, of melting/crystallization at the glass/mineral interface. Are calculations of PEC% relevant in the case of reversely zoned olivine crystals?

Response: We scrutinized the olivine and inclusions and checked for cracks and decrepitation, but to the best of our knowledge we did not identify any of those. While we did not make an explicit reference, there is a correlation between olivine zoning and the inclusion composition. Normally zoned olivine has high-Fo core (Fig. 3), thus the mafic group on the basis of our grouping (< 55 % SiO₂). Reversely zoned olivine has low-Fo and belong to the felsic group. As the revised the text, we described the compositional correlation carefully, we believe it illustrates the systematics better now.

PEC is calculated between the melt inclusion and small immediate vicinity of the surrounding olivine. The fact that the olivine is reversely zoned has nothing to do with the correction at the time of the eruption. The reverse zoning likely happened sometimes after the entrapment of the melt inclusion.

P10, 110-13. Could the calculated mixing curves be reported in the plots (H₂O-S-Cl) of Fig. 5?

Response: In the revised text, we decided not to include volatile elements in the mixing model, mainly due to difficulty separating degassing from mixing. Fig. 5 was kept but the mixing line was not added.

P10, 135. "The mafic endmember magma is expected to be volatile- rich, notably in sulfur (up to 4000 ppm; Fig. 3)." Yes but the end-member which has been chosen for the modeling of the magma mixing process contains 0.29 wt% S? Moreover, in the Figure 3d and as it is written p 9 and in the abstract, the S concentration reaches 3745 ppm in one MI (KKO sample) and most of them are <3745 ppm.

Response: The reviewer is right. The value of "4000 ppm" written in the text was a mistake, "3750 ppm" is right. Thus, we replaced the number in the text with "3750 ppm". This corresponds to the highest S concentration measured in a KKO olivine-hosted melt inclusion and we took this value as the S composition of the mafic endmember. We explicit this in the text.

P11, 114-17. I think that it is important to write here that P_{H_2O} is assumed to be equivalent to the total pressure of fluids, neglecting the role of CO_2 .

Response: Yes absolutely. Now it reads “[Here the total pressure of fluids is in fact equivalent to \$P_{H_2O}\$, neglecting the role of \$CO_2\$.](#)” [Line 560-561]

P1, 125. Are the depths of 2 and 4 km, below sea level? or below the vents?

Response: Yes these 2 numbers are below sea level every time because they come from the magnetotelluric work of Hata. When we calculated the lithostatic pressure we did it from the vent so we added 1km which corresponds to the height of the volcano (so 3 to 5 km below the vent). In the revised document, the depths are referenced to the common point= the vent.

P11, 135. VolatileCalc is calibrated for MORB at low pressure. The authors could make their pressure calculations using Shishkina et al., (Chem Geol 2014), who provide an extensive experimental dataset on the CO_2 concentrations in basalts. As fully proved in this paper the solubility of CO_2 , contrary to H_2O , widely varies with the melt compositions.

Response: As pointed out here, we have explored alternative saturation pressure calibration available in the community (Supplementary material S4). In the revision, we mention the range of pressure that we found. SolEx and MagmaSat (Ghiorso and Gualda 2015) are shown to be comparable. [Line 582-583]

P11, 135: “ the mafic-endmember H_2O concentration as 4.43 – 4.68 wt.%. Thus, the initial primitive H_2O concentration is at least 4.5 wt. %.”. In the modeling of mixing reported in ESM2 the end-member are KSS-2m1 and KSS-2d-m1. The former contains 2.9 wt% H_2O and 0.29 wt% S (SIMS corrected data). I am confused here.

Response: Yes indeed, our writing was not clear enough. We used the maximum H_2O determined with the hygrometer (4.68wt.%) as the H_2O concentration of the mafic endmember. The S concentration of the mafic endmember is the maximum S concentration measured in the melt inclusion 3750 ppm. We modified the text accordingly.

P11, 138. “2400 kg/m^3 for the first km and... ” first km of what?

Response: we meant the first 1 km of crust. We modified text and it reads “[2200 \$kg/m^3\$ for less than 1 km deep in the crust](#)” to clarify. Furthermore, we have revised the near surface density to 2200 g/m^3 after carefully inspecting Komazawa’s figure. [Line 564]

P11-12. “Gas bubbles in MIs...increases the pressure entrapment...”. Not the bubble, the CO_2 trapped in the bubble because the total fluid pressure = $P_{H_2O}+P_{CO_2}$.

Response: We modified text, and now reads: “[As gas bubbles were seen in melt inclusions, large amounts of \$CO_2\$ incorporated in such shrinkage bubbles significantly increases the entrapment pressure estimation \(e.g. Moore et al. 2015\).](#)” [Line 585-587]

More than 40–90% of the initial CO_2 that was dissolved in the melt inclusions at the time of trapping was lost to shrinkage bubbles, with an average loss of 75-80% (Wallace et al., 2015; Moore et al. 2015; Hartley et al., 2014). Hence the initial dissolved amount of CO_2 in Aso MIs could imply a much higher total fluid pressure

($P_{CO_2}+P_{H_2O}$) than 300 MPa (~10 km depth equivalent). The discussion needs to be more elaborated here to demonstrate that there is a good agreement between the petrology and the depth of the seismic-low velocity layer at Aso. I also suppose that the magma ponding zone is not unique between 10 and 24 km beneath Aso, and that magma batches could mix altogether at various depths?

Response: The argument of the reviewer is correct and we took it into account in our discussion. On former page 12 line 3, we added the following text “Recent melt inclusion studies reported more than 40-90 % of the initial CO₂ that was dissolved in the melt at the time of entrapment was lost to shrinkage bubbles, with an average loss of 75-80 % (Wallace et al. 2015; Moore et al. 2015; Hartley et al. 2014). If 90 % of initial CO₂ is present in the shrinkage bubble and a maximum CO₂ value of 340 ppm is assumed in the melt (from Saito et al. 2018), then the expected initial value of the melt would reach 3400 ppm. This value is in the same order of magnitude as the initial CO₂ concentration in a typical primary arc magma (Aster et al. 2016), and saturation pressure would exceed 5 kbar (~19 km depth equivalent) However, at the time of this study, bubble sizes were not documented with impossibility to go back to measuring them *a posteriori* since most are now polished away. In this case we chose not to use the CO₂ data of the melt inclusions.” [Line 589-599]

Regarding the magma ponding zone, we don't have any information to argue for multiple ponding zones. Therefore, further discussion is currently difficult.

P12, l35. As written above, the S concentration reaches 3745 ppm in one MI (KKO sample) and most of them are <3745 ppm (not 4000 ppm). Such an amount is not higher but typical of subduction-related magmas -related basalt in which sulfur is dissolved dominantly or totally dissolved as sulfate. As another example, the H₂O-rich MIs of Augustine volcano display similar high S concentration (i.e., Webster et al., 2010; in The 2006 eruption of Augustine volcano, Alaska, US Prof paper 1769).

Response: It was our error to stress the high S content. We revised the text, “Dissolved S concentrations, up to 3750 ppm in the mafic endmember melt inclusions, are higher than many in subduction-like hydrous basalt (Fig. 6a, mostly S between 900 and 2500 ppm; e.g. Wallace 2005), while similar high S content appears to occur in oxidized magmas (Roggensack 2001; Webster et al., 2010).” [Line 493-496]

P12, l17-19. I am confused also here. How are calculated these ratios? There is no sulfur concentration as high as 5050 ppm? What are they representative of?

Response: We admit it was confusing. Now we only use the maximum ratios S/K₂O (0.711), Cl/K₂O (0.170) and F/K₂O (0.047) as representative of the primitive composition, and we did not demonstrate a strong ground to choose a concentration of K₂O. The endmember composition is now defined by melt inclusion values. The text now reads: “Because the composition of the mafic endmember points towards that of the primitive magma, the maximum values are, taken as the primitive volatile ratios: S/K₂O = 0.711, Cl/K₂O = 0.170, and F/K₂O = 0.047.” [Line 489-492]

P12, l23-24. “In fact, as shown in the previous section, we assessed the mafic-endmember H₂O concentration as 4.43 – 4.68 wt.%. Thus, the initial primitive H₂O concentration is at least 4.5 wt. %”. This sentence is redundant. Could it be just one section where the volatile (H₂O, S, Cl) contents of the end-member are clearly described: what is the best candidate (KKO, KSS)? Why is it representative of THE parental melt of the ASO series?

Response: Absolutely agree. We decided to rewrite the section about “Characterization of mixing endmembers”, and “Volatile concentrations of primitive basaltic melt”. We have paid particular attention to suppress redundancy.

P14, 110-14. What is the pressure of sulfur exsolution in such magma? The question of the sulfur supply from deep basalt magmas is detailed in Wallace and Edmonds (2011).

Response: In the passage here, we did not specify the exact depth as the discussion is developed later Fig. 8. As the conclusion of the paper, we think S is degassed between 9 - 10 km and we added a summary figure to synthesize our finding to the reader.

P15, 11-7. It is well known that CO₂ is almost totally exsolved as a gas phase at pressure less than 500 MPa (see Wallace and co-authors).

Response: Indeed, that is the point of our discussion as well. Now, in our new revision, we simplified the discussion regarding CO₂. CO₂ is nearly all degassed at shallow depth, and all the inclusions have low CO₂. We have no information regarding the CO₂ at the source. Taking high values of CO₂, it is possible to infer the depths of equilibrium, however the inclusions were degassed already. Our conclusion is that observed gas composition is consistent with the equilibrium pressure of 2.2-2.3 kb which is derived from 400-750 ppm initial CO₂. Our finding is therefore coherent with the point mentioned here. Yes, the major degassing and segregation occurs at depth shallower than 5 kb.

P16, 119. What are the gas species exsolved at 300MPa (\pm equivalent to 9 km)? I suppose that it 9 km below the vents? Geophysicists generally indicate depth below sea level.

Response: yes the 9 km here is from the vent. The difference between vent and sea level is 1000m the height of the volcano, so 9km from the vent, means 8 km below sea level. As SolEx model ignores gas speciation completely, the gas species at the depth must be H₂O-CO₂-(dissolved S, Cl, and F).

Other remarks

Table S1. Analysis OP2-M1. Is there an error in the Na₂O concentration (0.63 wt%) that is very low?

The data with the Na₂O outlier was suppressed from the Table.

Table S3 some of the analyses have a relatively low total (among others: OJSU olivine a2c& a4c: 95.8; c1c: 96.2; c5c: 91.2) or >102wt%.

Response: we have deleted these low total data after check the stoichiometry. Data of olivine and plagioclase presented in S3 are those measured by an EDS detector in SEM. Since stoichiometry of minerals are good, even for these with low total, we remained these EDS data as 100 wt.% normalized value unless total is too low (± 4 wt.%), and suppressed all low total data. For WDS data, while stoichiometry of minerals is excellent, we decided to suppress data with low or high total (>102 wt.% or <98 wt.%).

Fig. 4. Temperature

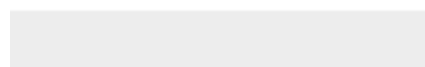
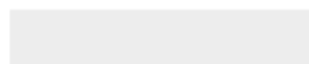
ESM 2: $C_{obs}^i - C_B^i$ written two times

Response: The spelling error is corrected, so is the error of the equation.



Click here to access/download

Electronic supplementary material
ESM1.xlsx





[Click here to access/download](#)

Electronic supplementary material
ESM2.pdf

